

Fox

AEDC-TR-88-31

User's Guide to CUNIFLOW

James T. Curtis
Calspan Corporation/AEDC Operations

April 1989

Final Report for Period October 1, 1981 – September 30, 1988

Approved for public release; distribution is unlimited.

**ARNOLD ENGINEERING DEVELOPMENT CENTER
ARNOLD AIR FORCE BASE, TENNESSEE
AIR FORCE SYSTEMS COMMAND
UNITED STATES AIR FORCE**



NOTICES

When U. S. Government drawings, specifications, or other data are used for any purpose other than a definitely related Government procurement operation, the Government thereby incurs no responsibility nor any obligation whatsoever, and the fact that the Government may have formulated, furnished, or in any way supplied the said drawings, specifications, or other data, is not to be regarded by implication or otherwise, or in any manner licensing the holder or any other person or corporation, or conveying any rights or permission to manufacture, use, or sell any patented invention that may in any way be related thereto.

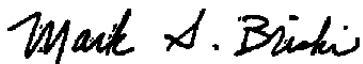
Qualified users may obtain copies of this report from the Defense Technical Information Center.

References to named commercial products in this report are not to be considered in any sense as an endorsement of the product by the United States Air Force or the Government.

This report has been reviewed by the Office of Public Affairs (PA) and is releasable to the National Technical Information Service (NTIS). At NTIS, it will be available to the general public, including foreign nations.

APPROVAL STATEMENT

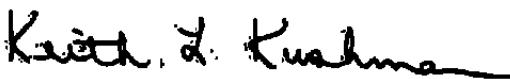
This report has been reviewed and approved



MARK S. BRISKI, Capt, USAF
Directorate of Technology
Deputy for Operations

Approved for publication:

FOR THE COMMANDER



KEITH L. KUSHMAN
Directorate of Technology
Deputy for Operations

UNCLASSIFIED

SECURITY CLASSIFICATION OF THIS PAGE

REPORT DOCUMENTATION PAGE				Form Approved OMB No. 0704-0188		
1a REPORT SECURITY CLASSIFICATION Unclassified			1b. RESTRICTIVE MARKINGS			
2a. SECURITY CLASSIFICATION AUTHORITY			3 DISTRIBUTION/AVAILABILITY OF REPORT Approved for public release; distribution is unlimited.			
2b DECLASSIFICATION/DOWNGRADING SCHEDULE						
4 PERFORMING ORGANIZATION REPORT NUMBER(S) AEDC-TR-88-31			5 MONITORING ORGANIZATION REPORT NUMBER(S)			
6a NAME OF PERFORMING ORGANIZATION Arnold Engineering Development Center		6b OFFICE SYMBOL (if applicable) DOT	7a NAME OF MONITORING ORGANIZATION			
6c ADDRESS (City, State, and ZIP Code) Air Force Systems Command Arnold Air Force Base, TN 37389-5000			7b ADDRESS (City, State, and ZIP Code)			
8a. NAME OF FUNDING/SPONSORING ORGANIZATION Arnold Engineering Development Center		8b OFFICE SYMBOL (if applicable) DOT	9 PROCUREMENT INSTRUMENT IDENTIFICATION NUMBER			
8c ADDRESS (City, State, and ZIP Code) Air Force Systems Command Arnold Air Force Base, TN 37389-5000			10 SOURCE OF FUNDING NUMBERS			
			PROGRAM ELEMENT NO 65807F	PROJECT NO DC71PW	TASK NO	WORK UNIT ACCESSION NO.
11 TITLE (Include Security Classification) User's Guide to CUNIFLOW						
12 PERSONAL AUTHOR(S) Curtis, James T., Calspan Corporation/AEDC Operations						
13a. TYPE OF REPORT Final		13b TIME COVERED FROM 10/1/81 TO 9/30/88		14. DATE OF REPORT (Year, Month, Day) April 1989	15 PAGE COUNT 118	
16. SUPPLEMENTARY NOTATION Available in Defense Technical Information Center (DTIC).						
17. COSATI CODES			18 SUBJECT TERMS (Continue on reverse if necessary and identify by block number) hypersonic flow planar body thermochemical model axisymmetric body			
FIELD	GROUP	SUB-GROUP				
12	01					
19 ABSTRACT (Continue on reverse if necessary and identify by block number) CUNIFLOW is a fast, mature code for calculating the hypersonic flow of an inviscid reacting gas over an axisymmetric or planar body. The thermochemical model allows for the finite-rate chemical relaxation of an arbitrary mixture of perfect gases and the coupling of dissociation with nonequilibrium vibrational relaxation. Options for calculating the effects of radiant energy loss, of nonuniform free-stream conditions, and of boundary-layer displacement are available. A particular advantage of the code, in addition to its speed, is that it can often be made to complete a calculation for near-equilibrium situations where other reacting flow codes encounter difficulties. This report summarizes the thermophysical models and the computational methods embodied in the code and provides instructions for inputting a problem and interpreting the output. The computational time for a standard configuration is plotted as a function of centerline velocity for various values of the binary scaling parameter.						
20 DISTRIBUTION/AVAILABILITY OF ABSTRACT <input type="checkbox"/> UNCLASSIFIED/UNLIMITED <input checked="" type="checkbox"/> SAME AS RPT <input type="checkbox"/> DTIC USERS			21 ABSTRACT SECURITY CLASSIFICATION Unclassified			
22a NAME OF RESPONSIBLE INDIVIDUAL Carlton L. Garner			22b TELEPHONE (Include Area Code) (615) 454-7813		22c OFFICE SYMBOL DOCS	

DD Form 1473, JUN 86

Previous editions are obsolete.

SECURITY CLASSIFICATION OF THIS PAGE

UNCLASSIFIED

PREFACE

The work reported herein was performed by Arnold Engineering Development Center (AEDC), Air Force Systems Command (AFSC), under Program Element 65807F. The Air Force Program Manager was Dr. K. L. Kushman. This work was performed by Calspan Corporation/AEDC Operations, operating contractor for the Aerospace Flight Dynamics testing effort at the AEDC, AFSC, Arnold Air Force Base, Tennessee. The work was performed in the Aerospace Systems Facility (ASF) under AEDC Project Number DC71PW. The task in the DC71 project addressed here was to document the current version of the CUNIFLOW analysis code. This report was submitted for publication on January 23, 1989.

CONTENTS

	<u>Page</u>
1.0 INTRODUCTION	5
2.0 OPTIONS, ASSUMPTIONS, AND RESTRICTIONS	6
2.1 Body Shape	6
2.2 Thermochemical Models	7
2.3 Chemical and Vibrational Relaxation	11
2.4 Radiation	15
2.5 Free-Stream Options	15
2.6 Boundary-Layer Options	16
3.0 NUMERICAL METHODS	18
3.1 The Nose Region Program	19
3.2 Transition to M.O.C. Code	24
3.3 The Hyperbolic Region	24
4.0 USING CUNIFLOW	30
4.1 System Requirements	31
4.2 Input	31
4.3 Output	44
4.4 Diagnostics	47
4.5 Operating Envelope	51
5.0 CONCLUDING REMARKS	51
REFERENCES	53

ILLUSTRATIONS

<u>Figure</u>	<u>Page</u>
1. Typical Configuration for CUNIFLOW	6
2. Physical and Computational Geometries for the Blunt Body Code	20
3. Overall Geometry for the Afterbody Program	25
4. Schematic of Geometry for Calculation of an Internal Point	27
5. Geometry of Boundary-Layer Interaction Procedure	28
6. Computing Mesh in Presence of Secondary Shock	30
7. Input Schematic	32
8. Converged Values for Radius of Curvature of Nonequilibrium Shock	37
9. Effect of Free-Stream Conditions on CPU-Time for Nonequilibrium Blunt Body Solutions	50
10. Nonequilibrium Air Solutions on Missile-Like Bodies	52

TABLES

	<u>Page</u>
1. File Usage	31
2. Variables in Namelist UPSTREAM	33
3. Input Format for Nonuniform Free-Stream Flow	34
4. Variables in Namelist OPTIONS	35
5. Parameters in Namelist SHOCK	37
6. Variables in Namelist BODY	38
7. Entries in Namelist CONTROL	39
8. Controls in Namelist SUPER	41
9. Entries in Namelist RESTART	43
10. Namelist CHANGE	44
11. Interpretation of the B2 Array	47

APPENDIXES

A. MATHEMATICAL DETAILS	57
B. INPUTTING THERMOCHEMICAL PROPERTIES	62
C. CHANGES SINCE 1967	72
D. CODE STRUCTURE	73
E. SHOCK SHAPE PARAMETERS	85
F. EXAMPLES	86
 NOMENCLATURE	 109

1.0 INTRODUCTION

Current interest in hypersonic vehicles such as the National Aerospace Plane (NASP) and the Aeroassisted Orbital Transfer Vehicle (AOTV) has prompted renewed attention to high-temperature thermochemical effects, including a radiative heat load to the body and the formation of a plasma sheath which will affect communication with the vehicle. At somewhat lower altitudes, the partially dissociated, vibrationally excited air ingested by the NASP engines may well affect the efficiency of the combustion process within the engines. Since reproduction of the hypersonic operating environment within a ground-based facility appears to be impractical, there exists a powerful impetus for numerical simulation of the flight conditions.

The Computational Fluid Dynamics (CFD) community is actively working to develop the capability for making such computations. Gnoffo, et al. (Ref. 1), Li (Ref. 2), Prabhu, et al. (Ref. 3), and Candler, et al. (Ref. 4) have recently reported Navier-Stokes codes incorporating nonequilibrium thermochemistry, but these codes have not yet reached a production stage, and, as Barber and Cox (Ref. 5) point out, the use of such codes for design purposes is prohibitively expensive.

The current report describes a mature and well-developed code which provides a large part of the capability for analyzing the aerophysical problems described above and may be as close to production status as any code of similar capabilities will ever be. This code, CUNIFLOW, is now operational on the AEDC Cray X/MP and on several other machines around the country (Refs. 6 - 9). The original version of CUNIFLOW and its first extension were thoroughly documented in Refs. 10 and 11, but these documents are getting hard to find and there have been many changes to the code since 1967, cf., Appendix C.

CUNIFLOW calculates the inviscid, hypersonic, chemically reacting flow field about a blunt axisymmetric or two-dimensional body like that in Fig. 1. The chemical composition, pressure, density, and velocity components of the free stream may be specified as functions of position, but it is also possible to input only the vehicle velocity and altitude and let the code calculate the other free-stream variables from fits to the 1953 *U. S. Standard Atmosphere*. Embodied in the code are thermochemical models for treating either equilibrium air or a chemically relaxing arbitrary gas mixture. Additionally, nonequilibrium vibrational relaxation for two diatomic species and radiant energy loss from the gas may be modeled. Since the displacement effect of the boundary layer is approximated by a semi-empirical method, CUNIFLOW is well adapted for use with a reacting boundary-layer code such as BLIMP (Ref. 12).

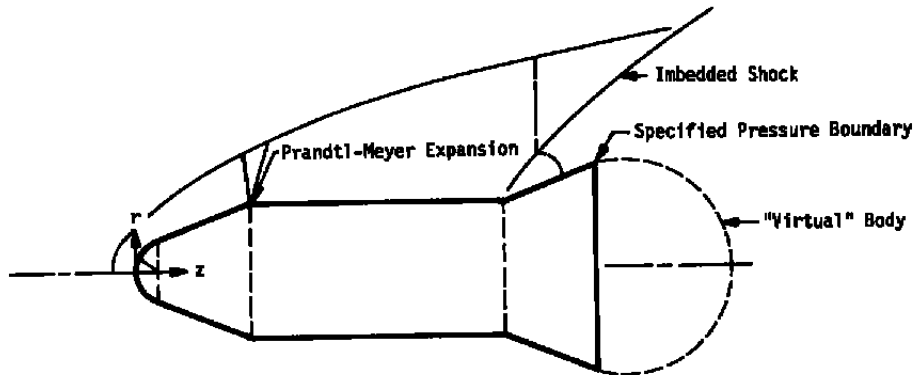


Figure 1. Typical configuration for CUNIFLOW.

The advantage of the interface with BLIMP is especially apparent at low altitudes ($\approx 23,000$ ft) where more sophisticated programs fail to converge. Other advantages of CUNIFLOW include moderate storage requirements and high speed. As currently dimensioned, CUNIFLOW requires only 250,000 words of memory. Run times, of course, will depend on the body size, the complexity of the thermochemical model, and the specified free-stream conditions. However, a fairly typical shock tunnel simulation (a 7-deg blunt cone with a 1-in. nose radius and an overall length of 10 in.) was calculated in 69 sec of CPU time on a Cray X/MP.

This report guides the user through the current version of the code and its usage without repeating all the details contained in Refs. 10 and 11. Sections 2.0 and 3.0, together with Appendix A, present without formal derivation the mathematical models and numerical methods employed, with some comment on their validity. Section 4.0 and Appendix B describe the input procedures and suggest some cures for common difficulties which may arise. The overall code structure is presented by the tables and charts of Appendix D.

2.0 OPTIONS, ASSUMPTIONS, AND RESTRICTIONS

2.1 BODY SHAPE

A typical configuration which may be analyzed with CUNIFLOW is shown in Fig. 1. The body must be convex and continuous; that is, steps are not allowed, but sharp expansion corners and **one** sharp compression corner are permissible.

The desired body may be specified by up to six equations of the form

$$(r - r_j)^P = (z - z_j)^Q [C_0 + C_1(z - z_j) + C_2(z - z_j)^2 \dots C_4(z - z_j)^4] \quad (1)$$

where z and z_j are measured from the body apex. Since the stagnation point is determined under the assumption that the body is a sphere, it is necessary that r_1 and z_1 be zero.

As indicated by Fig. 1, the inviscid calculation may be extended beyond the end of the vehicle by the artifice of introducing a "virtual body" and replacing the tangency condition by a specified pressure distribution. The surface pressure is determined as part of the computation. At present, only a constant pressure may be specified.

The physical significance of this constant pressure curve is minimal; it should be considered as a numerical boundary condition which is required by the numerics of the reference-plane characteristics method (Ref. 13). Although the computed flow field in the base flow region is of dubious validity, the flow field above the left-running characteristic from the corner will be valid.

2.2 THERMOCHEMICAL MODELS

Five separate thermochemical models are embedded in CUNIFLOW and may be selected through the input constant MODEL (Section 4.2.4). If the constant is not specified, the default model described in Section 2.2.1 will be used.

2.2.1 MODEL = 0 (Default)

The gas in the shock layer consists of N_S monatomic and diatomic species. The specific molar concentration of the j th species is $\bar{\gamma}_j$ moles/gm.* Because the finite-rate relaxation of the vibrational degrees of freedom of N_{vib} species is to be modeled, the caloric equation is taken in the form

$$\bar{h}_j = \bar{I}_j + \bar{h}_j^\circ + \bar{\epsilon}_j \text{ ergs/mole} \quad (2)$$

where $\bar{\epsilon}_j$ is the vibrational energy and \bar{h}_j° is the heat of formation. The energies of translation, of rotation, and of electronic excitation are included in the term \bar{I}_j , which may be written (Ref. 14)

$$\bar{I}_j = \left| \frac{5 + 2(n_j - 1)}{2} \right| RT + \left| \frac{\sum_{\ell=1}^m E_{j\ell} g_{j\ell} e^{-\bar{E}_{j\ell}/T}}{\sum_{\ell=1}^m g_{j\ell} e^{-\bar{E}_{j\ell}/T}} \right| \quad (3)$$

where n_j denotes the number of atoms per molecule, $\bar{E}_{j\ell}$ is the energy of the ℓ th electronic level of the j th species, and $g_{j\ell}$ is the degeneracy of this level.

*The bar (—) signifies a dimensional quantity.

The chemical potential of the j^{th} species is given by

$$\frac{\bar{\mu}_j^{\circ} - \bar{h}_j^{\circ}}{\bar{T}} = - \left\{ b_j + \left(\frac{3 + 2n_j}{2} \right) \ell n \bar{T} + (n_j - 1) \ell n (1 - e^{-\bar{\theta}_j/\bar{T}}) + \ell n \left[\frac{\sum_{\ell=1}^n g_{j\ell} e^{-\bar{E}_{j\ell}/\bar{T}}}{g_{j1}} \right] \right\} \quad (4)$$

The constant, b_j , includes the translational and rotational contributions, as well as the logarithm of the ground-level degeneracy. The characteristic vibrational temperature is $\bar{\theta}_j$.

For the species in vibrational equilibrium, the simple harmonic oscillator approximation, (Ref. 14)

$$\bar{\epsilon}_j = \mathcal{R} \bar{\theta}_j \frac{(n_j - 1)}{[\exp(\bar{\theta}_j/\bar{T}) - 1.0]} \quad (5)$$

is used for the vibrational energy. For the nonequilibrium diatomic species, the vibrational energy is obtained by integration of a differential equation relating $\bar{\epsilon}_j$ to the temperature, \bar{T} , and to the rates of certain reactions.

Each of the component gases may be assumed to be thermally perfect, so that one may write for the equation of state

$$\bar{p} = \bar{\rho} \bar{T} \mathcal{R} \sum_{j=1}^{N_s} \bar{\gamma}_j \quad (6)$$

where \mathcal{R} is the universal gas constant, 8.313405×10^7 ergs/mole $^{\circ}\text{K}$.

The default thermodynamic model (MODEL = 0) is based on certain common simplifications of molecular physics. These assumptions are useful in describing the thermal behavior of a low-temperature, low-density gas, but become increasingly inapplicable as the temperature increases. In particular, the simple-harmonic oscillator assumption of Eq. (5) must be supplemented by anharmonicity corrections (Ref. 15) for temperatures above approximately 1000°K . Furthermore, the separability of the vibrational, rotational, and electronic modes implied by Eqs. (2) and (3), although commonly assumed, is not in fact true (Refs. 15 and 16) and may become significant at temperatures greater than 2500°K (Ref. 16). Fortunately, at the very high temperatures ($T \approx 50,000^{\circ}\text{K}$) predicted for the AOTV,

MODEL = 0 is adequate because dissociation is so rapid that the vibrational and rotational modes contribute very little to the mixture energy.

2.2.2 MODEL = 1

The gas is assumed to be perfect with a specific heat ratio of 1.4. If the user does not specify the free-stream composition, air will be assumed. There is very little reason for selecting this option, as the code numerics are not well adapted to it.

2.2.3 MODEL = 2

Equilibrium air (O₂ and N₂ only) is assumed. The well-known RGAS and SERCH routines (Ref. 17) are used to obtain the thermal properties. No composition data are output and the radiation option is turned off.

2.2.4 MODEL = 3

The fluid is assumed to be an arbitrary mixture of thermally perfect gases — monatomic, diatomic, polyatomic — with fully equilibrated internal states. The specific heat, enthalpy, entropy, and chemical potential of each species are calculated from polynomial fits to existing property tables (Refs. 18 and 19).

$$\frac{\bar{c}_{p_j}}{\mathcal{R}} = a_{1j} + a_{2j} \bar{T} + a_{3j} \bar{T}^2 + a_{4j} \bar{T}^3 + a_{5j} \bar{T}^4 \quad (7)$$

$$\frac{\bar{h}_j}{\mathcal{R}\bar{T}} = a_{1j} + \frac{a_{2j}}{2} \bar{T} + \frac{a_{3j}}{3} \bar{T}^2 + \frac{a_{4j}}{4} \bar{T}^3 + \frac{a_{5j}}{5} \bar{T}^4 + \frac{a_{6j}}{\bar{T}} \quad (8)$$

$$\frac{\bar{S}_j}{\mathcal{R}} = a_{1j} \ln \bar{T} + a_{2j} \bar{T} + \frac{a_{3j}}{2} \bar{T}^2 + \frac{a_{4j}}{3} \bar{T}^3 + \frac{a_{5j}}{4} \bar{T}^4 + a_{7j} \quad (9)$$

$$\frac{\bar{F}_j}{\mathcal{R}\bar{T}} = \frac{\bar{h}_j}{\mathcal{R}\bar{T}} - \frac{\bar{S}_j}{\mathcal{R}} \quad (10)$$

Gordon and McBride (Ref. 20) have fitted the data of Ref. 18 with polynomials of the form of Eqs. (7) – (9), and furnish an extensive tabulation of the fit coefficients with the

NASA LeRC Chemical Equilibrium Code (Ref. 20) in the format required by CUNIFLOW. The LeRC Code fits are valid only in the ranges 300°K to 1000°K and 1000°K to 5000°K.

MODEL = 3 requires that the internal modes — rotation, vibration, electronic — be in equilibrium with the translational temperature. This assumption is justified for most propulsion problems to which CUNIFLOW might be applied and in many lower-speed, higher-density flow problems, except directly behind a thin shock.

Both the JANNAF (Ref. 18) and the Browne (Ref. 19) property tables incorporate a variety of empirical corrections for anharmonicity and vibration-rotation effects so that they are more accurate than the MODEL = 0 formulae quoted in Section 2.2.1. The accuracy of the CUNIFLOW results will depend on the precision of the curve fits, which usually deteriorate rapidly outside the announced limits. CUNIFLOW will not issue any messages when extrapolation occurs. The effect of such extrapolations on the solution will depend on the species concentration, on the reactions in which the species is involved, and on the magnitude of the extrapolation error.

2.2.5 MODEL = 4

The thermodynamic model presumed for MODEL = 4 is very similar to MODEL = 3. The thermal properties are calculated from the equations:

$$\bar{c}_{p_j} = \bar{a}_{3j} + \bar{a}_{4j} \bar{T} + \bar{a}_{5j} \bar{T}^2 \quad (11)$$

$$\bar{h}_j = \bar{a}_{1j} + \bar{a}_{2j} + \bar{a}_{3j} (\bar{T} - 3000) + \frac{\bar{a}_{4j}}{2} (\bar{T}^2 - 9.0 \times 10^6) - \bar{a}_{5j} \left(\frac{1}{\bar{T}} - \frac{1}{3000} \right) \quad (12)$$

$$\bar{S}_j = \bar{a}_{6j} + \bar{a}_{3j} \ln \left(\frac{\bar{T}}{3000} \right) + \bar{a}_{4j} (\bar{T} - 3000) - \frac{\bar{a}_{5j}}{2} \left(\frac{1}{\bar{T}^2} - \frac{1}{3000^2} \right) \quad (13)$$

which are those used by the KBLIMP-A (Ref. 12) boundary-layer code.

If this option is selected, the pressure, entropy, and composition at the body surface or boundary-layer edge are output on Fortran logical Unit 3 in a format acceptable to BLIMP.*

*File usage is described in Table 1, Section 4.1.

2.3 CHEMICAL AND VIBRATIONAL RELAXATION

The rate of change of the concentration of the j^{th} species along a streamline is described by two equations:

$$\sum_{j=1}^{N_S} a_{jk} \frac{\partial \bar{\gamma}_j}{\partial S} = 0 \quad k = 1, \dots, N_c \quad (14)$$

$$\frac{\partial \bar{\gamma}_j}{\partial S} = \sum_{i=1}^{N_R} \frac{\bar{Q}_{ij}(\bar{T}, \{\bar{\gamma}\})}{\bar{\rho} \bar{U}} \quad j = N_c + 1, \dots, N_s \quad (15)$$

in which N_c represents the number of elements and a_{jk} the number of atoms of k^{th} element in species j . Equation (14) states the principle of atom conservation. Conservation of electric charge is secured by treating the electron as an atom and assigning $a_{jk} = -1$ if the j^{th} species is a positive ion.[†]

The source term on the right of Eq. (15) is a function of the temperature and of all of the species concentrations $\{\bar{\gamma}\}$. When vibrational nonequilibrium is considered, the chemical source term \bar{Q}_{ij} also becomes dependent on the rate of change of the vibrational energy $\bar{\epsilon}_j$ of certain species.

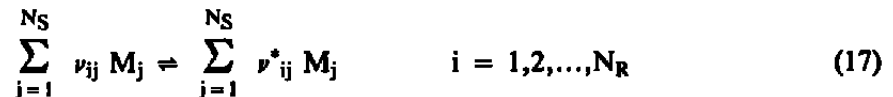
For the N_{vib} species not in vibrational equilibrium, the vibrational energy is determined from

$$\frac{\partial \bar{\epsilon}_j}{\partial S} = \bar{w}_j \quad j = N_c + 1, \dots, N_c + N_{\text{vib}} \quad (16)$$

where \bar{w}_j is coupled to the chemical source terms \bar{Q}_{ij} in Eq. (15).

2.3.1 Reactions

To lend generality to the program, the N_R reactions are written in the form



[†]Note that the convention for numbering the species lists the monatomic elements, including the electron, first, followed by the molecular species with nonequilibrium vibrational energies.

where M_j represents the j^{th} chemical species, and the stoichiometric coefficients are represented by ν_{ij} and ν_{ij}^* .

The forward and backward rate constants for the i^{th} reaction are related by

$$k_{fi}/k_{bi} = (\mathcal{R}\bar{T})^{-\Delta_i} \exp \left[- \frac{\Delta \bar{F}_i^0}{\mathcal{R}\bar{T}} \right] \quad (18)$$

where

$$\frac{\Delta \bar{F}_i^0}{\mathcal{R}\bar{T}} = \sum_{j=1}^{N_S} (\nu_{ij}^* - \nu_{ij}) \frac{\bar{A}_j^0}{\bar{T}} \quad (19a)$$

and

$$\Delta_i = \sum_{j=1}^{N_S} (\nu_{ij}^* - \nu_{ij}) \quad (19b)$$

By using Eq. (18), either the forward or backward reaction rate may be specified and the other computed from it. The temperature dependence of the reaction rate constants is assumed in the form

$$\bar{k}_{fi\text{eq}} \text{ or } \bar{k}_{bi\text{eq}} = \bar{A}_{ki} \bar{T}^{\bar{B}_{ki}} \exp \left[- \frac{\bar{C}_{ki}}{\bar{T}^{\bar{D}_{ki}}} \right] \quad (20)$$

The source term \bar{Q}_{ij} is written†

$$\begin{aligned} \bar{Q}_{ij} = & W_i \left\{ (\nu_{ij}^* - \nu_{ij}) k_{fi} e^{\sum_l \nu_{il}} \prod_{l=1}^{N_S} \bar{\gamma}_l^{\nu_{il}} \chi_{li} \right\} \\ & + D_i \left\{ \left[\frac{(\nu_{ij}^* - \nu_{ij})}{(\sum \bar{\gamma}_j)^{-1}} \bar{k}_{fi} e^2 \right] \prod_{j=1}^{N_S} \bar{\gamma}_j^{\nu_{ij}} \chi_{li} \right\} \\ & + Z_i \left\{ \left[(\nu_{ij}^* - \nu_{ij}) \bar{k}_{fi} e^{2\bar{\gamma}_j} \sum_{j=1}^{N_S} (\nu_{ij}^* - \nu_{ij} + 1) \nu_{ij} \bar{\gamma}_j \right] \chi_{li} \right\} \end{aligned} \quad (21)$$

†These formulae assume that Z and D reactions are binary in the forward direction.

In Eq. (21), the parameters W_i , D_i , Z_i may be either zero or one and serve to denote the type of reaction. Thus, the first term alone ($W_i = 1$, $Z_i = 0$, $D_i = 0$) accounts for specific collision partners as in the reaction $O_2 + O \rightleftharpoons 2O + O$. The second term is used when all collision partners are lumped together, as in the reaction $O_2 + M \rightleftharpoons 2O + M$. The third term is used when some collision partners are lumped and others specified. Note that for a Z-type reaction, the specified reactant may not be included among lumped collision partners. For instance, $N_2 + M \rightleftharpoons 2N + M$ with M including N_2 will not permit N_2 to collide with itself if the reaction is specified as a Z type. This must be written as a separate reaction of type, i.e.,



The parameter χ_i appearing in Eq. (21) is defined as

$$\chi_i = 1 - \frac{\exp\left(-\sum_{j=1}^{N_S} (\nu_{ij}^* - \nu_{ij})\right)}{\prod_{j=1}^{N_S} V_j^{A_{ij}} K_i} \prod_{n=1}^{N_S} \gamma_n^{\nu_{ij}^* - \nu_{ij}} \quad (22)$$

where K_i is the equilibrium constant. The significance of χ_i is that it represents the degree of nonequilibrium

$$\chi_i = 1 - \frac{\text{reverse rate}}{\text{forward rate}} \quad (23)$$

and is obviously equal to zero at final equilibrium. Immediately behind the shock $\chi_i = 1^{**}$, while in a region of rapid recombination, χ_i may assume large negative values.

2.3.2 Vibrational Relaxation

Since the energy required for dissociation is diminished by the internal energy stored in vibration, a finite rate of vibrational relaxation affects the dissociation rates. On the other hand, the upper vibrational levels are selectively depopulated by dissociation. In other words,

*These formulae assume that Z and D reactions are binary in the forward direction.

**If all reactions are input with dissociation on left side of Eq. (17).

vibrational and chemical relaxation are coupled. The effect of the nonequilibrium vibrational energy on the reaction rates is described by

$$k_{fi} = k_{fi,eq} \prod_{j=1}^{N_{S_{vib}}} V_j^{A_{ij}} \quad (24)$$

and the subscript "eq" on the reaction rates indicates that these are evaluated for equilibrium vibration. The exponent A_{ij} may be either 0 or 1 and is used to specify which reaction will be affected by the vibration-dissociation coupling factor, V_j [Eq. (28)].

In developing an estimate of the so-called CVDV coupling terms which describe these opposing effects, it is assumed that the vibrational energy levels are those of a truncated simple harmonic oscillator, that the levels are populated according to a Boltzmann distribution with a vibrational temperature T_{vib} , and that the probability of dissociation depends only on the collision energetics. For this model (Refs. 21, 22), the relaxation rate ω_j is

$$\begin{aligned} \bar{\omega}_j \equiv \frac{d\bar{\epsilon}_j}{dS} &= \frac{\bar{\epsilon}_{j,eq} - \bar{\epsilon}_j}{\bar{\tau}_j \bar{U}} + \frac{1}{e\bar{U}} \left\{ \frac{\bar{\theta}_j}{\exp(\bar{\theta}_j/\bar{T}_{mj}) - 1} - \frac{N_j \bar{\theta}_j}{\exp(\bar{\theta}_j N'_j / \bar{T}_{mj}) - 1} - \bar{\epsilon}_j \right\} \sum_{i=1}^{N_R} \frac{A_{ij}}{\bar{\gamma}_j} \\ &- \frac{1}{e\bar{U}} \left\{ \left(\frac{1}{2} N'_j - 1 \right) \bar{\theta}_j - \bar{\epsilon}_j \right\} \sum_{i=1}^{N_R} \frac{A_{ij} Q_{ij}}{\bar{\gamma}_j} \left(\frac{1 - x_i}{x_i} \right) \end{aligned} \quad (25)$$

where N'_j is the number of vibrational levels in the truncated oscillator and

$$\frac{1}{\bar{T}_{mj}} = \frac{1}{\bar{\theta}_j} \ln \left(\frac{\bar{\theta}_j + \bar{\epsilon}_j}{\bar{\epsilon}_j} \right) - \frac{1}{\bar{T}} \quad (26)$$

The characteristic relaxation time $\bar{\tau}_j$ is assumed to be of the form

$$\bar{\tau}_j = \frac{\tau_{aj} \bar{T}^{\tau_{bj}}}{\bar{P}} \exp \left[\frac{\tau_{cj}}{\bar{T}^{\tau_{dj}}} \right] \quad (27)$$

where $\bar{\tau}_{aj}$, $\bar{\tau}_{bj}$, $\bar{\tau}_{cj}$, $\bar{\tau}_{dj}$ are user-supplied constants. For the nonpreferential model (Ref. 21), the coupling factor is

$$V_j = \frac{1}{N'_j} \left[\frac{1 - \exp(-N_j \bar{\theta}_j / \bar{T}_{mj})}{\exp(\bar{\theta}_j / \bar{T}_{mj}) - 1} \right] \left[\frac{\exp(\bar{\theta}_j / \bar{T}_{vj}) - 1}{\exp(\bar{\theta}_j / \bar{T}) - 1} \right] \quad (28)$$

where the vibrational temperature \bar{T}_{vj} is just the reciprocal of the first term on the right-hand side of Eq. (26), and \bar{T} is the translational temperature.

At very high velocities (greater than 30,000 ft/sec), the vibrational coupling model outlined above breaks down, resulting in the unstable growth of vibrational energy and temperature. Since the rate of dissociation is high, only a small fraction of the total enthalpy is involved in the vibrational modes, so that the use of equilibrium vibration is a reasonable approximation.

Note also that the coupling model is intended only as a correction to empirical reaction rates measured under conditions that assure equilibrium vibration. The CVDV coupling model has recently been discussed and modified by Park, et al., (Refs. 23, 24) and by Carlson, et al (Ref. 25) and is currently in a state of flux.

2.4 RADIATION

If the nonequilibrium option (MODEL = 0) is selected, it is also possible to consider a class of reactions which result in the emission of radiation. Since the shock layer is assumed to be optically thin, this radiant energy is lost to the gas.

The radiation from the excited particles is computed as if it were in equilibrium with the local translational temperature; i.e., the energy states which are involved in radiative transitions are assumed to be populated according to a Boltzmann distribution with the translational temperature as an independent variable. The overall rates of radiation from the various radiating systems were taken from Ref. 26. These rates can be fitted over a considerable range by expressions of the type

$$\bar{A}_k \bar{N}_j \exp(-\bar{B}_k / \bar{T}) \quad (29)$$

where \bar{A}_k and \bar{B}_k are input constants and \bar{N}_j is the nonequilibrium number density of the j^{th} species.

2.5 FREE-STREAM OPTIONS

To study entry into a nonterrestrial atmosphere or phenomena in, say, an arc-heated tunnel, the chemical composition, pressure, density, and velocity components of the free stream may

be specified as functions of position. Most of the time, however, it is appropriate to consider a uniform stream of standard air and input only a velocity (ft/sec) and an altitude (feet) and let the code calculate the other free-stream variables from fits to the 1953 *U. S. Standard Atmosphere* (subroutine HATM).

2.6 BOUNDARY-LAYER OPTIONS

One of the strong features of CUNIFLOW is its ability to approximate some of the effects of a boundary layer without ever actually calculating a viscous profile. This procedure needs a wall enthalpy ratio (or wall temperature, T_w) which must be input.

While the boundary-layer procedure increases the realism of the simulation and allows the program to avoid the difficult "reaction layer" near the wall, it slows down the calculation and sometimes introduces numerical instability. Because the numerical methods used at slope discontinuities are incompatible with the presence of a boundary layer, the boundary-layer calculation should be omitted when discontinuities are present.

2.6.1 Transport Properties

The viscosity must be evaluated in connection with the boundary-layer matching procedures to be described later. Since the boundary layer is calculated only approximately, an exact calculation of the viscosity is not required. At the stagnation point, a program based on the work of Peng and Pindroh (Ref. 27) is used to compute the stagnation density and stagnation viscosity. In the program, an equilibrium air composition involving 14 species is obtained as a function of temperature and pressure. After computing the density, the program lumps the original 14 species into 4 (molecules, atoms, ions, electrons) with molecular weights $m_1 = 28.8$ gm/mole, $m_2 = 14.4$ gm/mole, $m_3 = 14.4$ gm/mole, and $m_4 = 5.5 \times 10^{-4}$ gm/mole, respectively. Using the same subscripts for the lumped mole fractions, \bar{X}_i , one may write an approximate expression for the mixture viscosity as follows:

$$\bar{\mu} = \sum_{i=1}^4 \left[\frac{1}{\bar{\mu}_i} + \frac{1.45 \mathcal{R} \bar{T}}{e \bar{X}_i m_i} \sum_{k=1, k \neq i}^4 \frac{\bar{X}_k}{D_{ik}} \right]^{-1} \quad (30)$$

where the viscosity of the pure species is

$$\bar{\mu}_i = \frac{\sqrt{m_i \bar{T}}}{11920 \phi_{22}} \sqrt{m_\infty \bar{T}_\infty} \quad (31)$$

$$\frac{1}{D_{ij}} = 171.1 \left(\frac{\bar{m}_i \bar{m}_j}{\bar{m}_i + \bar{m}_j} \right)^{1/2} \bar{T}^{-3/2} \phi_{ij} P \quad (32)$$

The cross sections for viscosity ϕ_{ii} and binary diffusion ϕ_{ij} were obtained by a least-squares curve fit of the results of Peng and Pindroh.

The stagnation point viscosity evaluated from Eqs. (30) to (32) is used as a reference for viscosity calculations at all other points of the nose-region boundary layer since it may be rather safely assumed that the flow close to the body is chemically frozen at a composition near that of the stagnation point equilibrium. Away from the stagnation point in the nose-region, the viscosity is computed as

$$\bar{\mu} = \bar{\mu}_0 \sqrt{\bar{T}/T_0} \quad (33)$$

Over the afterbody, temperatures get low enough ($\sim 3000^\circ \text{K}$) that the Sutherland formula

$$\bar{\mu} = \frac{(1.4582 \times 10^{-5}) \bar{T}^{3/2}}{\bar{T} + 110.3} \text{ gm/cm-sec} \quad (34)$$

is applicable. The reader should note that Eq. (34) applies only to air.

2.6.2 Displacement

If $\text{INBLR} = 1$ (Section 4.2.4), the displacement interaction between the viscous and inviscid flow fields is computed using a simplified boundary-layer theory. While this boundary layer is approximate, the neglected items — chemical reactions and species diffusion — have no significant effect on the variables which affect the inviscid flow field, namely, the mass flux, $\bar{\psi}_2$, through the viscous layer and the velocity thickness, $\bar{\delta}$.* The basic relations governing these variables are

$$\bar{\psi}_2 = (2\pi)^{\omega} \sqrt{2 \bar{s}} F_1 (\Pi, G_{\text{wall}}) \quad (35)$$

$$\bar{\delta} = \frac{\sqrt{2 \bar{s}}}{q_e u_e r_b^{\omega}} \left(\frac{H_c}{h} F_2 + F_3 \right) \quad (36)$$

*The displacement thickness is not used because it tends to be negative under hypersonic flight conditions.

where

$$\bar{s} = \int_0^s \frac{\bar{\rho}_e \bar{\mu}_e \bar{u}_e \bar{r}_b^{2\omega}}{dS} \quad (37)$$

is the transformed arc length used in laminar compressible boundary-layer theory. Away from the nose, it is necessary to replace the customary pressure gradient parameter, π , by its average over the length of the boundary layer.

$$\langle \bar{\pi} \rangle = \frac{1}{\bar{s}} \int_0^{\bar{s}} \left(2 \frac{H_e \bar{s}'}{h_e \bar{u}_e} \frac{dU_e}{d\bar{s}'} \right) d\bar{s}' \quad (38)$$

For consistency this usage was extended to the nose region boundary layer. The quantities F_1 , F_2 , and F_3 appearing in Eqs. (35) and (36) are integrals over the ideal gas boundary-layer profiles reported by Cohen and Reshotko (Ref. 28). The values of these integrals, taken from Ref. 28, were fitted by the third-degree polynomials:

$$F_1 = \int_0^\infty f d\eta = a_{10}(G_{\text{wall}}) + a_{11}(G_{\text{wall}}) \bar{\pi} + a_{12}(G_{\text{wall}}) \bar{\pi}^2 + a_{13} \bar{\pi}^3 \quad (39)$$

$$F_2 = \int_0^\infty (G - f^2) d\eta = a_{20} + \dots + a_{23}(G_{\text{wall}}) \bar{\pi}^3 \quad (40)$$

$$F_3 = \int_0^\infty f^2 d\eta = a_{30}(G_{\text{wall}}) + \dots + a_{33}(G_{\text{wall}}) \bar{\pi}^3 \quad (41)$$

where

$$G = H(\eta)/H_e; f = \frac{df}{d\eta} = U(\eta); \eta = \int_0^\infty \frac{g_e}{\rho} dy$$

For a given value of G_{wall} , the coefficients a_{ij} are obtained by table look-up and linear interpolation. The evaluation of the F_i is performed by subroutine INTGRL.

3.0 NUMERICAL METHODS

A complete presentation of all the numerical details would make this report unwieldy and contribute little to the would-be user's understanding of what is going on in the calculation. Since most of this information is available in Refs. 10 and 11, this section will attempt to

present only the information necessary for understanding the input procedures and for evaluating the output of the code. Additional information will be found in Appendixes A and D.

Since the shock layer flow is both subsonic and supersonic, distinct numerical methods are required for the flow field over the nose, which is described by elliptic partial differential equations, and for the remainder of the body, which is described by hyperbolic flow equations which permit the use of the method of characteristics. The evaluation of the thermochemical properties and of the reaction rates is common to both procedures, as is the evaluation of the boundary conditions at the thin shock.

This distinction in numerical methods is reflected in the structure of CUNIFLOW (cf., Appendix D) which consists of a small MAIN program which calls BREGN to compute the blunt body flow, FRMAIN to calculate the supersonic flow, and BRIDGE as a transition between the two. The program is arranged so that the named segments can be loaded as overlays, although this is not required for most modern computers such as the Cray X/MP.

3.1 THE NOSE REGION PROGRAM

3.1.1 General

The elliptic partial differential equations which describe the flow in the subsonic-transonic region between the body and the detached shock wave are solved by the "Method of Lines" (Ref. 29). That is, derivatives parallel to the shock are evaluated numerically so that the partial differential equations may be converted to a set of ordinary differential equations which are then integrated by an explicit marching procedure starting from the shock and marching inward toward the body.

The body surface is located by mass conservation. An iterative procedure is used to vary the shock shape until the resulting body shape corresponds to that specified. When the boundary-layer displacement option is elected, the mass balancing takes place at the edge of the boundary layer.

3.1.2 The Nose-Region Mesh

The geometry for the nose-region calculation is shown in Fig. 2. The mesh consists of data surfaces parallel to the shock and rays normal to the shock. Since the data surfaces are parallel to the shock, there is a discrepancy between grid and body which increases as one moves away from the axis. The calculation on the six outer rays is not carried completely to the body surface (Section 3.1.4). A minimum of seven equally spaced rays is required;

25 rays are allowed. The ray spacing, Δx , and the position of the first off-axis ray, x_0 , may be adjusted to ensure a satisfactory supersonic ray for starting the M.O.C. (hyperbolic region) program. If $x_0 \leq \Delta x$, BREGN will make use of symmetry to create three virtual rays so that x-derivatives on the axis will be handled properly by the standard derivative routines. The axis will then appear in the printout as ray number 4.

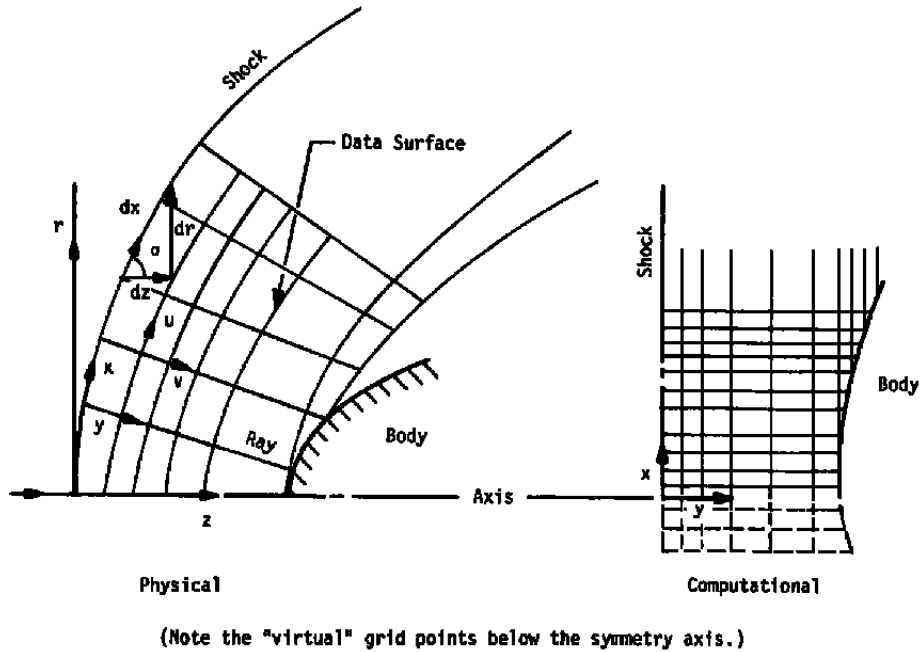


Figure 2. Physical and computational geometries for the blunt body code.

The spacing in the y-direction (normal to the shock) is determined dynamically (within user-specified limits) by the program. Spacing will be fine near the shock and near the body.

To relate the physical coordinates z and r to the computational coordinates x and y , it is necessary to specify a shock shape in some parametric form. The shape recommended by Lomax and Inouye (Ref. 17)

$$\frac{\bar{z}}{\text{RSH}} = \frac{\left(\frac{\bar{r}}{\text{RSH}}\right)^2 + \text{SlP}\left(\frac{\bar{r}}{\text{RSH}}\right)^4}{1 + \text{Sl}\left(\frac{\bar{r}}{\text{RSH}}\right)^3} \quad (42)$$

is used for this purpose. This shock has a radius of curvature (RSH) at the axis.

The metric for the nose-region mesh is

$$dS^2 = (1 + \kappa y)^2 dx^2 + dy^2 + r^2 d\phi^2 \quad (43)$$

where $\kappa(x)$ is the local shock curvature, $d\sigma/dx$ (Fig. 2).

3.1.3 Boundary Conditions

When the free stream is nonuniform, the local pre-shock conditions are calculated by linear interpolation in the two-dimensional tables input via Unit 4 (cf., Table 1).

Since the shock is assumed to be thin, the composition of the gas does not change during its passage through the shock unless equilibrium has been assumed (MODEL = 2). The vibrational energies of NVIB (Section 4.2.4) molecules are held at their free-stream values during the shock passage. The vibrational energies of the remaining molecules are equilibrated to the post-shock translational temperature.

Because of the variety of possible thermochemical options involved, the shock conservation conditions are solved by an iterative process.

3.1.4 Marching

Sections 3.1.4 and 3.1.5 describe the inviscid procedure. The optional viscous corrections are discussed in Section 3.1.6. In the following discussion, "step" means advancing by the same increment Δy on each ray.

A marching cycle begins by using the most recent data to evaluate the derivatives in the x-direction. A seven-point algorithm (Appendix A) derived from filter theory (Ref. 30) is used.

Since the x-derivatives are now known, one has on each ray a coupled set of ordinary differential equations which are integrated for a single y-step by an algorithm attributed to Lomax (Ref. 31). The algorithm, which consists of an explicit predictor and 4, 6, 8, or 10 implicit correctors, is presented in Appendix A.

The Lomax algorithm was devised to overcome the step size limitations associated with the "stiffness" of the differential equations. A set of differential equations is said to be stiff when the set possesses large negative "parasitic" eigenvalues which limit the step size but

are uninteresting physically, and some very much smaller "driving" eigenvalues which convey the interesting physics.

Failure of an integration step is indicated by a negative value for a dependent variable or by an excessive change (15 percent) in the temperature. When a failure is detected, the previous (successful) step size is halved and the entire step is repeated. The possible repetition of a successful step requires that storage be provided for two complete data surfaces (B0 and B1 in Fig. 2) as well as the surface under construction, B2.

If a step is successful, the data in array B0 are written to Unit 9, B1 is copied to B0, B2 is copied to B1, and the size of the next step is increased according to the rule

$$\text{STEP} = \text{STEP} \times (1.0 + 1.0/\text{FLOP}) \quad (44)$$

where FLOP is initialized to 1.0 and incremented by 1.0 at each failure. In addition, the estimated distance to the body, calculated at each step, is used as an upper bound on the step size.

The body is located by mass balancing. At a general point on ray M, the mass flux across the ray between the point and the body is

$$\psi_M = \psi_{Sh}^M(x) - \int_0^y (2\pi r)^\omega \rho u dy \quad (45)$$

where ψ_{Sh}^M is the nondimensional mass flux into the shock between the axis and the point $(x,0)$. The inward integration on a ray is continued until $\psi_M \leq$ some specified fraction of $\psi_{Sh}^M(x)$. When a ray "reaches the body," the results on that ray are "frozen" and the ray is dropped from the computation. Since seven rays are required for evaluation of the x derivatives, the integration stops when the number of active rays becomes less than seven. It is desirable that the rays drop one at a time from the axis outward, but frequently they will be dropped in clumps depending on step sizes and the degree of parallelism between shock and body.

3.1.5 Shock Iteration Procedure

When the inviscid flow calculation stops, data for the last three points on each ray are left in the arrays B0, B1, and B2.

The first step in the shock iteration procedure is to linearly extrapolate the remaining mass flux across each ray to zero. This defines the points $(z_{ed}(m), r_{ed}(m))$ at the surface of

the computed body. The desired body is then translated along the axis of symmetry to bring it into coincidence with the point z_{ed} (MATCH), r_{ed} (MATCH), where MATCH is the first ray off the axis. The intersection of each ray with the desired body is designated as $z_B(m)$, $r_B(m)$.

The scheme for correcting the shock shape involves translating each ray along its length to bring the point (z_{ed}, r_{ed}) into coincidence with z_B, r_B . In practice, this idea is expressed in the equations.

$$\begin{aligned} z'_{sh}(m) &= z_{sh}(m) + \alpha[1 - \lambda\alpha][z_B(m) - z_{ed}(m)] \\ r'_{sh}(m) &= r_{sh}(m) + \alpha[1 - \lambda\alpha][r_B(m) - r_{ed}(m)] \end{aligned} \quad (46)$$

Only a fraction $\alpha[1.0 - \lambda\alpha]$ of the z and r errors is removed at each iteration. Appropriate values for α and λ have been found to be $\alpha = 0.35$, $\lambda = -0.5$.

Two tests for convergence of the shock iteration must be simultaneously satisfied:

1. The RMS deviation between extrapolated points and body points must be less than an input constant, RMSTST, which is defaulted to 5.0×10^{-4} .
2. The extrapolated flow angle error at the junction point with the M.O.C. calculation must be $\leq 10.0 \times \text{RMSTST}$.

If these criteria have not been met, the shock shape parameters RSH, S1P, and S1 of Eq. (42) for the next iteration are determined by a least-squares fit of the revised shock coordinates x'_{sh} , r'_{sh} .

3.1.6 Viscous Interaction Option

When the viscous interaction option is invoked, the calculation proceeds as above except that z_{ed} , r_{ed} are determined by interpolating to the boundary-layer mass flux from the previous iteration instead of to zero. After z_B, r_B have been determined, the boundary-layer edge and mass flux are calculated. The mass flux is used to re-evaluate z_{ed}, r_{ed} and the edge coordinates are substituted for the body coordinates in Eq. (46).

3.2 TRANSITION TO M.O.C. CODE

When BREGN returns to MAIN with a converged shock shape, the amount of data on Unit 9 is highly variable — anywhere from 20 to 1,000 y-steps. Subroutine BRIDGE reads Unit 9 and selects NOUT records as nearly equally spaced in mass flux as possible and calls Subroutine OUT to print the data in dimensional form.

Starting the M.O.C. program is a little “touchy,” especially when a boundary layer is present. The supersonic program is sensitive to any inconsistency between the body shape and the flow angle determined from the flow-field calculation. Such inconsistencies arise because the shock iteration process satisfies the flow tangency condition only on the average. To remove or reduce these inconsistencies, BRIDGE calls Subroutine BLAYST, which adjusts the axial position and the scale (nose radius) of the body to make the body slope match the flow angle. The changes in scale and position are small if a reasonable shock fit has been obtained. (Section 4.2.7)

When the body adjustments are completed, the flow-field data on the junction ray at the selected y-stations are written to Unit 2 for transfer to the M.O.C. code.

Finally, the flow-field data are extrapolated or interpolated to the boundary-layer edge or the body surface. These data are also printed by Subroutine OUT.

3.3 THE HYPERBOLIC REGION

3.3.1 General

The flow-field calculation in the supersonic region is performed by the method of characteristics using the so-called reference-plane form which is sometimes attributed to Hartree (Ref. 13). This procedure, described in Section 3.3.3 below, converts the hyperbolic partial differential equations into ordinary differential equations — the “compatibility equations” — which apply along the Mach lines and the streamlines in the flow.

Chemical kinetic effects appear directly in the compatibility equations (Appendix A) and also indirectly through their influence on temperature and molecular weight. Since the latter effects are secondary, it is possible to converge the fluid dynamic properties at the downstream point while holding the chemistry frozen. After convergence is obtained, the downstream composition is calculated by integrating the species conservation equations (A-27) – (A-29) along the streamline through the point.

The bow shock is "fitted," i.e., the infinitely thin wave is located by matching the pressure calculated with the Rankine-Hugoniot equations with the pressure calculated by applying a compatibility equation along a characteristic from the interior of the shock layer.

3.3.2 The Mesh

3.3.2.1 General

As shown in Fig. 3, the M.O.C. data surfaces — often referred to as rays in the text — are cones (or planes) which intersect the body surface in a right angle. When the input data surface is prepared by subroutine BRIDGE as is usually the case, the first "ray" is normal to the shock rather than to the body surface. Then, as indicated in Fig. 3, the next NROTAT rays are pivoted about the foot of the input ray to adjust to the body-normal mesh. The default value $NROTAT = 4$ (Section 4.2.8) is usually satisfactory.

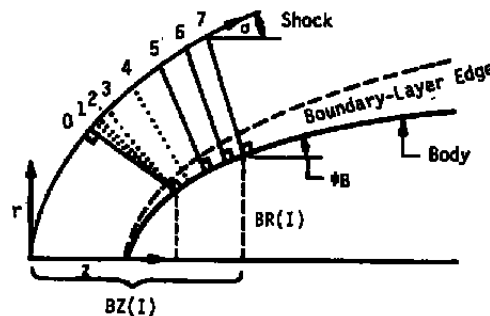


Figure 3. Overall geometry for the afterbody program.

The mesh consists of points at the intersection of each ray with the body surface (or the boundary-layer edge), each of the selected streamlines, and the shock wave. Ray spacing is discussed in Section 3.3.3.4. Following a given streamline from ray to ray is facilitated by assigning an index NUM which never changes. Since the boundary-layer edge is not a streamline, it is assigned the special value $NUM = 0$. The true streamlines are numbered consecutively outward, beginning with $NUM = 2$.

Occasionally, the growing boundary layer will swallow a numbered streamline, and the corresponding value for NUM will simply disappear from the output.

In the natural order of events, a new point would be added to the mesh at each ray-shock intersection. Because of the continually decreasing curvature of the shock, these added streamlines would be tightly clustered near the shock and would soon overwhelm the available storage. To avoid this situation, a streamline is started from the shock only if the increment

is more than an input fraction CSST (Section 4.2.7) of the spacing between the two existing streamlines closest to the shock.

When the number of streamlines threatens to overflow the existing storage, the program drops odd-numbered streamlines.

3.3.2.2 Exceptions

The mesh just described is sometimes interrupted to accommodate body slope discontinuities such as expansion and compression corners. These exceptions will be explained in Section 3.3.5.

3.3.3 Marching

3.3.3.1 Interior Point

In Fig. 4, the flow field is completely known at the points designated by solid symbols on rays A and B. The flow field at point IT on ray B is to be calculated by an iterative process. The calculation is initialized by extending the streamline through IK to intersect ray B and by estimating the pressure and flow angle at IT. Using the composition at IK and the pressures at IT and IK, Eqs. (A-26) and (A-30) are integrated along IK-IT to determine the "frozen" temperature and velocity at IT. The Mach angle $\beta(IT)$ is calculated, and the intersections IR and IS of the characteristic lines with ray A are found. The fluid dynamic properties at IR and IS are interpolated linearly, and the compatibility equations are integrated along the characteristics to obtain a pair of algebraic equations which are then solved simultaneously for the pressure and flow angle at IT.

If the relative pressure change from the previous cycle exceeds the allowed tolerance, IT is relocated, $f(IT)$ is averaged with $\phi(IK)$, and new values for temperature and velocity at IT are computed. In general, three or four iterations are required to converge the solution at an interior point to a relative error of 1×10^{-6} in pressure.

When the solution is converged, the species conservation equations are integrated along the streamline from IK to IT and the temperature is updated. This integration is performed with the Lomax algorithm described in Section 3.1.4. If a concentration becomes negative at any phase of the procedure, the marching step is halved. The calculation is aborted after eight unsuccessful attempts. Although several applications of the Lomax algorithm may be required to get from IK to IT, only the point IT is stored.

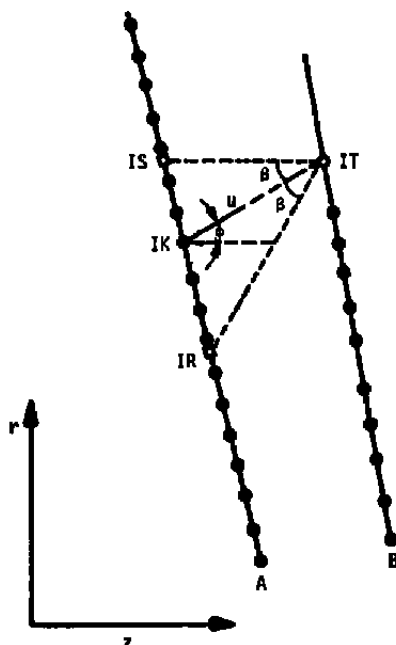


Figure 4. Schematic of geometry for calculation of an internal point.

3.3.3.2 Interpolating Along the Boundary

One or the other of the backward characteristics from points near the extremities of ray B may not intersect ray A. This difficulty is overcome by calculating the shock and body points before starting the interior points. Two shock points and two body points are calculated to improve the accuracy of the interpolation.

3.3.3.3 Data Storage

To economize on storage, data for points on a completed ray and also for points on a ray under computation are stored in the same arrays. At the beginning of a marching cycle, the data for points on the completed ray are shifted upwards by MDELAY points, where MDELAY is the number of points saved for interpolation.

The default value of MDELAY is 5. A larger value restricts the number of streamlines in the mesh while a smaller value restricts the size of the marching step. Since the first nine positions in the data arrays are reserved for special uses such as characteristic base points and intermediate body and shock points, the effective number of streamlines is NMAX where $NMAX = NY - MDELAY - 9$. NY is currently fixed at 50 by PARAMETER statements.

Since the point B_2 is known, specifying a value for δ locates the point IT on the ray. Estimate a value for the flow angle ϕ_{IT} on the streamline IR-IT which enters the growing boundary layer at IT. The pressure, composition, etc., at IR may be determined by interpolation along the previous ray. The Mach angle, β , may be determined by integrating along the streamline, and one application of the compatibility equations along IS - IT yields the pressure, $p(IT)$. With the external flow conditions known at IT, one can solve the boundary-layer equations to evaluate δ' and the boundary-layer mass flow, Ω , between B_2 and IT. Interpolation for Ω along the initial ray locates a new position for the streamline base IR. Finally,

$$\phi' = \tan^{-1}[(r_{IT} - r_{IR})/(z_{IT} - z_{IR})] \quad (47)$$

Thus, the interaction problem is reduced to the solution of equations of the form

$$\delta' - \delta = f(\delta, \phi, \pi, s) - \delta = 0 \quad (48a)$$

$$\phi' - \phi = g(\delta, \phi, \pi, s) - \phi = 0 \quad (48b)$$

where the functions f and g are known implicitly. Equations (48a) and (48b) are solved simultaneously by a Newton-Raphson procedure.

3.3.5 Body Discontinuities

If there is no boundary layer, the M.O.C. code will treat a body with one or more expansion corners and one sharp compression corner. The program will not follow the coalescence of Mach waves into a secondary shock.

At a discontinuity, the fluid dynamic variables are multivalued. For the finite reaction rate models, the composition is frozen for calculations at the discontinuity but is allowed to relax downstream.

3.3.5.1 Prandtl-Meyer Expansion

Since most of the calculation through an expansion fan is identical with the usual characteristics procedure, it is necessary only to set up the new ray directions, (subroutine RAYB), and to calculate the conditions at the singular point on the body, (subroutine PRANDTL). An iterative procedure is used to vary the temperature at the singularity until the Prandtl-Meyer angle computed from the Mach number matches the required turning angle.

3.3.5.2 Imbedded Shock

When a compression corner is present, the mesh is altered to that shown in Fig. 6. Below the secondary shock, the rays are normal to the flared surface; above the secondary shock, the rays are kept parallel to the corner ray, which is normal to the original body at that point. In the printed output, there is a double point at the secondary shock. If the identifying number (Section 3.2.2.1) assigned to the double point is greater than 1,000, it represents a streamline which was interpolated to better define the secondary shock but will not be continued into the secondary flow field.

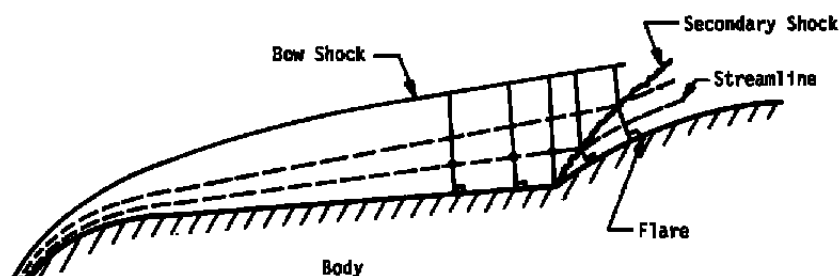


Figure 6. Computing mesh in presence of secondary shock.

Although the presence of the secondary shock complicates the logic of the program, no new techniques are required. The imbedded shock is located first and then treated as if it were the bow shock for computation of the secondary flow field. In the computation of the primary flow field, the front face of the secondary shock serves as a virtual body. The run will abort when the secondary shock intersects the primary bow wave.

The run will also be aborted with an explanatory message if an abrupt expansion corner (NCORN = 1) is encountered following a flare. However, a sharp compression corner may be followed by a smooth convex surface, as indicated in Fig. 6.

3.3.5.3 Downstream Continuation

If the continuation option has been selected (IBODY > NBODY), CUNIFLOW will add a tangent sphere to the prescribed body (Fig. 1) and switch to a constant pressure boundary condition. This pressure, PLIMIT, may be input. The default value for PLIMIT is the last body pressure calculated.

4.0 USING CUNIFLOW

Sections 2.0 and 3.0 have presented the physical models and some of the numerical techniques employed in the CUNIFLOW program. The application of the code will now be discussed. Sections 4.1 through 4.3 present the information necessary to set up the input

and to execute different types of CUNIFLOW calculations. Interpretation of the printed output is discussed in Section 4.4. Section 4.5 presents data relevant to the problem of defining the "operating envelope" for CUNIFLOW.

4.1 SYSTEM REQUIREMENTS

CUNIFLOW is written in the Cray version of FORTRAN77. The Cray extensions to the basic FORTRAN language include Namelist input and comments on the same line as a statement. The source code contains 5,704 statements filling 8,250 lines. The field length of the current version on the AEDC Cray X/MP 12 is approximately 250,000 64-bit words.

CUNIFLOW will run in single precision on a 32-bit machine, although with reduced reliability; that is, there are a number of places in the code where the reduced precision might occasionally lead into a wrong branch or cause a lack of convergence. However, the code was originally developed on IBM machinery and the default values for the convergence criteria have been set from years of experience on 32-bit machines.

Table 1 lists the assignments of the 10 I/O units referenced in the code.

Table 1. File Usage

<u>Unit</u>	<u>Use</u>
1	Input for a restart
2	Scratch file used in BRIDGE
3	Edge conditions for input to BLIMP
4	Input nonuniform free-stream conditions
5	System input
6	System output
7	Output for plotting
8	Input gas property and reaction rates
9	Output for a restart in nose region
10	Output for a restart in M.O.C. region

4.2 INPUT

Figure 7 is a schematic of typical input. The first record of the input file contains only one entry — the eight-character run number NRUN which will appear on each page of output. Enter NRUN with an "A" format. The second record contains an 80-character comment or description of the run, HEAD. If the word NONUNIFORM appears in the first ten positions (columns), the code will read the free-stream conditions from Unit 4 and bypass Namelist UPSTREAM.

The problem — free-stream conditions, body shape and thermochemical model — is specified through the Namelists UPSTREAM, OPTIONS, BODY, SHOCK, and CONTROL (Tables 2,4 - 7), which are read in subroutine BBIN, and SUPER, which is read in subroutine START.

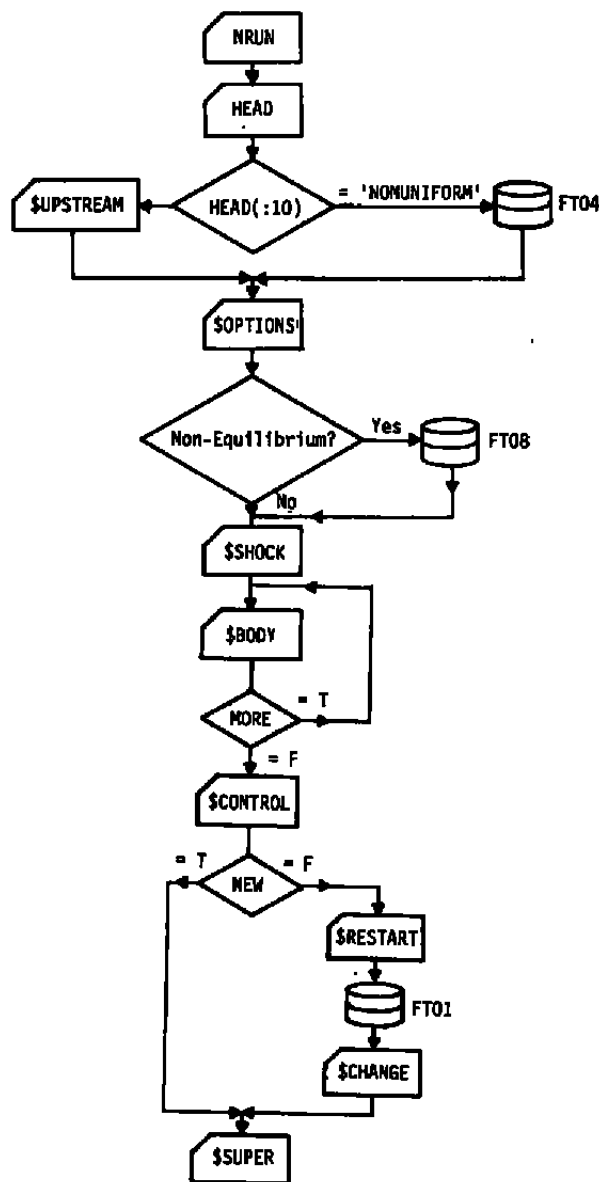


Figure 7. Input schematic.

The SHOCK and CONTROL namelists supply initial estimates for the shock shape parameters and values for convergence criteria, grid spacing, and print controls. Namelists RESTART

and CHANGE are read only when a run is to be restarted after some interruption. Namelist BODY is read once for each body segment.

Thermodynamic and reaction rate data are read from a formatted file assigned to Unit 8. For equilibrium cases, Unit 8 is referenced in subroutine RGAS; for nonequilibrium cases, Unit 8 is read in subroutine CHEMIN. Since the thermochemical data are rarely changed, it is advantageous to maintain a semi-permanent file which may be copied and edited as required. The equilibrium data file should never be touched.

4.2.1 Units

The user may choose the English engineering system (feet, slugs, seconds), the "cgs" system (centimeters, grams, seconds) or the SI system (meters, kilograms, seconds) for input. Composition data may be input as mole-fractions, as mass-fractions, or as moles per gram. Unless otherwise specified, "cgs" units and moles per gram are assumed. Output is in the cgs system.

Units for the thermochemical input data depend on the value of MODEL (cf., Appendix B).

4.2.2 Free-Stream Conditions

The flow field upstream of the bow shock is input through the Namelist UPSTREAM and/or a formatted file on Unit 4. The entries in UPSTREAM are defined in Table 2.

Table 2. Variables in Namelist UPSTREAM

<u>Item</u>	<u>Array Length</u>	<u>Default Value</u>	<u>Definition</u>
ALT		---	Geometric altitude
DENS		---	Free-stream density
PRES		---	Free-stream pressure
VEL		---	Centerline axial velocity
FRACTN	30	---	Chemical composition
EPS	2	---	EPS(I) is vibrational energy of species OSC(I). Use erg/gm or ft-lb/slug or J/kg
OSC	2		Name of oscillating species
TEMP		---	Free-stream temperature
SPEC	30	---	Names of species in free stream. Enclose in single quotes and left-adjust.

For a typical reentry problem, the only required entries are the velocity, VEL, and the altitude, ALT — if cgs units are acceptable.

If the airflow about a wind tunnel or ballistic range model is to be investigated, one should specify IUNIT = 1 and input values for the velocity VEL and for two of the three state variables PRES, TEMP, DENS. Also specify the units, the composition, and vibrational energies EPS if not in equilibrium. If units other than moles/gm are used, specify by selecting either 'MOLE' for mole-fraction or 'MASS' for mass-fraction as the value for FRAC. The species names are entered into the SPEC array, and the identifiers for species with nonequilibrium vibration are entered into the OSC array. These names are to be left-adjusted and enclosed in single quotes. The run will stop with a diagnostic message if the input species name has no match in the user-supplied thermochemical data.

4.2.3 Nonuniform Free Stream

If the free stream is spatially nonuniform, the comment card HEAD must begin with the keyword NONUNIFORM in column 1, IUNIT in OPTIONS namelist must equal 2, and a table of aerodynamic and composition variables as functions of position must be assigned to Unit 4. The position is specified in "cgs" units using the shock-based cylindrical coordinate system of Fig. 2. Composition is assumed to be in mole fractions.

The format of the free-stream file is shown in Table 3. The first few records define the size and contents of the file, including the names of the free-stream species and the two species which may be in vibrational nonequilibrium. The flow field is to be input with the radius increasing at each axial station. Centerline data must always be included.

Table 3. Input Format for Nonuniform Free-Stream Flow

<u>Card</u>	<u>Column</u>	<u>Format</u>	<u>Item</u>	<u>Description</u>
1	5	I5	NZZ	Number of axial stations
	10	I5	NRR	Number of radial stations
	15	I5	NSP	Number of species ≤ 30
	20	I5	NVIB	Number of nonequilibrium vibrators ≤ 2
2	1-4	A4	SPEC(1)	Name of free-stream species
	5-8	A4	SPEC(2)	Name of free-stream species
	9	---	---	---
	---	A4	SPEC(NSP)	Name of free-stream species

Table 3. Concluded

<u>Card</u>	<u>Column</u>	<u>Format</u>	<u>Item</u>	<u>Description</u>	
2 (Contd.)	---	A4	OSC(1)	Name of vibrator	
	---	---	OSC(NVIB)	Name of vibrator	
3	1-10	E10.4	ZSPOT	Z coordinate from shock vertex	
	11-21	E10.4	RSPOT	R coordinate from centerline	
	21-30	E10.4	VINF	Radial velocity component	
	31-40	E10.4	PRES	Pressure, dyne/cm ²	
	41-50	E10.4	DENS	Density, gm/cm ³	
	51-60	E10.4	UINF	Axial velocity component, cm/sec	
	61-70	E10.4	FRACTN(1)	Mole-fraction of species 1	
	71-80	E10.4	FRACTN(2)	Mole-fraction of species 2	
			---	---	
			E10.4	FRACTN(NSP)	Mole-fraction of species NSP
		E10.4	EPSINF(1)	Vibrational energy, erg/gm	
		E10.4	EPSINF(NVIB)	Vibrational energy, erg/gm	

Notes:

1. Card 2 is read only if NSP > 0.
2. NSP is number of species in free stream, not number in model.
3. VINF must be zero on the centerline.
4. For each axial station, NRR sets of card 3 are needed. The centerline (RSPOT = 0) must be included at each axial station.

4.2.4 Namelist OPTIONS

Table 4 defines the variables in Namelist OPTIONS. The options for including sharp corners and for the downstream continuation will be discussed in connection with Namelist SUPER (Table 8).

Table 4. Variables in Namelist OPTIONS

<u>Item</u>	<u>Type</u>	<u>Default</u>	<u>Function</u>
FRAC	Character	'M/GM'	Composition unit. Choose 'MASS' or 'MOLE' or 'M/GM'
INAFT	Integer	1	0 Do only nose region 1 Do both regions 2 Do only aft region

Table 4. Concluded

<u>Item</u>	<u>Type</u>	<u>Default</u>	<u>Function</u>
INBLR	Integer	0	0 No viscous interaction
			1 Include viscous interaction
INDIM	Integer	1	0 Planar (2-D) flow
			1 Axisymmetric flow
IUNIT	Integer	0	0 standard atmosphere; supply only VEL and ALT
			1 Uniform free stream; supply composition and any 2 state variables
			2 Nonuniform free stream. Use Unit 4
MODEL	Integer	0	0 Nonequilibrium model Sec. 2.2.1
			1 Perfect gas Sec. 2.2.2
			2 Equilibrium air Sec. 2.2.3
			3 Nonequilibrium Sec. 2.2.4
			4 Nonequilibrium Sec. 2.2.5
NEW	Logical	"T"	Set NEW = "F" for a restart
*NVIB	Integer	0	Number of nonequilibrium vibrators, NVIB ≤ 2
UNIT	Character	'CGS'	Input unit system. Use 'ENG' for ft-slug-sec system; 'CGS' for cm-gm-sec system; 'MKS' for SI system

*NVIB = 0 unless MODEL = 0

4.2.5 Namelist SHOCK

Table 5 defines the three initial shock parameters input through Namelist SHOCK. No default values are provided. The initial estimate for the shock radius of curvature RSHP must be non-zero and in the units specified in UPSTREAM. Initial non-zero values for the other two parameters, S1 and S1P, are useful but not essential. A plot of shock radii RSH normalized by the nose radius for a number of converged nonequilibrium solutions is shown in Fig. 8. The significance of the parameter $\rho_{\infty} R_N$ is discussed in Section 4.5. Table E-1 of Appendix E presents more detail as well as the corresponding values of S1 and S1P.

For equilibrium air (MODEL = 2), the tabulated results of Inouye (Ref. 32) are helpful. (S1P corresponds to Inouye's A7 and S1 to $2A7/\sqrt{(M^2_{\infty} - 1)}$). The equilibrium air shock parameter values are also reasonable estimates for nonequilibrium. For flow conditions not

encompassed by the tables of Ref. 32, use $RSHP = 1.1 \times R_N$, $S1P \approx 0.1$ and $S1 \approx 0.01$ where R_N is the centerline radius of curvature of the nose.

Table 5. Parameters in Namelist SHOCK

<u>Item</u>	<u>Default</u>	<u>Definition</u>
RSHP	--	Dimensional radius of curvature at centerline.
S1P	--	Coefficient of r^4 in Eq. (42)
S1	--	Coefficient of r^3 in denominator of Eq. (42)

An initial shock which is too blunt (too open) for the flow conditions will occasionally cause a run to abort with diagnostic messages indicating negative species or temperatures on the higher numbered rays. When this is the case, either make the initial shock "tighter" (by decreasing RSHP or increasing S1P) or else decrease the ray spacing DELX.

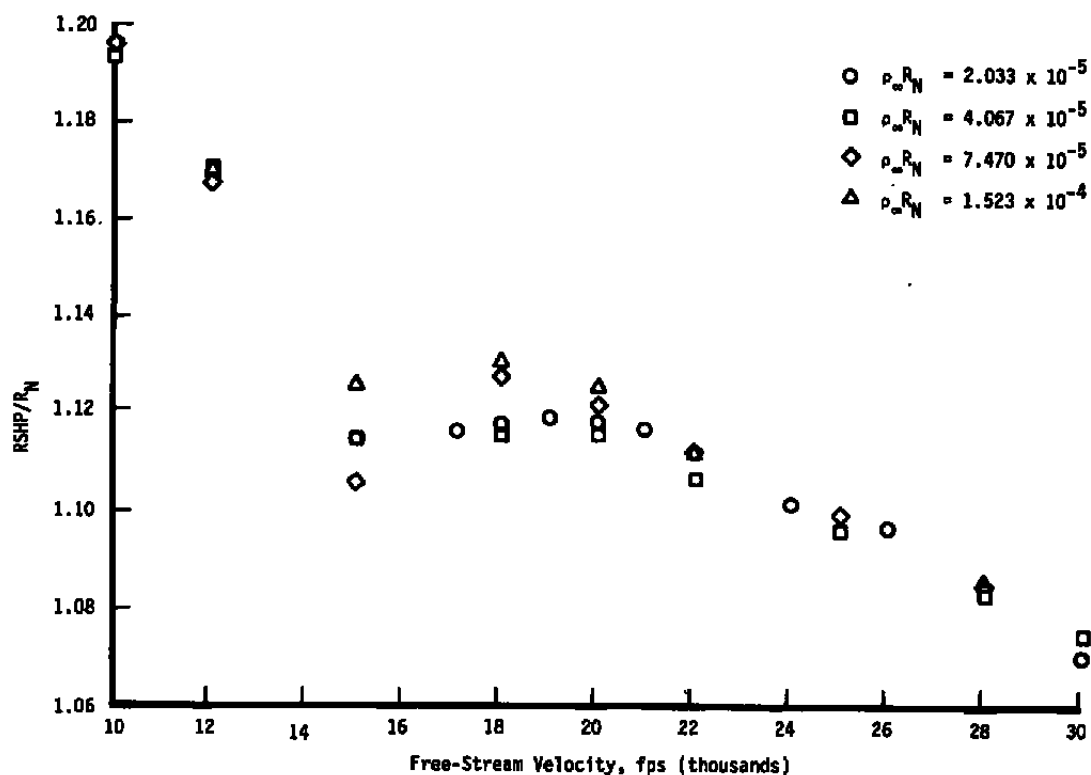


Figure 8. Converged values for radius of curvature of nonequilibrium shock.

4.2.6 Namelist BODY

Table 6 defines the entries in Namelist BODY:

Table 6. Variables in Namelist BODY

<u>Variable</u>	<u>Default</u>	<u>Description</u>
C0	---	C_0 in Eq. (49)
C1	---	---
C2	---	---
C3	---	---
C4	---	C_4 in Eq. (49)
MORE	"F"	If "T" another segment follows. Read BODY again
REXP	---	Exponent "P" of radius in Eq. (49)
RJUNC	---	Radius at junction point " r_j ", Eq. (49)
ZEXP	---	Exponent of axial coordinate "q", Eq. (49)
ZJUNC	---	Axial coordinate of junction point between body segments. " z_j " in Eq. (49)

The body is assumed to consist of NBDY segments ($NBDY \leq 6$). Each segment is described by an equation of the form

$$(r - r_j)^P = (z - z_j)^q [C_0 + C_1(z - z_j) + C_2(z - z_j)^2 \dots + C_4(z - z_j)^4] \quad (49)$$

where z and z_j are measured from the nose of the body. The code will adjust to the shock-based coordinates used internally. The first equation must represent a sphere, i.e.,

$$r^2 = 2zR - z^2 \quad (50)$$

At the junction points z_j, r_j the radius, r , must be continuous.

BODY is read once for each segment. The logical flag MORE is used to indicate that another segment follows. The segment equations are input in dimensional form using the system specified by UNIT (Table 2).

4.2.7 Namelist CONTROL

Table 7 defines the entries in Namelist CONTROL:

Table 7. Entries in Namelist CONTROL

<u>Item</u>	<u>Default</u>	<u>Definition</u>
DELMAX	5.0×10^{-3}	Maximum step in y-direction
DELMIN	1.0×10^{-6}	Minimum step in y-direction
DELX	0.04	Ray spacing
ERROR	1.0×10^{-6}	Convergence criterion for all iterations except shock
GAMTST	1.0×10^{-7}	Minimum mole-fraction for inclusion in source term
IPRNT	0	If non-zero, print status line every IPRNT steps
ISW6	0	Print diagnostic information if non-zero
JOIN	NXDIV-7	Junction ray to M.O.C. code
METHOD	6	Use 4, 6, 8, 10 to select integration algorithm
NBSIT	1	Number of bow shock iterations
NOUT	15	Number of points saved for M.O.C. code; also number of full printout stations
NXDIV	20	Number of DELX increments ≤ 21
PSIRAT	0.10	Flux ratio to stop integration
RMSTST	5.0×10^{-4}	Convergence criterion for shock iteration
SKAP	0.35	Damping factor in Eq. (46)
SLAM	-0.50	Damping factor in Eq. (46)
TESTM	1.10	Minimum Mach number on junction ray
TIME	28	Maximum run time in seconds
TTEST	0.15	Maximum relative change in temperature over a y-step
X0	0.04	Position of first non-axis ray

The default values which are provided for the parameters in the CONTROL namelist are adequate for nonequilibrium problems in the central part of the operating envelope, Section 4.5. The value for TIME is based on experience with the Cray X/MP12 and is consistent with NBSIT = 1, a chemical model with 10 reactions and a body length of approximately 15 nose radii. A single iteration of the bow shock shape is rarely sufficient unless the problem amounts to a small perturbation of an existing solution with accurately known shock parameters.

The shock iteration process is regulated by the controls RMSTST, SKAP, SLAM, and PSIRAT, as well as NBSIT. The default value for RMSTST is probably too lax since root-mean-square deviations between desired and calculated body points $\leq 10^{-4}$ are readily obtained. The control for ending the integration of the flow equations is PSIRAT, which is defaulted to 0.1 to avoid the region of "stiff" chemistry near the body surface. If inspection of the status reports indicates few problems near the surface, PSIRAT might well be decreased

to 0.05 or even 0.03 to increase the precision of the shock iteration process. The convergence rate of the shock iteration process is affected by the damping factor SKAP which has been set conservatively. If RMSDEV increases or oscillates from iteration to iteration, decrease SKAP. Shock convergence has been obtained with SKAP as large as 0.6. There is no reason to change SLAM unless MAXDEV begins to increase.

The forebody computational grid is regulated by the controls DELMAX, DELMIN, DELX, NXDIV, and X0. The grid consists of NXDIV evenly spaced rays normal to the shock. The spacing between the rays is DELX and the first ray is located at X0. If $X0 \leq DELX$, the axis will be included in the mesh and NXDIV will be increased by 4 to account for the axis and the three "virtual" rays which allow the use of the seven-point differentiation algorithm at the axis. One might choose $X0 > DELX$ in a situation where the species conservation equations were very stiff near the stagnation point and interest was in the afterbody flow field.

The marching step in the "y" direction is internally controlled between the limits DELMIN and DELMAX. At the shock, CUNIFLOW will try an initial integration step

$$y = 100 \times DELMIN$$

and will halve this value four times or until the integration is successful. The default value for DELMIN is adequate for most equilibrium and many nonequilibrium problems, but a smaller value will be required for exceptionally strong shocks or stiff chemistry. Too small a value for DELMIN may cause unacceptable run times. Since the nondimensional shock layer thickness is ≈ 0.05 , the default value for DELMAX is probably the largest step which will give adequate flow-field resolution.

The integration algorithm is selected by METHOD which may assume the values 4, 6, 8, 10. The stability of the Lomax procedure and the number of derivative evaluations increase with METHOD. For equilibrium air problems, the standard Runge-Kutta algorithm, METHOD = 4, works well. For many nonequilibrium problems it is necessary to use METHOD = 10.

GAMTST represents the smallest mole-fraction which will be used in computing the source terms in the species conservation equations. Also, if $\gamma_i < GAMTST$, the code sets $d\gamma_i/dy = \max(d\gamma_i/dy, 0)$. Note that γ_i is left unchanged. The foregoing GAMTST artifice is useful where the stream contains small amounts of some species such as O_2 , which will continue to dissociate at the prevailing temperatures such as those behind a strong shock or near the stagnation point. Since GAMTST perturbs the composition, the minimum value of GAMTST which will allow the run to finish should be selected. Trouble will also be experienced if $0 < GAMTST < \text{machine zero}$ ($\sim 10^{-14}$ for Cray).

Output from the nose region part of the code is controlled by IPRNT, NOUT, and ISW6. If IPRNT is non-zero, a one-line status report is printed every IPRNT successful integration steps. A non-zero value for ISW6 produces diagnostic information from certain subroutines. The amount of data can be overwhelming so that care should be taken when this option is used. NOUT is the number of records to be printed and also the number of points on the starting line for the Method-of-Characteristics (afterbody) code. $NOUT < NMAX$, where NMAX (see Table 8) is the maximum number of points per afterbody ray.

If the minimum Mach number on the junction ray (designated by ray index $M = JOIN$) $< TESTM$, the nose region code will increase DELX and X0 on the next shock iteration. The default value for TESTM is as low as is safe, typically 1.10. The maximum allowable value for JOIN is NXDIV-6. The default values for JOIN, X0, and DELX put the junction line at 40 to 45 deg from the axis.

4.2.8 Input to the Hyperbolic Flow Code

The controls for the Method-of-Characteristics code are input through Namelist SUPER, which is read by subroutine START. The initial data surface is usually read from a file on Unit 2, but if INAFT = 2 (Table 4), the starting line is read from the system input (Unit 5). The entries in Namelist SUPER are defined in Table 8.

Table 8. Controls in Namelist SUPER

<u>Item</u>	<u>Default</u>	<u>Definition</u>
CSST	1.0	Controls streamline spacing at shock
IBODY	0	Downstream continuation (Sec. 2.1) if IBODY \geq number of input body segments
IPOLY	1	Current body equation
ION	1	Plasma properties calculated if ION > 0
MAXRAY	0	Maximum number of rays to be calculated
METHOD	6	Algorithm order. Will equal blunt body value unless otherwise specified
MODRAY	1	Print ray if MOD (NRAY,MODRAY) = NRAOUT
NRAOUT	0	Print ray if MOD (NRAY,MODRAY) = NRAOUT
NCHI	0	ERROR = 10^{NCHI} if NCHI not = 0
NCORN(6)	6×0	0 This junction is smooth 1 This junction is expansion corner 2 This junction is compression corner
NFIL1	1	Write restart record every NFIL1 rays
NITER	10	Maximum number of iterations
NMAX	35	Maximum number of points on ray. $NMAX \leq 35$

Table 8. Concluded

<u>Item</u>	<u>Default</u>	<u>Definition</u>
NMOD4	1	Print diagnostics from certain subroutines if
NREM4	2	MOD(NRAY,NMOD4) = NREM4
NMOD6	1	Print diagnostics from certain routines if
NREM6	2	MOD(NRAY,NMOD6) = NREM6
NPRROT	1	Number of rays in Prandtl-Meyer expansion
NROTAT	4	Number of rays used for initialization
PLIMIT	---	Fixed boundary pressure for continuation option
TIME	---	Time limit default = value from blunt body code
TSTGAM	GAMTST	Same role as GAMTST
ZMAX	---	Axial station to end calculation
ZETAMAX	0.8	Safety factor in ray spacing algorithm. ZETAMAX < 1.0

The spacing between data surfaces grows as the calculation progresses downstream because the local Mach number increases. The rate of growth is regulated by ZETAMX but is also affected by the streamline spacing. A streamline is added at the shock when the distance between the shock point and the first streamline below the shock exceeds CSST times the separation between that streamline and the next lower. When the number of streamlines exceeds NMAX, approximately half of the streamlines are removed from the grid with the effect that the ray spacing is approximately doubled from that station downstream. The initial ray spacing is also affected by NOUT, the number of points on the initial line. Halving ZETAMX triples, at least, the number of rays and the CPU time for a run. The practical limits for ZETAMX are roughly $0.2 \leq ZETAMX \leq 0.9$. The default value CSST = 1.0 has proven to be optimum for 80 percent of the calculations made with CUNIFLOW. Experience has shown that any adjustments should be kept in the range $0.9 \leq CSST \leq 1.2$.

The maximum value for NMAX is NY - 15; NY is set by PARAMETER statements in the source program. The user may specify either MAXRAY, the maximum number of rays to be calculated, or the final axial station ZMAX, but not both. ZMAX is entered as a dimensional number in the same units as RSHP. If both ZMAX and MAXRAY are entered, the code will use MAXRAY.

The default value for MODRAY, the number of rays to skip between printouts, is less than desirable in most cases; MODRAY = 10 is frequently fine enough. The data on the

initial ray, on ray NROTAT, on rays at each corner, and on rays where streamlines are dropped are always printed. Default values for NMOD6, NREM6, NMOD4, and NREM4 have been selected to prevent the printing of the auxiliary output from each iteration at each point, since the amount of this output would be overwhelming.

To invoke the downstream continuation option, the user must input a nonzero value for PLIMIT and set IBODY equal to the number of input body equations. If IBODY is greater than the number of equations, the code will construct an aft-facing tangent sphere as shown in Fig. 1. Whether input or internally created, segment IBODY serves only to define the ray geometry.

4.2.9 Restarting

The blunt body code writes a restart record on Unit 9 after each successful step. The current number of records is printed every IPRNT steps as part of the status report and also when the body is reached. Unit 9 is rewound at the beginning of each shock iteration. The M.O.C. code writes a restart record to Unit 10 and prints the number of records after each NFIL1 rays.

To restart in either code segment, assign the appropriate file to Unit 1, set NEW = .FALSE. in Namelist OPTIONS, and add Namelists RESTART and CHANGE as shown in Fig. 7. Table 9 defines the entries in RESTART:

Table 9. Entries in Namelist RESTART

<u>Entry</u>	<u>Default</u>	<u>Definition</u>
NRUN	Old run ident.	Run identifier can be changed
ITAPE	0	1-Restarts in blunt body code 2-Restarts in M.O.C. code
NRCORD	0	Resume computation after NRCORD

There is no record on either Unit 9 or 10 with NRCORD = 0. It is always wise to set NRCORD less than the maximum value printed in the status report.

Most of the blunt body controls and all of the M.O.C. controls may be changed during a restart. Also, any part of the body definition which has not been used may be altered safely. Table 10 lists the blunt-body controls which may be changed.

Table 10. Namelist CHANGE

<u>Entry</u>	<u>Default</u>	<u>Definition</u>
DELMAX	5.0×10^{-3}	Maximum step in y-direction
DELMIN	1.0×10^{-6}	Minimum step in y-direction
ERROR	1.0×10^{-6}	Convergence criterion for all iterations except shock
GAMTST	1.0×10^{-7}	Minimum mole-fraction for inclusion in source term
INAFT	1	Change 1 to 0 or 0 to 1 if desired; do not use INAFT = 2 on restart
IPRNT	0	If non-zero, print status line every IPRNT steps
ISW6	0	Print diagnostic info if non-zero
JOIN	NXDIV-7	Junction ray to M.O.C. code
METHOD	6	Use 4, 6, 8, 10 to select integration algorithm
NBSIT	1	Number of bow shock iterations
NOUT	15	Number of points saved for M.O.C. code; also number of full printout stations
PSIRAT	0.10	Flux ratio to stop integration
RMSTST	5.0×10^{-4}	Convergence criterion for shock iteration
SKAP	0.35	Damping factor in Eq. (46)
SLAM	-0.50	Damping factor in Eq. (46)
TESTM	1.10	Minimum Mach number on junction ray
TIME	28	Maximum run time in seconds
TTEST	0.15	Maximum relative change in temperature over a y-step

4.3 OUTPUT

This section describes the output produced during the course of a completely successful run. Examples are contained in Appendix F. Diagnostic messages are interpreted in Section 4.4.

The first page begins with a largely self-explanatory "echo" of the input. Units have been converted to the cgs system and concentrations are expressed in moles per gram. Only the centerline values of the free-stream parameters are printed. XLMBDA is the dimensionless combination $\bar{U}_\infty^2 \bar{M}_\infty / \mathcal{R} \bar{T}_\infty$ which serves as an inverse gas constant in the nondimensionalized equations. HINF is the dimensionless total enthalpy and BIGAM is the isentropic exponent in the free stream.

The quantities AK(I), BK(I), CK(I), and DK(I) printed in connection with each reaction are the rate parameters defined in Eq. (21). The reaction type is defined by Eq. (22). The matrix elements A_{ik} couple the i^{th} reaction to the k^{th} oscillator when nonequilibrium vibration is specified.

4.3.1 Blunt Body Output

The blunt body output begins with a tabulation of the current shock parameters and geometry. Since this table is printed before the optional rearrangement for including the axis of symmetry is performed, the first ray ($M = 1$) will be off the centerline by $X0$. The shock angle, $SIGMA$, is in radians, but the local curvature $CURV$ has been normalized by its centerline value $1.0/RSHP$.

As the computation marches inward, a progress message is printed every $IPRNT$ steps. The information presented consists of the number of records on Unit 9 ($NRCORD$); the number of failures ($FLOP - 1$); the index of the lowest numbered ray still in the computing grid, $MINRAY$; the last three y -values, and the last y -increment. Since the dimensionless nonequilibrium shock standoff distance is of the order of 0.05 on the stagnation line, the last y printed gives a crude estimate of relative position within the shock layer.

If $ISW6 = 2$, the quantities involved in the shock iteration process (Section 3.1.5) are printed for each ray; otherwise, only the rms deviation between extrapolated and desired body points, the flow-angle error at the junction point, the normalized stagnation line standoff distance ($ZSTAG$), and the current and proposed shock parameters are output.

When convergence has been obtained or the allowable number of global iterations has been performed, the nondimensional body coordinates ZB , RB , the body angle in radians, the boundary-layer thickness, and boundary-layer mass flux are printed.

Each page of the blunt body flow-field data corresponds to a constant y value which is printed in the upper right corner. If the stagnation line was included in the computation, it is printed as ray number 4. All data are dimensional except for the Mach number, the equilibrium indicator, labeled $AVER.CHI$, and the ratio of the mass flux across the ray between the given y -station and the body to the mass flux into the shock between the ray and the stagnation line. The equilibrium indicator $AVER.CHI$ is defined as $[\sum_i \chi_i]/N_R$ where χ_i is defined by Eq. (24). The flow angle is defined as the angle (in degrees) between the z -axis and the resultant velocity $VTOT$.

The flow-field printout includes only rays $MINRAY$ through $JOIN$. The data on rays $JOIN + 1$ through $NXDIV$ are of lesser quality than the data on the lower numbered rays because of the inadequacies of the x -differentiation algorithm, and will be replaced with $M.O.C.$ data. As the integration on a given ray reaches the body surface or boundary-layer edge, the data on that ray stop changing and the ray is dropped from the printout to prevent confusion.

Following the printout of the integrated flow field, the dimensionless body shape parameters corrected for the latest shock radius are printed before and after the adjustment process described in Section 3.2 is performed. The last page of the blunt-body printout represents

the results of a linear extrapolation of all flow-field data to the body surface or boundary-layer edge.

4.3.2 Plotting File

At each y-station, the dimensional flow-field properties are written in unformatted form to a file assigned to Unit 7. The first record contains, in order, MINRAY, JOIN, NVIB, and CSIG, where $CSIG(N) = \cos(\sigma_n)$. Each of the following $JOIN - MINRAY + 1$ records contains the data for a ray. The data entries are z,r,P,T,RHO,XMW,VTOT, flow angle, total enthalpy, entropy, average chi, electron density, Mach number, flux ratio, specific radiation rate, mass flux, and species mole-mass ratios (mole/gm). Note that the entries are arranged in the same order as on the printout.

4.3.3 M.O.C. Output

Printout from the Method-of-Characteristics code begins with an echo of the input Namelist SUPER. ZMAX and PLIMIT will be dimensional (cgs units). The principal control parameters are then tabulated in nondimensional form.

The following output data are arranged so that each of the selected rays starts a new page. The first block labeled with $NPT = 0$ is either at the body surface or at the boundary-layer edge, which is not, of course, a streamline. The last block presents the flow data immediately behind the shock. The other blocks present data on successive streamlines numbered from the body outward. A streamline keeps the same identification number from ray to ray. Occasionally, the growing boundary layer will "swallow" a streamline, and the corresponding identification number will disappear. From time to time, alternate streamlines are removed from the grid to keep the number of points within bounds; their identification numbers are not reused. Two adjacent blocks with the same identification and the same coordinates represent points on an imbedded shock. An "I.D." number greater than 1,000 represents an auxiliary shock point which will not start a new streamline. Note that the angle of the imbedded shock is printed as the last item on the previous page, Appendix F.

With the exception of the Mach number and the equilibrium indicator, the printed data are dimensional. The plasma frequency is defined as $\Omega_p = (56.4104 \times 10^3) \sqrt{n_e}$ radians/sec. The electrical conductivity of the plasma is stated in mho/m and is calculated under the assumption that the electron temperature is equal to $T_{vib}(N_2)$ if $NVIB > 0$, and to T otherwise.

4.3.4 Edge Conditions File

For interfacing with BLIMP, the blunt body and the M.O.C. parts of the code write an unformatted file of dimensional boundary-layer edge data to Unit 3 (Table 1). The entries in each record are, in order arc, radius, pressure, entropy, and concentrations, where arc

is the surface distance from the nose vertex. Both the surface distance and the body radius are stated in feet. Species concentrations are stated in mass fractions and the entropy in calories/gm°K. Pressure is in dyne/cm².

4.4 DIAGNOSTICS

Diagnostic messages, which are sometimes helpful, are printed by CUNIFLOW whenever the computation departs from the usual course.

4.4.1 Non-Fatal Conditions

In the blunt body part of the code, an integration step is repeated with a smaller y-increment if any dependent variable goes negative or if the relative change in temperature over the interval exceeds the input constant TTEST. When this occurs, either of the following messages is printed:

B2(---) NEGATIVE ON RAY---, RUNGE-KUTTA STEP---, Y=---, DELY=---
 or
 T TEST FAILED ON RAY---, RUNGE-KUTTA STEP---, Y=---, DELY=---

The elements of the B2 array are defined in Table 11 below.

Table 11. Interpretation of the B2 Array

J	1	2	3	4	5	6	7	36
VARIABLE	ϵ_1	ϵ_2	v	p	q	u	γ_1	γ_{30}

The information in this output is sometimes useful in understanding the chemical processes taking place in the shock layer or in assessing the effects of a tentative change in the thermochemical model. As the step-size will be cut several times before the run finally aborts, a study of the dynamic output might reveal insidious input errors such as misplaced decimals. It must be emphasized that step cutting is a normal part of a nonequilibrium run.

Another nonfatal diagnostic is:

ITERATION IN SUBROUTINE _____ IS NOT CONVERGING.

To interpret the accompanying data, it is necessary to find the call to CNVRGE in the named subroutine. This message is printed whenever the local iteration counter is \geq NITER-3. CNVRGE is an entry in subroutine DIGNOS.

A message which may or may not indicate a physically real situation is

“SHOCK LAYER FULLY VISCOUS”

which means that the calculated mass flux through the boundary layer at some station is greater than the flux into the shock. When this condition is detected, the shock shape iteration is abandoned and the calculation proceeds as if the shock shape were converged. The user should review the input data carefully, paying special attention to ALT, DENS, and TWALL, and the body nose radius. An RSHP which is much too small for the body could be the culprit. If TWALL is much too low, the density within the boundary layer will be too high.

Programmed stops are produced by a call to either TRUBEL or PAUSE. TRUBEL prints the location of the call before stopping. PAUSE prints the location of the call and then calls POINT to print the data at all locations on the ray, including those which are reserved for special storage and, consequently, do not appear in the usual output. The first two blocks give interpolated data at the bases IR and IS of the two characteristics (Fig. 4); the third block contains data at the starting point of the streamline integration. This will differ from the point on the previous ray only if the integration step size has been cut. The next blocks present data at the three successive shock points and the three successive boundary-layer or body points. The following blocks, up to the first out-of-sequence change in the point number, present the data at the new points. The remaining blocks present the data on the previous ray. When the trouble occurs while calculating the flow over a flare, the diagnostic output becomes somewhat confusing because of the repeated transfer of data in and out of special storage. The key to interpretation in this case is to remember that data on the downstream side of a shock are always stored in rows 4-6 of the data arrays. Information on the upstream side of the imbedded shock will be stored in rows 5-9.

4.4.2 Fatal Conditions

Frequently occurring error messages are discussed below.

The following messages indicate that the time limit has been exceeded:

ERROR AT STATEMENT 1201 OF ROUTINE BREGN

or

ERROR AT STATEMENT 1601 OF ROUTINE BREGN

“Timing out” in BSHCK on the first iteration means that something is terribly wrong with the input and/or program. Excessive time in BREGN may be attributable to bad input; check free-stream density, velocity, temperature, and composition. Excessive time may also be caused by free-stream compositions containing small amounts of some substance which would tend to further dissociate at the high temperatures behind the shock. For example, if the free stream were partially dissociated air, the step sizes needed to keep the O₂ mole fraction non-negative behind the shock may be very small. A possible cure for this condition would be to increase GAMTST. Sometimes it is necessary to neglect some insignificant free-stream species. If the

input is correct and the calculation has made significant progress, use the restart procedure and possibly change TIME, DELMIN.

ERROR AT STATEMENT 1208 SUBROUTINE LINK 2:

“LINK 2” is the former name of BREGN. The significance of this statement is that the marching procedure could not get started. Check the input, reduce the initial step size by reducing DELMIN, and/or increase METHOD.

ERROR AT STATEMENT 1425 OF SUBROUTINE LINK 2:

Significance of this statement is that continuation of the marching procedure requires a step-size less than DELMIN. A clue to the cause may possibly be obtained from the dynamic dumps. If the input is satisfactory, change METHOD and/or DELMIN and restart at a station well upstream of the point where the catastrophic instability occurred.

ERROR AT STATEMENT 30 OF SUBROUTINE BDYFCT:

A value of ZJUNC < 0.0 was input for first body segment, or PSIRAT ~ 1.0 was input, or RSHP < 0 was input.

ERROR AT STATEMENT 90 OF SUBROUTINE INTR:

The significance of this message is that the intersection of a characteristic with the previous ray is not within the range of points saved for interpolation. The coordinates of the offending point will be in either the second or first block of the following output. The third block is the base of the streamline from which one can determine the “troubled” process. Most appearances of this message are caused by a discontinuity at the junction between two body equations. If the message appears while the nose is still being calculated, it is possible that the junction Mach number, TESTM, is too small, that the computational mesh is becoming too skewed because the flow direction is steeply inclined with respect to the ray direction, or that there are not enough points on the starting line. To fix these conditions, rerun the nose portion of the code with a larger TESTM and smaller DELMAX. Also try a smaller value for ZETAMX. If the error occurs well back on the afterbody, it is probably attributable to a divergent iteration process somewhere and possibly may be fixed by decreasing the step-size (adjusting ZETAMX, CSST, and/or NMAX).

ERROR AT STATEMENT 11 OF SUBROUTINE CFFCNT:

The significance of this error statement is that the Mach number < 1.0. If the message occurs early in the M.O.C. calculation, it is probably because of an inadequate starting line from the nose code. The statement may, of course, correspond to reality if the flare angle is too steep.

4.5 OPERATING ENVELOPE

Figure 9 is a plot of the CPU time required to execute three shock iterations, including the boundary-layer displacement procedure. The shock iteration time is controlled by the number of integration failures with the accompanying step repetitions and step-size cutting and, therefore, is affected somewhat by the step-size controls, by the input shock parameters, the integration method, and the thermochemical model. The same thermochemical model (MODEL = 0, eight species, ten reactions, and equilibrium vibration) and control settings (METHOD = 10, DELMIN = 10^{-9} , and GAMTST = 10^{-7}) were used for all the calculations. The shock damping factor, SKAP, was increased from 0.35 to 0.50 for the high-velocity cases to secure better convergence. The procedure for constructing the graph was to start at 15,000 ft/sec and build outwards in both directions using as initial shock parameters for each case the final (converged) values from the previous calculation.

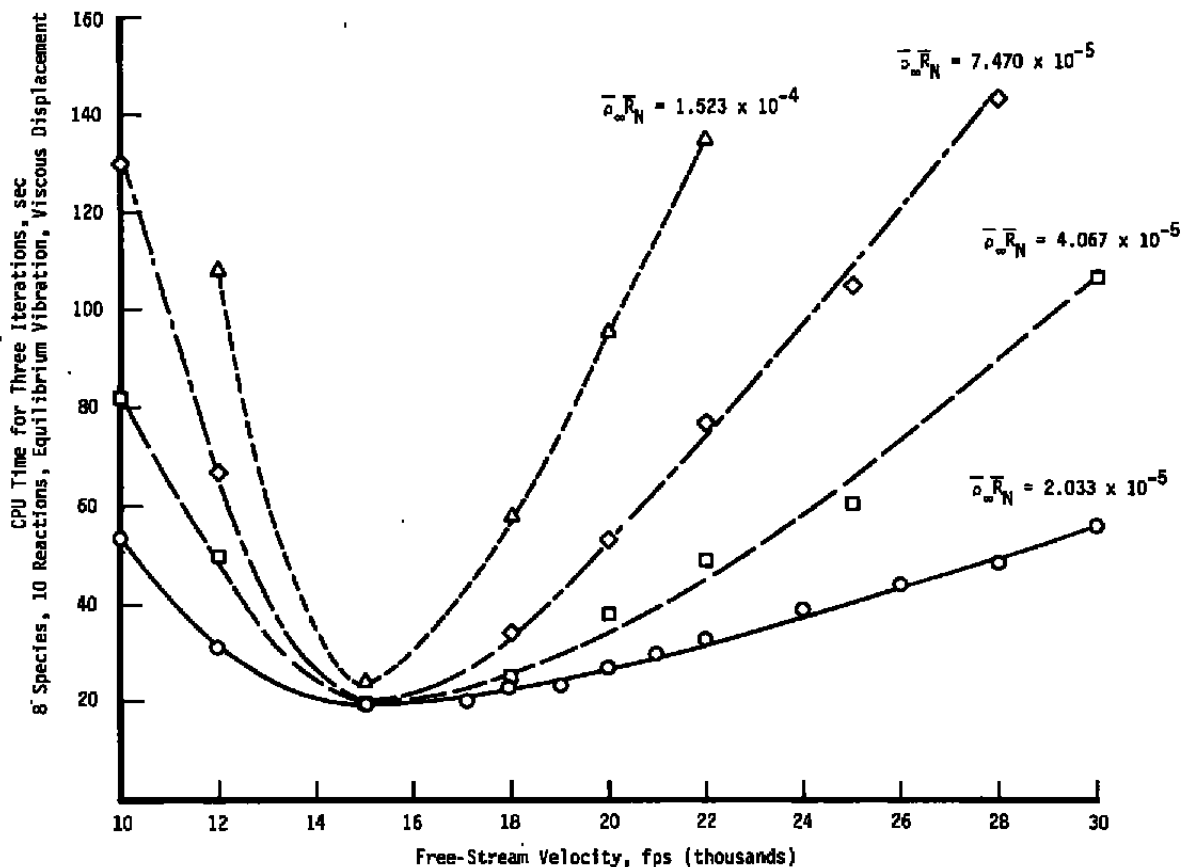


Figure 9. Effect of free-stream conditions on CPU-time for nonequilibrium blunt body solutions.

The increase in CPU time at low speed was caused by the presence of a minute amount of nitrogen atom ($\gamma = 1.8 \times 10^{-9}$) which was being consumed by the reaction, $N + O$

= $\text{NO}^+ + \bar{e}$, faster than it was being produced and could have been forestalled by choosing a larger value for GAMTST, such as 10^{-6} .

The increase at high speed arose from the virtually complete dissociation of O_2 near the stagnation point, where the flow is nearly in equilibrium ($\text{AVER.CHI} = 3.3 \times 10^{-5}$). In contrast, at the lowest speed, the flow is far from equilibrium ($\text{AVER.CHI} = 0.98$) at the boundary-layer edge. This increase illustrates the difficulty in using a nonequilibrium code in near equilibrium conditions.

The curves of Fig. 9 are labeled with the parameter, $\bar{\rho}_\infty \bar{R}_N$. It has been shown (Ref. 33) that the product of the free-stream density with a characteristic body length constitutes a simple and exact similitude for nonequilibrium processes which involve two-body collisions only. Since the full chemistry of high-temperature air involves the three-body recombinations of oxygen, nitrogen, and nitric oxide, binary scaling cannot apply exactly to air, especially at lower altitudes where the flow is close to equilibrium, or over the afterbody where the flow is recombining.

Figure 10 is a plot of the scaling factor against velocity for a number of nonequilibrium solutions which have been obtained over the years using various versions of CUNIFLOW and various reaction sets. It is probably safe to assume that CUNIFLOW will run for free-stream conditions which can be plotted on the figure below the indicated upper boundary. Near the upper boundary it will probably be necessary to include both radiation and thermal nonequilibrium options. For very blunt bodies or bodies with large cone angles, the base radius might be a more appropriate characteristic length than the radius of curvature of the nose.

5.0 CONCLUDING REMARKS

The structure and use of the CUNIFLOW code has been discussed. CUNIFLOW is a very fast, robust, reacting flow code which has become the standard method at AEDC for computing the nonequilibrium flow about axisymmetric or two-dimensional bodies. By combining CUNIFLOW with the well-known BLIMP boundary-layer code, it has been possible to obtain nonequilibrium solutions at low-altitude, high-speed conditions where other external flow codes will not converge. Furthermore, it is possible to make computations for flow media other than air and for nonuniform upstream conditions. The economy and robustness of the code are illustrated by plots (Section 4.5) of CPU time as a function of velocity and binary scaling parameters.

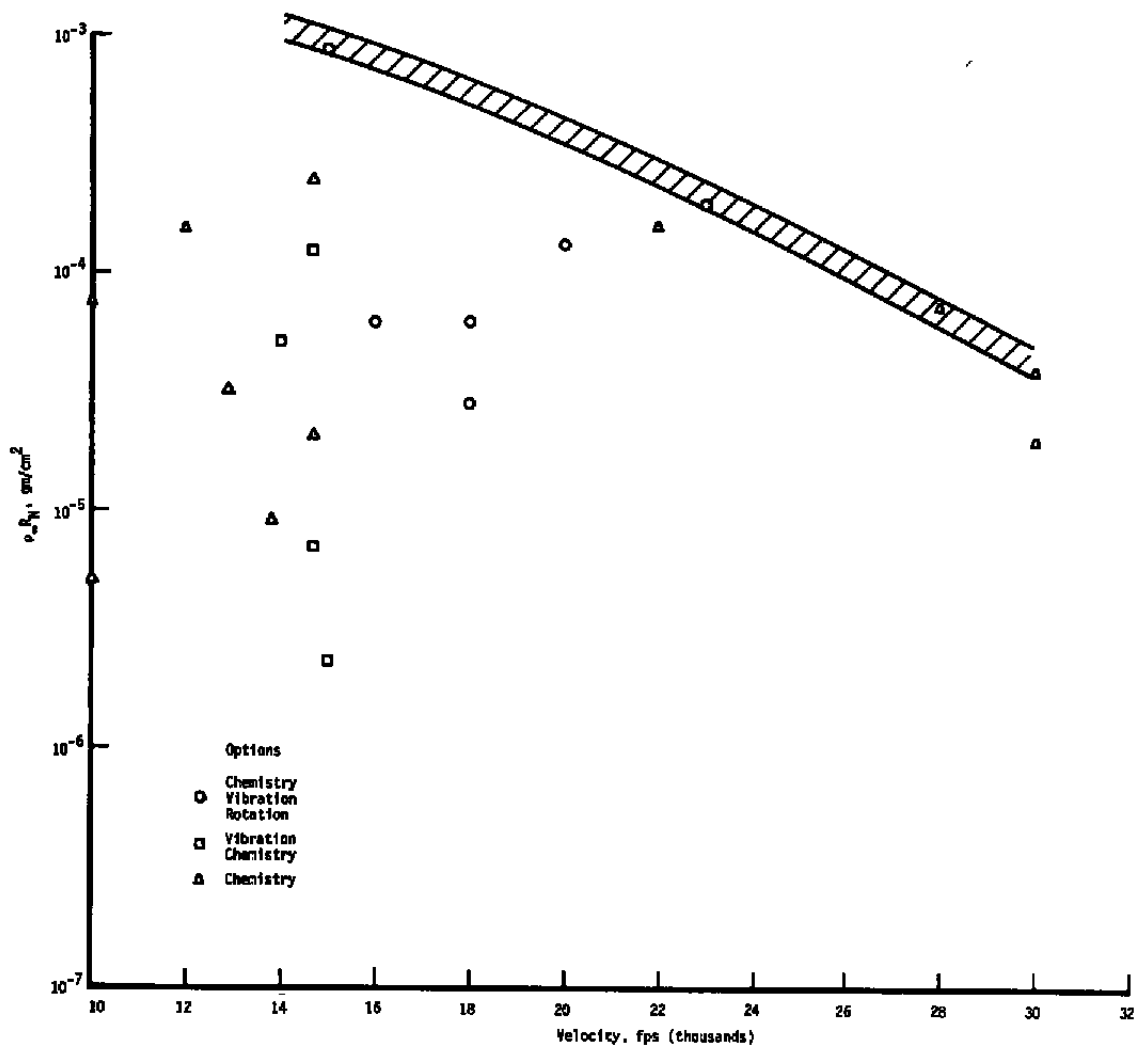


Figure 10. Nonequilibrium air solutions on missile-like bodies.

The available thermochemical models, the flow and geometry options, and the overall code structure are presented in Sections 2.0 and 3.0. The procedures for determining the location of the bow shock, as well as an imbedded shock and for approximating the displacement effect of the boundary layer have been explained in Section 3.0.

Instructions for using CUNIFLOW are presented in Section 4.0 and in Appendixes B, E, and F. Appendixes A and D present mathematical details and the code structure. Differences between the present and previous versions of CUNIFLOW are listed in Appendix C.

REFERENCES

1. Gnoffo, P. A. and McCandless, R. S. "Three-Dimensional AOTV Flow Fields in Chemical Nonequilibrium." AIAA Paper 86-0230, January 1986.
2. Li, C. P. "Implicit Computation of Chemically Reactive Flow About Hypersonic Vehicles." AIAA Paper 87-0282, January 1987.
3. Prabhu, D. K., Tannehill, J. C., and Marvin, J. G. "A New PNS Code for Three-Dimensional Chemically Reacting Flows." AIAA Paper 87-1472, June 1987.
4. Candler, G. and MacCormack, R. "The Computation of Hypersonic Ionized Flows in Chemical and Thermal Nonequilibrium." AIAA Paper 88-0511, 1988.
5. Barber, T. J. and Cox, G. B., Jr. "Hypersonic Vehicle Propulsion: A CFD Application Case Study." AIAA Paper 88-0475, January 1988.
6. Moreno, J. B. "Inverse-Method and Method-of-Characteristics Flow Field Programs." Sandia Laboratories, SC-DR-67-652, 1967.
7. Lordi, J. A., et al. "Description of Nonequilibrium Effects on Simulation of Flows About Hypersonic Vehicles." AIAA Paper 88-0476, January 1988.
8. Kaplan, A. E. "Ballistic Missile Defense Advanced Development Program, Reentry Physics Studies Report, RMP-B Flow Field Calculations II: Computational Package Description." Bell Telephone Laboratories, RPSR 71-6, July 1971.
9. Patterson, J. L. and Lewis, A. B. "An Investigation of Nonuniform Hypersonic Free-Stream Flows About Blunt Axisymmetric Bodies." Air Force Flight Dynamics Laboratory Technical Report AFFDL-TR-69-57, November 1969.
10. Curtis, J. T. and Strom, C. R. "Computation of the Nonequilibrium Flow of a Viscous Radiating Fluid About a Blunt Axisymmetric Body — Vol. I." AFFDL-TR-67-40 (AD660104), June 1967.
11. Curtis, J. T. and Strom, C. R. "Computation of Equilibrium Hypersonic Flow About Blunt Bodies with Sharp Corners." Sandia Laboratories Report SC-CR-67-2749, August 1967.
12. Evans, R. M. "User's Manual: Boundary-Layer Integral Matrix Procedure Including Gas Phase Kinetics KBLIMP-A." AEROTHERM Report UM75-62.

13. Hartree, D. R. *Numerical Analysis*, 2nd Edition. Oxford University Press, 1952.
14. Mayer, J. E. and Mayer, M. G. *Statistical Mechanics*. John Wiley and Sons, New York, 1940, pp. 149-178.
15. Herzberg, G., *Molecular Spectra and Molecular Structure. I, Spectra of Diatomic Molecules*, Van Nostrand Reinhold, New York, Second Edition, 1950.
16. Jaffe, R. L. "The Calculation of High-Temperature Equilibrium and Nonequilibrium Specific Heat Data for N₂, O₂, and NO." AIAA Paper 87-1633, June 1987.
17. Lomax, H. and Inouye, M. "Numerical Analysis of Flow Properties About Blunt Bodies Moving at Supersonic Speeds in an Equilibrium Gas." NASA TR-R-204, July 1964.
18. Stull, D. R. and Prophet, H. "JANNAF Thermochemical Tables, Second Edition." National Bureau of Standards Report NSRDS-NBS-37, 1972.
19. Browne, W. G. "Thermodynamic Properties of Some Diatoms and Diatomic Ions at High Temperatures." General Electric Company, Missiles and Space Division Technical Memo TM-8, 1962.
20. Gordon, S. and McBride, B. J. "Computer Program for Calculation of Complex Chemical Equilibrium Compositions, Rocket Performance, Incident and Reflected Shocks and Chapman-Jouguet Detonations." NASA SP-273, 1971.
21. Marrone, P. V. and Treanor, C. E. "Chemical Relaxation with Preferential Dissociation from Excited Vibrational Levels." *Physics of Fluids*, Vol. 6, 1963, pp. 1215-1221.
22. Treanor, C. E. and Marrone, P. V. "Effect of Dissociation on the Rate of Vibrational Relaxation." *Physics of Fluids*, Vol. 5, 1962, pp. 1022-1026.
23. Park, C. "Two-Temperature Interpretation of Dissociation Rate Data for N₂ and O₂." AIAA Paper 88-0458, January 1988.
24. Sharma, S. P., Huo, W. M., and Park, C. "The Rate Parameters for Coupled Vibration-Dissociation in a Generalized SSH Approximation." AIAA Paper 88-2714, June 1988.
25. Carlson, L. A., Bobskill, G. J. and Greendyke, R. B. "Comparison of Vibration Dissociation Coupling and Radiative Heat Transfer Models for AOTV/AFE Flow Fields." AIAA Paper 88-2673, June 1988.

26. Nardone, M. C., et al. "Radiance of Species in High Temperature Air." General Electric Corporation Missile and Space Division Report R63SD3, 1963.
27. Peng, T. C. and Pindroh, A. L. "An Improved Calculation of Gas Properties at High Temperatures: Air." Boeing Company Aerospace Division Report D2-11722, February 1962.
28. Cohen, C. B. and Reshotko, E. "Similar Solutions for the Compressible Laminar Boundary Layer with Heat Transfer and Pressure Gradient." NACA TR-1293, 1956.
29. Oran, E. S. and Boris, J. P. *Numerical Simulation of Reactive Flow*. Elsevier, New York, 1987, pp. 198-199.
30. Fleck, J. T. and Fryer, W. D. "An Exploration of Numerical Filtering Techniques." Cornell Aeronautical Laboratory Report XA-869-P-1, May 1, 1953.
31. Lomax, H. "On the Construction of Highly Stable, Explicit Numerical Methods for Integrating Coupled Ordinary Differential Equations with Parasitic Eigenvalues." NASA TN D-4547, April 1968.
32. Inouye, M. "Blunt Body Solutions for Spheres and Ellipsoids in Equilibrium Gas Mixtures." NASA TN D-2780, May 1965.
33. Birkhoff, G. *Fact, Logic, Similitude*. Princeton University Press, 1960, p. 109.
34. Hoffman, J. J., et al. "Low Density Real Gas Flows About Hypersonic Vehicles." AFWAL-TR-87-3112, March 1988.
35. Evans, J. S., Schexnayder, C. J., Jr., and Huber, P. W. "Boundary-Layer Electron Profiles for Entry of a Blunt Slender Body at High Altitudes." NASA TN-D-7332, July 1973.
36. Jensen, D. E. and Jones, G. A. "Reaction Rate Coefficients for Flame Calculations." *Combustion and Flame*, 32, 1978, pp. 1-34.
37. Marrone, P. V. "Inviscid, Nonequilibrium Flow Behind Bow and Normal Shock Waves, Part I General Analysis and Numerical Examples." Cornell Aeronautical Laboratory Report QM-1626-A-12(I), May 1963.

37. Marrone, P. V. "Inviscid, Nonequilibrium Flow Behind Bow and Normal Shock Waves, Part I General Analysis and Numerical Examples." Cornell Aeronautical Laboratory Report QM-1626-A-12(I), May 1963.

APPENDIX A MATHEMATICAL DETAILS

1.0 BLUNT BODY EQUATIONS

The nondimensional conservation equations in the curvilinear coordinate system of the blunt body code are

Mass: (A-1)

$$\frac{\partial \rho}{\partial y} + \frac{\rho}{v} \frac{\partial v}{\partial y} = - \frac{\rho}{v(1+xy)} \left[\frac{1}{\rho} \frac{\partial}{\partial x} (\rho u) + \frac{u}{r} \frac{\partial r}{\partial x} + (1+xy) \frac{v}{r} \frac{\partial r}{\partial y} + xv \right]$$

Normal Momentum: (A-2)

$$\frac{\partial p}{\partial y} + \rho v \frac{\partial v}{\partial y} = \frac{-\rho}{1+xy} \left[u \frac{\partial v}{\partial x} - xv^2 \right]$$

Longitudinal Momentum: (A-3)

$$\frac{\partial u}{\partial y} = - \frac{1}{v(1+xy)} \left[\frac{1}{\rho} \frac{\partial p}{\partial x} + u \frac{\partial u}{\partial x} + xv \right]$$

Species: (A-4)

$$\frac{\partial \gamma_j}{\partial y} = \frac{1}{v} \left[\frac{\sum_{i=1}^{N_R} Q_{ij}}{\rho} - \frac{u}{(1+xy)} \frac{\partial \gamma_j}{\partial x} \right]; \quad j = N_c + 1, \dots, N_s$$

Atoms: (A-5)

$$\sum_{j=1}^{N_s} \alpha_{jk} \left[\frac{u}{1+xy} \frac{\partial \gamma_j}{\partial x} + v \frac{\partial \gamma_j}{\partial y} \right] = 0; \quad k = 1, NC$$

Vibrational Energy: (A-6)

$$\frac{\partial \epsilon_i}{\partial y} = \frac{1}{v} \left[w_j - \frac{u}{1+xy} \frac{\partial \epsilon}{\partial x} \right]$$

Enthalpy:

$$v\Lambda \left(\frac{c_p M}{e} \right) \left(\frac{\partial p}{\partial y} - \frac{p}{e} \frac{\partial e}{\partial y} \right) + v^2 \Lambda \frac{\partial v}{\partial y} = v\Lambda \frac{c_p M^2}{e} p \sum_{j=1}^{N_s} \frac{\partial \gamma_j}{\partial y}$$

$$- \text{Rad} - v \left(\Lambda u \frac{\partial u}{\partial y} + \sum_{j=1}^{N_s} h_j \frac{\partial \gamma_j}{\partial y} \right) - v \sum_{k=1}^{N_{vib}} \gamma_{N_c + k} + k \frac{\partial \epsilon_k}{\partial y}$$

$$- \frac{u}{1 + xy} \left\{ \Lambda \left(\frac{c_p M}{e} \right) \left(\frac{\partial p}{\partial x} - p M \sum_{j=1}^{N_s} \frac{\partial \gamma_j}{\partial x} - \frac{p}{e} \frac{\partial e}{\partial x} \right) + \sum_{k=1}^{N_{vib}} \frac{\partial \epsilon_k}{\partial x} \gamma_{N_c + k} \right. \tag{A-7}$$

$$\left. + \sum_{j=1}^{N_s} h_j \frac{\partial \gamma_j}{\partial x} + \Lambda \left(u \frac{\partial u}{\partial x} + v \frac{\partial v}{\partial x} \right) \right\}$$

In these variables, the partial pressure of the *i*th species may be written

$$p_i = \left(\frac{\bar{\rho} \bar{T}_\infty}{M_\infty \bar{U}_\infty^2} \right) \frac{e_i T}{M_i} = \Lambda^{-1} \frac{e_i T}{M_i} \tag{A-8}$$

and Rad is the radiant energy lost by the gas.

The nondimensional quantities used above are defined according to the following system:

<u>Types of Quantity</u>	<u>Reference</u>
Length	\bar{R}_{sh}
Velocity	\bar{U}_∞
Density	$\bar{\rho}_\infty$
Pressure	$\bar{\rho}_\infty \bar{U}_\infty^2$

<u>Types of Quantity</u>	<u>Reference</u>
Energy of mixture	$\mathcal{R} \bar{T}_\infty / \bar{M}_\infty$
Energy of particular species	$\mathcal{R} \bar{T}_\infty$
Molecular weight	\bar{M}_∞
Concentration (γ_j)	$\sum_{j=1}^{NS} \bar{\gamma}_{j\infty} = \bar{M}_\infty^{-1}$

2.0 DERIVATIVE ALGORITHM

Derivatives in the x-direction (parallel to the bow shock) are evaluated in subroutine PART using the formula

$$\frac{dB_i}{dx} = \frac{5B_{i-3} - 12B_{i-2} - 39B_{i-1} + 39B_{i+1} + 12B_{i+2} - 5B_{i+3}}{96\Delta x} \quad (\text{A-9})$$

where B represents any variable and i, its position in the data array.

Close to the ends of the array, special formulae are necessary:

For $i = 1$,

$$\frac{dB_1}{dx} = \frac{-133B_1 + 84B_2 + 207B_3 - 192B_4 - 39B_5 + 108B_6 - 35B_7}{96\Delta x} \quad (\text{A-10})$$

For $i = 2$,

$$\frac{dB_2}{dx} = \frac{-35B_1 - 28B_2 + 49B_3 + 32B_4 - 17B_5 - 4B_6 + 3B_7}{96\Delta x} \quad (\text{A-11})$$

For $i = 3$,

$$\frac{dB_3}{dx} = \frac{3B_3 - 44B_2 - 25B_3 + 64B_4 + 17B_5 - 20B_6 + 5B_7}{96\Delta x} \quad (\text{A-12})$$

For $i = N-2$ or $N-1$, where N is the number of elements in the array,

$$\frac{dB_i}{dx} = \frac{B_{i+1} - B_{i-1}}{2\Delta x} \quad (\text{A-13})$$

For $i = N$,

$$\frac{dB_N}{dx} = \frac{B_{N-2} - 4B_{N-1} + 3B_N}{2\Delta x} \quad (\text{A-14})$$

3.0 INTEGRATION ALGORITHM

The explicit algorithm devised by Lomax for stiff equations is

$$B_{n+1}^{(1)} = B_n + h\beta(1,M)B_n \quad (\text{A-15})$$

$$B_{n+1}^{(k)} = B_n + h\beta(k,M)B_{n+1}^{(k-1)} \quad (\text{A-16})$$

$$B_{n+1} = B_n + h\beta(2M,M)B_{n+1}^{(2M-1)} \quad (\text{A-17})$$

where

$$B_n \equiv \left. \frac{dB}{ds} \right|_{s=s_n} \quad (\text{A-18})$$

$$h = s_n - s_{n-1} \quad (\text{A-19})$$

and B_n represents any variable evaluated at point s_n .

4.0 EQUATIONS FOR THE M.O.C. CODE

The afterbody program uses the "reference-plane" method of characteristics. The nondimensional compatibility and characteristic equations used are listed below:

$$C_A dp \pm d\phi = C_B d\xi \quad (\text{A-20})$$

$$C_A = (\cot \beta)/\rho u^2 \quad (\text{A-21})$$

$$C_B = \frac{\omega \sin \phi \sin \beta}{r} + F \sin \beta \quad (\text{A-22})$$

$$F = \frac{\mathcal{G}}{C_p T} - \mathcal{M} \sum_{j=1}^{N_s} \frac{\partial \gamma_j}{\partial S} \quad (\text{A-23})$$

$$\mathcal{G} = \sum_{j=1}^{N_s} h_j \frac{\partial \gamma_j}{\partial S} + \sum_{k=1}^{N_{\text{vib}}} \gamma_{N_c+k} \frac{\partial \epsilon_k}{\partial S} \quad (\text{A-24})$$

which must be satisfied along the curves

$$\frac{dr}{dz} = \tan(\phi \pm \beta) \quad (\text{A-25})$$

In addition, the thermodynamic and reaction equations

$$\frac{\partial T}{\partial S} = \frac{1}{C_p} \left(\frac{\Lambda}{e} - \frac{\partial p}{\partial S} - \mathcal{G} \right) \quad (\text{A-26})$$

$$\sum_{j=1}^{N_s} \alpha_{jk} \frac{\partial \gamma_j}{\partial S} = 0; \quad k = 1, \dots, N_c \quad (\text{A-27})$$

$$\frac{\partial \gamma}{\partial S} = \sum_{i=1}^{N_R} \frac{Q_{ij}}{eU} \quad j = N_c + 1, \dots, N_s \quad (\text{A-28})$$

$$U \frac{\partial \epsilon_j}{\partial S} = w_j; \quad j = 1, \dots, N_{\text{vib}} \quad (\text{A-29})$$

$$U \frac{\partial U}{\partial S} = - \frac{1}{e} \frac{\partial p}{\partial S} \quad (\text{A-30})$$

are applicable along the streamlines specified by

$$\frac{dr}{dz} = \tan \phi \quad (\text{A-31})$$

The density is calculated from the equation of state

$$e = \frac{\Lambda_c \mathcal{M} p}{T} \quad (\text{A-32})$$

APPENDIX B INPUTTING THERMOCHEMICAL PROPERTIES

If a problem involves chemical or vibrational nonequilibrium (MODEL = 0,3,4), subroutine CHEMIN is called to read a properties file from Unit 8. The format and contents of this file will depend on the model, but, in general, reaction data are input first — two logical records for each reaction — followed by thermodynamic data for each species. All input is formatted, and each block of data is terminated by a record with the characters "END" in the first three columns. The code will count the entries in each category and will select the data for the species specified in Namelist UPSTREAM (Section 4.2.2) or named by the reaction records from the data base on Unit 8. At present, dimension statements allow 72 reactions involving not more than 30 species.

A diagram of the input procedure is shown in Fig. B-1. The various record types are identified by the numbers in the upper right corners of the record symbol. The input file "NEWCHEM" which was used for the exploration of the operating envelope in Section 4.5 is shown in Fig. B-2.

Table B-2 from Ref. 8 lists a number of reactions among the components of heated air.

Other tabulations will be found in Refs. 15, 30, and 34-36.

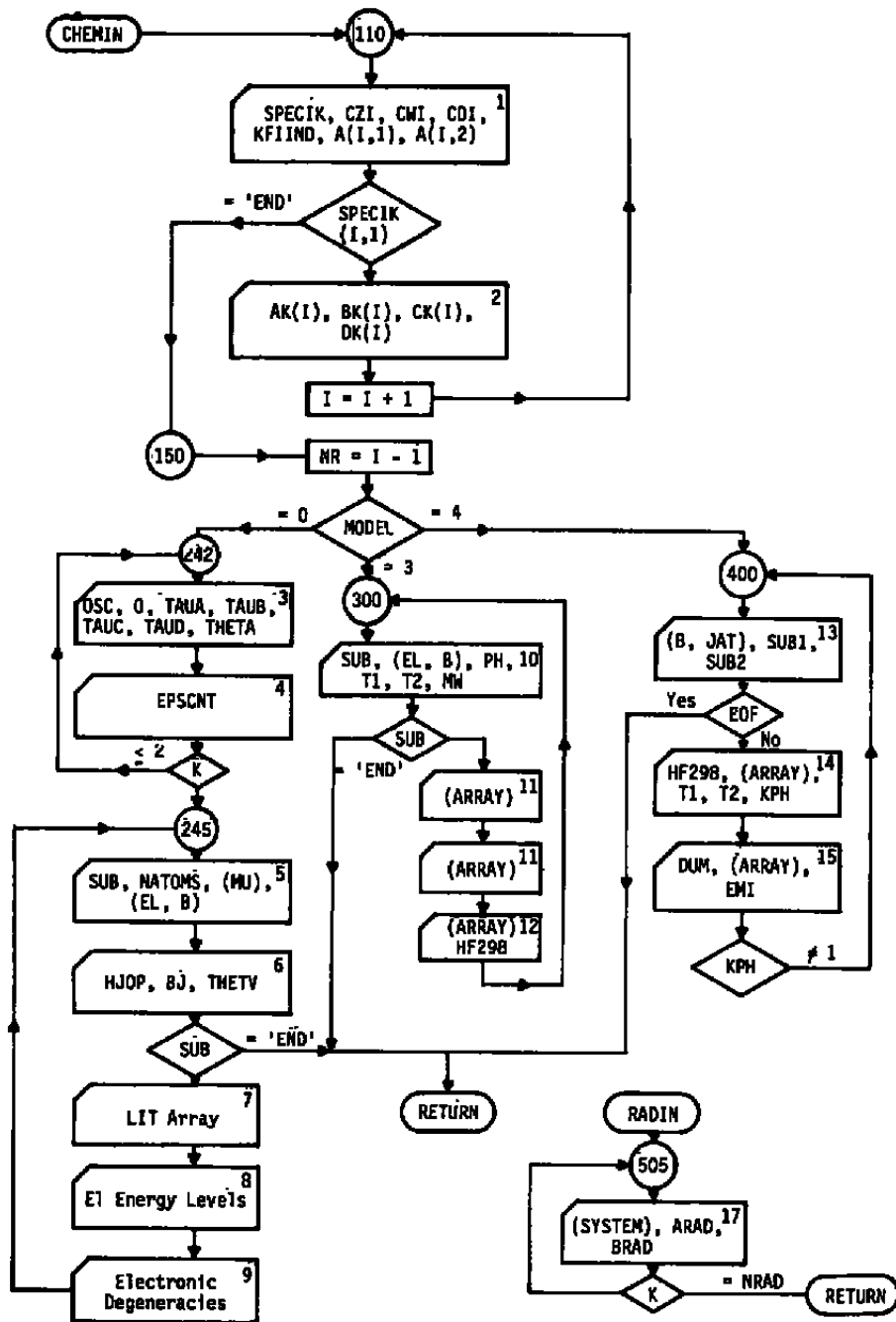


Figure B-1. Thermodata input schematic.

```

02 0      0 0 0      1      1.
      2.1 +18      - .50      5.938 +04      1.0
02 02     0 0 02     11.
      3.56+21      -1.5      5.938 +04      1.0
02 M      0 0 M      1.0      1.0
      1.19+21      -1.5      5.938 +04      1.0
N2 N      N N N      1.0      1 1.0
      7.5 +20      -1.5
N2 N2     N N N2     1.0      1 1.0
      1.5 +20      -1.5
N2 M      N N M      1.0      1 1.0
      5.0 +19      -1.5
NO M      N O M      1.0
      5.18 +21      -1.5      7.549 +04      1.0
N 02     NO 0      1.0
      1.0 +12      5.0      -01 3.12 +03      1.0
O N2     NO N      1.0
      5.0 +13
N 0      NO+ E-      1.0      1
      5.40 E+21 -1.5
END
02 26.0 1.6188 E-03      1.01444 E+02 3.333333E-01 2256.34 E+00
N2 33.0 1.1153 E-05 0.5      1.5400 +02 3.333333E-01 3374.03 E+00
0      1 0 1 0 0 0 1.0
      2.46855 E+12 2.1032 E+00 0.0 E+00
      1
0.0 E+00 7.548 E-22 1.077 E-21 7.532 E-20 1.604 E-19
5.0 E+00 3.0 E+00 1.0 E+00 5.0 E+00 1.0 E+00
N      1 0 1 0 0 N 1.0
      4.712342 E+12 1.67997 E+00 0.0 E+00
      1
0.0 E+00 9.127 E-20 9.152 E-20 1.369 E-19 4.1819E-19
4.0 E+00 6.0 E+00 4.0 E+00 6.0 E+00 1.2 E+01
E-      1 0 0 0 1, E-1.0
      0.0 E+00 -1.423517 E+01 0.0 E+00
      1 1
      1
2.0 E+00
AR      1 0 1 0 0 AR 1.
      0.0 E+00 1.86557 E+00 0.0 E+00
      1
0.0 E+00 4.4215E-19 4.4503E-19
1.0 E+00 5.0 E+00 3.0 E+00
02      2 1 0 0 0 2.0
      0.0 E+00 1.21618 E+00 2.23897 E+03
      1
0.0 E+00 3.7583E-20 6.2685E-20 1.713 E-19 2.3641E-19
3.0 E+00 2.0 E+00 1.0 E+00 3.0 E+00 3.0 E+00
N2      2 1 0 0 0 N 2.0
      0.0 E+00 -4.21630 E-01 3.35324 E+03
      1 1
0.0 E+00 2.3856E-19 2.830 E-19 2.848 E-19
1.0 E+00 3.0 E+00 6.0 E+00 1.0 E+00
NO      2 1 0 0 0 M 1.0 1.0
      8.98898 E+11 1.23256 E+00 2.69918 E+03
      1 1
0.0 E+00 5.744 E-22 2.087 E-19 2.180 E-19
2.0 E+00 2.0 E+00 2.0 E+00 4. E+00 0.0 E+00

```

Figure B-2. Thermochemical input file "NEWCHEM".

```

ND+  2  1  0  0  0  N  1.  0  1.  E-  -1
      9.834435 E+12  3.7861  E-01  3.37 95  E+03

0.0  E+00 1.9132E-19 2.8057E-19 3.4659E-19 3.4798E-19
1.0  E+00 6.0  E+00 3.0  E+00 6.0  E+00 2.0  E+00
END
D2  SCHUMAN-RUNGE  3.6  E-13  5.7  E+04
N2  FIRST POSITIVE  1.8  E-14  8.3  E+04
N2  SECOND POSITIVE  1.3  E-12  1.2  E+05
NO  BETA & GAMMA AVERAGE  3.0  E-13  6.7  E+04
NO  INFRA-RED  2.1  E-19  7.6  E+04
N  FREE-FREE  2.0  E-34  5.2  E+04
O  FREE-FREE  3.0  E-34  4.2  E+05

```

Figure B-2. Concluded.

Table B-1. Formats for Thermochemical Input

Record Type 1	Format (6A4,3F3.0,I3,2F3.0)
(SPECIK(I,K),K = 1,3)	Reactant names left justified
(SPECIK(I,K),K = 4,6)	Product names left justified beginning in Column 13.
CZI,CWI,CDI	Reaction type [Eq. (22), Sec 2.3.2]. Set just one to 1 and the others = 0.
KFIIND	Set = 1 if reaction rate constants apply to reverse of the reaction as written.
(A(I,K),K = 1,2)	Set = 1 if this reaction is coupled to the kth nonequilibrium vibrator. [Eq. (20)]
Record Type 2 Format (5E15.7)	
AK	Constant A_k of rate coefficient [Eq. (21)](cm ³ /mole-sec or cm ⁶ /mole-sec)
BK	Exponent of T in Eq. (21), B_{ki}
CK	Activation temperature [Eq. (21)], °K
DK	D_{ki} in Eq. (21)
Record Type 3 Format (A3, F4.0, 5E14.7)	
OSC	Vibrator name — left adjusted
O	Number of vibrational levels for this vibrator
TAUA	Coefficient in Eq. (27) (gm/cm/sec)
TAUB	Exponent of T_o , Eq. (27)
TAUC	Argument of exponential, Eq. (27)
TAUD	Temperature exponent in argument of Eq. (27)
THETA	Characteristic vibrational temperature (°K)

Table B-1. Continued

Record Type 4	Format (7E11.6)
EPSCNT	Reserved for coefficients of possible vibrational energy fit. Not used at present.
Record Type 5	Format (A4,4I3,8F3.0)
SUB	Name of species — left adjusted
NUMA	Number of atoms in species
LU(1)	1 if species is neutral molecule 0 otherwise
LU(2)	1 if species is neutral atom
LU(3)	1 if species is ionized atom
LU(4)	1 if species is electron
EL(1)	Name of element
B(1)	Number of atoms of EL(1) in molecule
EL(2)	Name of second element in molecule
B(2)	Number of atoms of EL(2) in molecule
EL(3)	Name of third element if present
B(3)	Number of atoms of EL(3) in molecule
EL(4)	Name of fourth element, if present
B(4)	Number of atoms of EL(4) in molecule

Table B-1. Continued

Record Type 6	Format (3E15.7)
HJOP	Heat of formation at 1 atm, ergs/mole
BJ	Constant b in Eq. (4), erg/mole
THETV	Characteristic vibrational temperature °K
Record Type 7	Format (17I3)
(LIT(I,J),J = 1, NRAD)	Matrix elements connecting this species to Jth radiating system
Record Type 8	Format (7E11.6)
HCFNT	Array of electron energy levels for this species — cal/molecule
Record Type 9	Format (7E11.6)
FCFNT	Degeneracies of electron-energy levels
Record Type 10	Format (4A4,8X,4(A2,F3.0),A1,2F10.3,F13.5)
(SUB(I),I = 1.4)	Species name — up to 16 characters
EL(1)	Name of element
B(1)	Number of atoms of EL(1) in molecule
EL(2)	Name of second element in molecule
B(2)	Number of atoms of EL(2) in molecule
EL(3)	Name of third element, if present
B(3)	Number of atoms of EL(3) in molecule

Table B-1. Continued

EL(4)	Name of fourth element, if present
B(4)	Number of atoms of EL(4) in molecule
PH	Enter "G"
T1	Boundary between lower and middle temperature ranges
T2	Boundary between middle and upper temperature ranges*
MW	Molecular weight

*Note: The thermal properties tables from Lewis Research Center have only two ranges: 100 - 1000 °K and 1000 - 5000 °K.

Record Type 11**Format (5E15.8)**

(ARRAY(N,1),N=1,5)	First 5 coefficients of mid-range polynomial fit, Eqs. (7)–(9)
(ARRAY(N,1),N=6,7), (ARRAY(N,2),N=1,3)	Rest of mid-range and first 3 low-range coefficients

Record Type 12**Format (5E15.8)**

(ARRAY(N,2),N=4,7)	Remainder of low-range thermofit coefficients
HF298	Heat of formation at 298.15 °K, cal/mole

Record Type 13**Format (7(F3.0,I3),30X,2A4)**

(B(N),JAT(N),N=1,7)	B(N) number of atoms of atomic number JAT in this molecule
SUB(1), SUB(2)	Species name — up to 8 characters

Table B-1. Concluded

Record Type 14	Format (6E9.6,2E6.0,I1)
HF298	Heat of formation at 298.15 °K, cal/mole
(ARRAY(J,1),J = 1,5)	Thermofit coefficients in Eq. (12); $a_2 = \text{ARRAY}(1,1)$ Lower temperature range, cal/mole or cal mole °K
T1	Upper limit of lower temperature range
T2	Reserved for upper limit of middle temperature range. Not currently implemented.
KPH	Enter 1 if this species is a gas Enter 0 if otherwise
Record Type 15	Format (6E9.6,2E6.0,I1)
HF298	Heat of formation at 298.15 °K. This must be the same as on previous record.
(ARRAY(J,2),J = 1,5)	Thermofit coefficients for upper range*
EMI	Molecular weight

*At present. If a third temperature range is necessary, alter subroutine CHEMIN to read a third record in record type 15 format; redimension EPSCNT for the number of species involved (30 at present), and enter appropriate value for T2. Use EPSCNT to carry the coefficients to subroutine THERMO, which will also need modification.

Table B-2. Reactions and Rates*

Reaction	Type	Direction	A_k	B_k	C_k	A_{11}	A_{12}	Units
$O_2 + O = 2O + O$	W	FWD	2.1×10^{18}	-0.5	59380	1	--	$cm^3/mole\text{-sec}$
$O_2 + O_2 = 2O + O_2$	W	FWD	3.56×10^{21}	-1.5	59380	1	--	$cm^3/mole\text{-sec}$
$O_2 + M = 2O + M$	Z	FWD	1.190×10^{21}	-1.5	59380	1	--	$cm^3/mole\text{-sec}$
$N_2 + N = 2N + N$	W	REV	7.50×10^{20}	-1.5	0		1	$cm^6/mole^2\text{-sec}$
$N_2 + N_2 = 2N + N_2$	W	REV	1.50×10^{20}	-1.5	0	--	1	$cm^6/mole^2\text{-sec}$
$N_2 + M = 2N + M$	Z	REV	5.00×10^{19}	-1.5	0	--	1	$cm^6/mole^2\text{-sec}$
$NO + M = N + O + M$	D	FWD	3.18×10^{21}	-1.5	75490	--	--	$cm^3/mole\text{-sec}$
$N + O_2 = NO + O$	W	FWD	1.0×10^{12}	+0.5	3120	--	--	$cm^3/mole\text{-sec}$
$O + N_2 = NO + N$	W	FWD	5.0×10^{13}	0	38016	--	--	$cm^3/mole\text{-sec}$
$N + O = NO^+ + e^-$	W	REV	1.8×10^{21}	-1.5	0	--	--	$cm^3/mole\text{-sec}$
$2O = e^- + O_2^+$	W	REV	1.9×10^{21}	-1.5	0	--	--	$cm^3/mole\text{-sec}$
$2N = e^- + N_2^+$	W	REV	9.6×10^{21}	-1.5	0	--	--	$cm^3/mole\text{-sec}$
$O + N = N + e^- + O^+$	W	REV	6.0×10^{24}	-2.5	--	--	--	$cm^6/mole\text{-sec}$
$2O = O + O^+ + e^-$	W	REV	6.0×10^{24}	-2.5	--	--	--	$cm^6/mole\text{-sec}$
$O + N_2 = N_2 + e^- + O^+$	W	REV	2.0×10^{26}	-2.5	--	--	--	$cm^6/mole\text{-sec}$
$O + O_2 = O^+ + e^- + O_2$	W	REV	9.0×10^{26}	-2.5	--	--	--	$cm^6/mole\text{-sec}$
$O + NO = NO + e^- + O^+$	W	REV	1.0×10^{28}	-2.5	--	--	--	$cm^6/mole\text{-sec}$
$2N = N + e^- + N^+$	W	REV	6.0×10^{24}	-2.5	--	--	--	$cm^6/mole\text{-sec}$
$N + O = O + e^- + N^+$	W	REV	6.0×10^{24}	-2.5	--	--	--	$cm^6/mole\text{-sec}$
$N + N_2 = N_2 + e^- + N^+$	W	REV	2.0×10^{26}	-2.5	--	--	--	$cm^6/mole\text{-sec}$
$N + O_2 = O_2 + e^- + N^+$	W	REV	9.0×10^{26}	-2.5	--	--	--	$cm^6/mole\text{-sec}$
$N + NO = NO + e^- + N^+$	W	REV	1.0×10^{28}	-2.5	--	--	--	$cm^6/mole\text{-sec}$
$N_2 + O^+ = O + N_2^+$	W	REV	7.8×10^{11}	0.5	--	--	--	$cm^3/mole\text{-sec}$
$N + NO^+ = N_2 + O^+$	W	REV	7.8×10^{11}	0.5	--	--	--	$cm^3/mole\text{-sec}$
$O + O_2^+ = O_2 + O^+$	W	REV	7.8×10^{11}	0.5	--	--	--	$cm^3/mole\text{-sec}$
$O + NO^+ = NO + O^+$	W	REV	7.8×10^{11}	0.5	--	--	--	$cm^3/mole\text{-sec}$
$N + O_2^+ = NO + O^+$	W	REV	7.8×10^{11}	0.5	--	--	--	$cm^3/mole\text{-sec}$
$N_2 + N^+ = N + N_2^+$	W	REV	7.8×10^{11}	0.5	--	--	--	$cm^3/mole\text{-sec}$
$N + O_2^+ = O_2 + N^+$	W	REV	7.8×10^{11}	0.5	--	--	--	$cm^3/mole\text{-sec}$
$O + NO^+ = O_2 + N^+$	W	REV	7.8×10^{11}	0.5	--	--	--	$cm^3/mole\text{-sec}$
$N + NO^+ = NO + N^+$	W	REV	7.8×10^{11}	0.5	--	--	--	$cm^3/mole\text{-sec}$
$O + N_2^+ = NO + N^+$	W	REV	7.8×10^{11}	0.5	--	--	--	$cm^3/mole\text{-sec}$
$N + O^+ = O + N^+$	W	REV	7.8×10^{11}	0.5	--	--	--	$cm^3/mole\text{-sec}$
$N_2 + O_2 = 2NO$	W	FWD	9.1×10^{24}	-2.5	65000	--	--	$cm^3/mole\text{-sec}$
$Ar^+ + 2e^- = Ar + e^-$	W	--	2.064×10^{17}	0.663	148000	--	--	$cm^3/mole\text{-sec}$

* Rates are of the form $k = A_k T^{B_k} \exp(-C_k/T^{D_k})$

APPENDIX C CHANGES SINCE 1967

Appendix C lists those features of CUNIFLOW which have been added, deleted, or substantially changed since the publication of Ref. 10.

Magneto-gas-dynamics — All references to magneto-gas-dynamic properties and related calculations have been removed from the blunt-body case.

Equilibrium wall temperature — Reference 10 describes an elaborate procedure for balancing the radiant and convective heat transfer to the body surface with the radiant energy emitted from the surface to determine the wall temperature. Since the wall temperature option was inaccurate and slow, it has been removed.

Integration Algorithm — The Lomax algorithm described in the text has replaced the Runge-Kutta and Treanor algorithms discussed in Ref. 10.

Nonuniform Free Stream — Inputting free-stream data in a tabular format and using linear interpolation for pre-shock properties has replaced the cumbersome polynomial fits described in Ref. 10.

Centerline — The original version of CUNIFLOW made no provision for including the centerline in the calculation.

Corners — The original version of CUNIFLOW (Ref. 10) made no provision for sharp corners. The facility for treating embedded shocks and Prandtl-Meyer corners was soon added and was described in Ref. 11. The current implementation differs significantly from that of the early version.

Input-Output — The current input procedure is entirely different from that of Refs. 10 and 11. The current printout is organized in roughly the same way as that of the original, but a number of quantities which were of interest only for code development have been omitted and the printout has been made dimensional. The binary plotting file, Unit 7, and the BLIMP communication file, Unit 3, have been added.

Equilibrium — Reference 11 described an elaborate equilibrium chemistry package which was supposed to furnish the equilibrium composition as well as the fluid dynamic quantities. Because the composition package was slow and temperamental, it was soon abandoned; only the RGAS and SERCH routines have been retained.

APPENDIX D CODE STRUCTURE

The overall structure of CUNIFLOW is displayed schematically in Figs. D-1 through D-4. A matrix of subroutine references is shown in Table D-1. SMALLH is actually an ENTRY point in subroutine THERMO; CNVRGE is an ENTRY in DIGNOS; FELDA is an ENTRY in subroutine FELD; STRIP is an ENTRY in ISTRIP; and QUELLE is an ENTRY point in subroutine SOURCE. A directory of unit operations is presented in Table D-2.

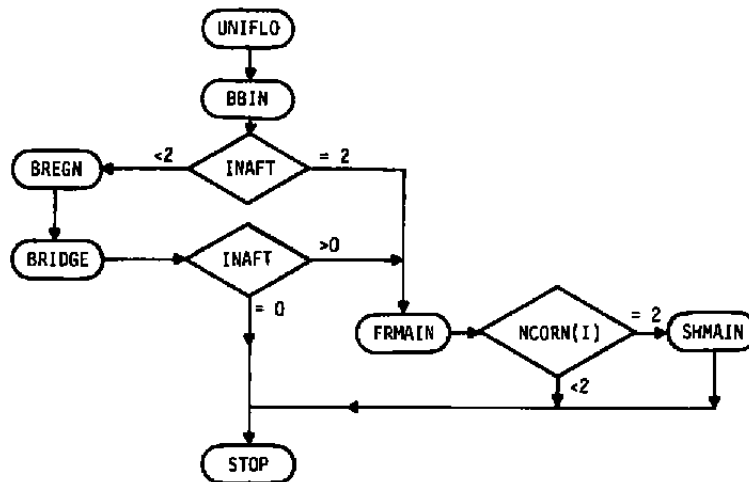


Figure D-1. Overall program control.

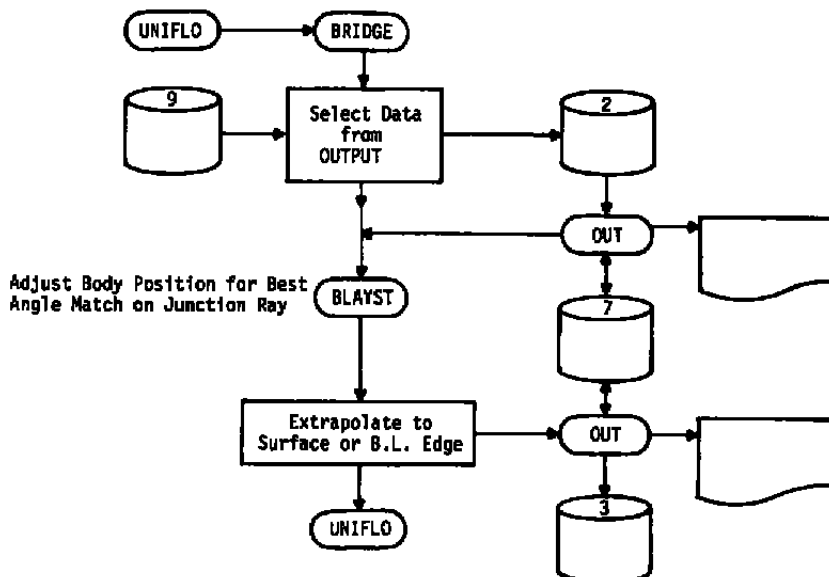


Figure D-2. Transition from elliptic to hyperbolic region.

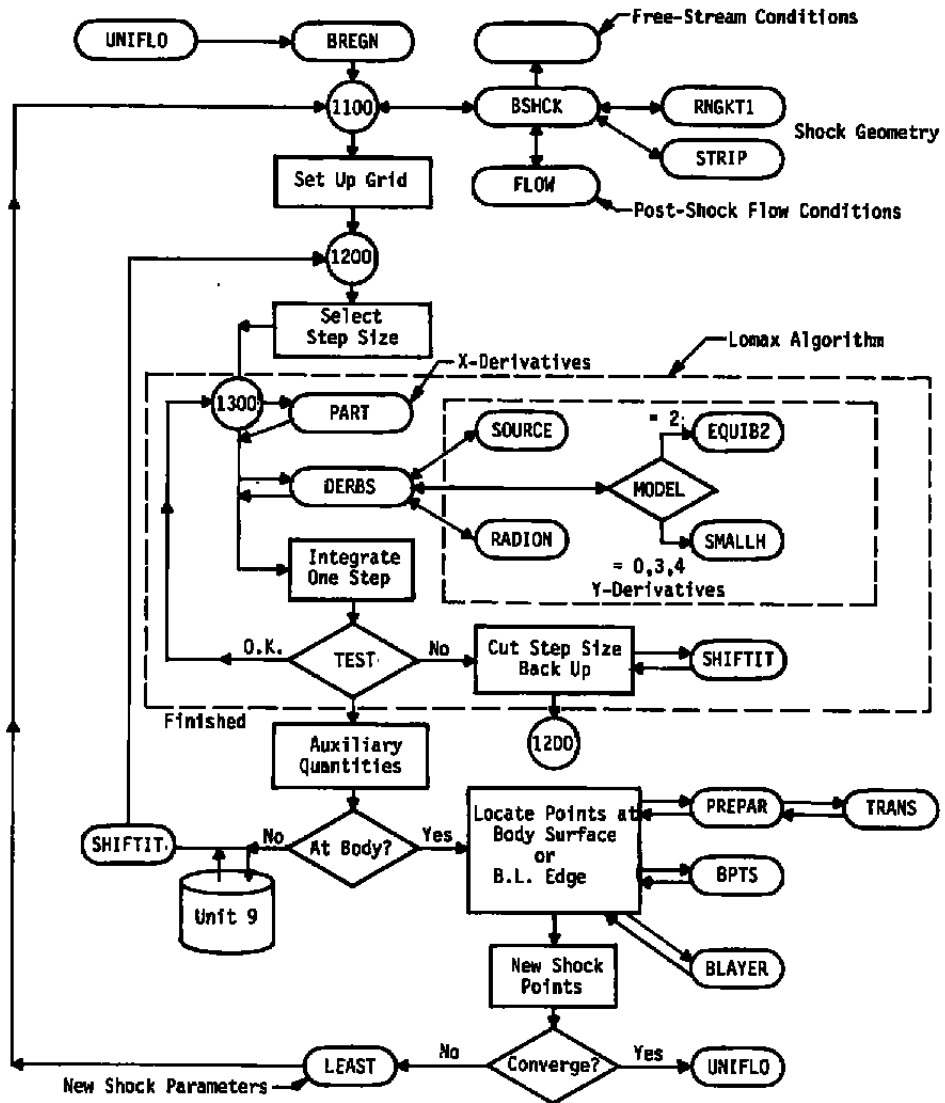


Figure D-3. Elliptic region calculation.

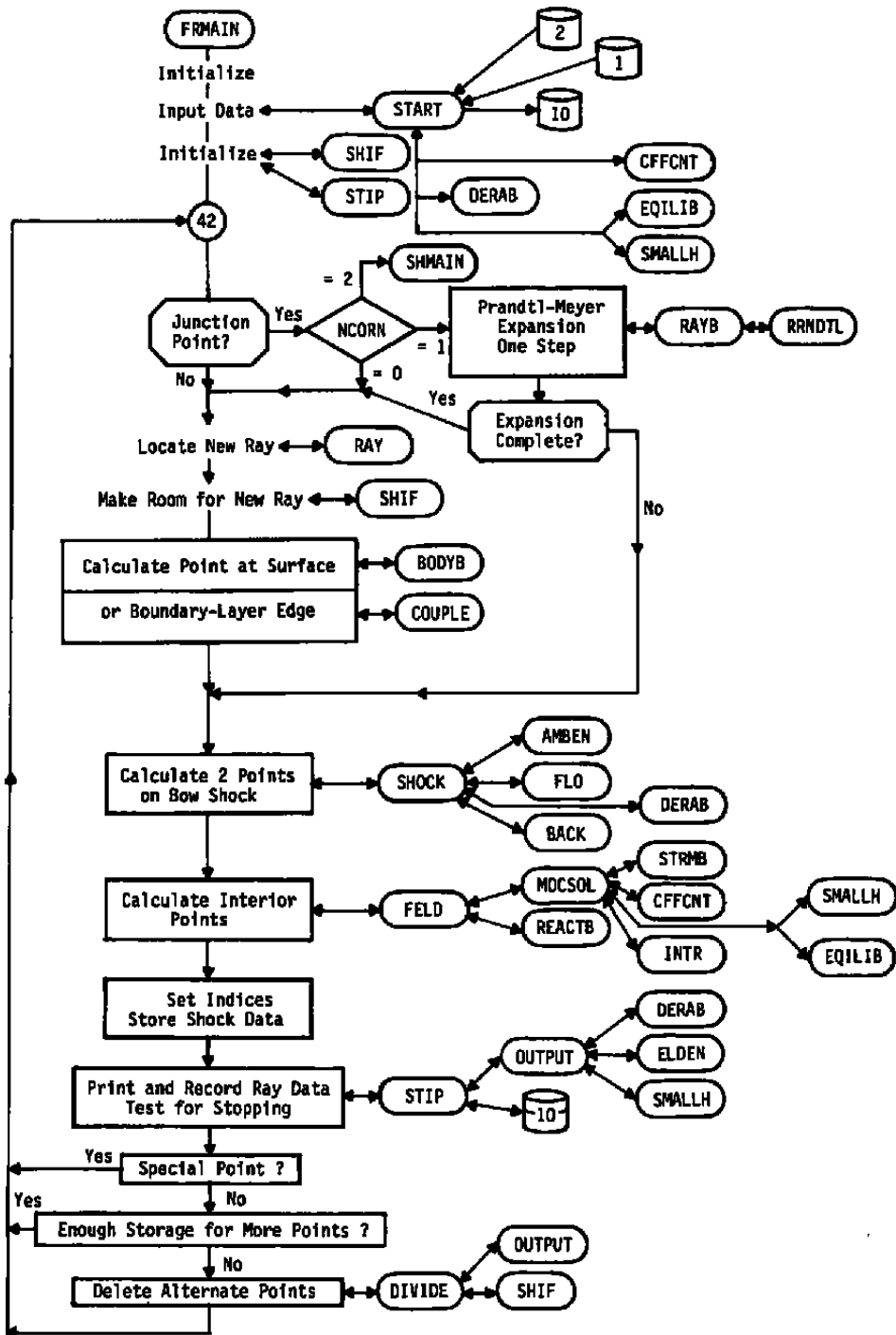


Figure D-4. Hyperbolic region calculation.

Table D-1. Subroutine Cross-Reference Chart

SUB Called	1	2	3	4	5	6	7	8	9	10	11	12	13	14	15	16	17	18	19	20	21	22	23	24	25	26	27	28	29	30	31	32	33	34	35			
Calling																																						
1																																						
2																																						
3																																						
4																																						
5																																						
6																																						
7																																						
8																																						
9																																						
10																																						
11																																						
12																																						
13																																						
14																																						
15																																						
16																																						
17																																						
18																																						
19																																						
20																																						
21																																						
22																																						
23																																						
24																																						
25																																						
26																																						
27																																						
28																																						
29																																						
30																																						
31																																						
32																																						
33																																						
34																																						
35																																						

Table D-1. Continued

SUB Called	1	2	3	4	5	6	7	8	9	10	11	12	13	14	15	16	17	18	19	20	21	22	23	24	25	26	27	28	29	30	31	32	33	34	35				
Calling																																							
36																																							
37												●												●											●				
38																																							
39																			●				●																
40																																							
41																																							
42																																							
43																																							
44																									●														
45												●												●															
46																																							
47																																							
48				●																																			
49				●																																			
50																																							
51																			●																				
52																																							
53																		●																					
54																																							
55																																							
56								●																															
57				●			●															●					●	●						●					
58	●	●																●					●					●											
59																																							
60																																							
61																																							
62																																							
63												●							●					●															
64																																							
65																								●															

Table D-1. Continued

SUB Called	36	37	38	39	40	41	42	43	44	45	46	47	48	49	50	51	52	53	54	55	56	57	58	59	60	61	62	63	64	65	66	67	68	69		
Calling																																				
1																																				
2																																				
3																																				
4																																				
5																																				
6																																				
7																																				
8																																				
9																																				
10																																				
11																																				
12																																				
13																																				
14																																				
15																																				
16																																				
17																																				
18																																				
19																																				
20																																				
21																																				
22																																				
23																																				
24																																				
25																																				
26																																				
27																																				
28																																				
29																																				
30																																				
31																																				
32																																				
33																																				
34																																				
35																																				

Table D-1. Concluded

SUB Called	36	37	38	39	40	41	42	43	44	45	46	47	48	49	50	51	52	53	54	55	56	57	58	59	60	61	62	63	64	65	66	67	68	69	
Calling																																			
36																																			
37																																			
38																																			
39																																			
40																																			
41							●																												
42								●																											
43																																			
44																																			
45																																			
46																																			
47																																			
48																																			
49																																			
50																																			
51																																			
52																																			
53																																			
54																																			
55																																			
56																																			
57																																			
58																																			
59																																			
60																																			
61																																			
62																																			
63																																			
64																																			
65																																			

Key to Subroutines

- | | |
|-------------|------------|
| 1. AMBEN | 36. LEAST |
| 2. BACK | 37. MOCSOL |
| 3. BBIN | 38. OUT |
| 4. BDYFCT | 39. OUTPUT |
| 5. BLAYER | 40. PART |
| 6. BLAYST | 41. PAUSE |
| 7. BODYB | 42. POINT |
| 8. BPTS | 43. POLATE |
| 9. BREGN | 44. PREPAR |
| 10. BRIDGE | 45. PRNDTL |
| 11. BSHCK | 46. RADAB |
| 12. CFFCNT | 47. RADION |
| 13. CHEMIN | 48. RAY |
| 14. CHEMOUT | 49. RAYB |
| 15. CNVRG | 50. RAYC |
| 16. COUPLE | 51. REACTB |
| 17. DAUX | 52. RGAS |
| 18. DERAB | 53. RNGKT1 |
| 19. DERBS | 54. SERCH |
| 20. DIGNOS | 55. SHIF |
| 21. DIVIDE | 56. SHIFIT |
| 22. ELDENT | 57. SHMAIN |
| 23. EQILIB | 58. SHOCK |
| 24. EQUIB2 | 59. SIMEQ |
| 25. ERRMSG | 60. SIMSOL |
| 26. FELD | 61. SMALLH |
| 27. FLARE | 62. SOURCE |
| 28. FLO | 63. START |
| 29. FLOW | 64. STIP |
| 30. FRMAIN | 65. STRMB |
| 31. HATM | 66. THERMO |
| 32. IMBED | 67. TRANS |
| 33. INTGRL | 68. TRUBEL |
| 34. INTR | 69. WRITE2 |
| 35. ISTRIP | |

Table D-2. Directory of Unit Operations

<u>Operation</u>	<u>Location</u>
Input free-stream conditions	BBIN
Input options and controls	BBIN
Input body shape equations	BBIN
Input initial shock shape parameters	BBIN
Free-stream conditions at z,r	AMBEN
Evaluate shock equation for blunt body shock coordinates	BSHCK
Iterate for M.O.C. shock points	SHOCK
Post-shock flow — elliptic region	FLOW
Post-shock flow conditions — hyperbolic region	FLO
Calculate pressure at trial shock location from interior flow-field data	BACK
Copy dependent variable data from one array to another — elliptic region	SHIFTIT
Copy data from one cell to another — hyperbolic region	SHIF
Evaluate x-derivatives — elliptic	PART
Evaluate y-derivatives — elliptic	DERBS
Evaluate species source terms	SOURCE
Evaluate vibrational relaxation rates	SOURCE
Evaluate radiant energy loss rate — elliptic	RADION
Evaluate radiant energy loss rate — M.O.C.	RADAB
Input nonequilibrium thermo properties	CHEMIN
Input equilibrium thermodynamic tables	RGAS
Evaluate nonequilibrium thermo properties	SMALLH
Evaluate equilibrium thermo properties	RGAS

<u>Operation</u>	<u>Location</u>
Arguments for RGAS — elliptic	EQUIB2
Arguments for RGAS — hyperbolic	EQILIB
Integrate from shock to body — elliptic	BREGN
Intersect ray with body — elliptic	BPTS
Intersect ray with body — hyperbolic	RAY
Evaluate polynomials for radius and slope	BDYFCT
Input body polynomials	BBIN
Evaluate viscosity at stagnation point	TRANS
Look up boundary-layer integrals	INTGRL
Calculate mass flux and velocity thickness	BLAYER
— elliptic region	
Iterate for point at edge of boundary-layer	COUPLE
— hyperbolic region	
Adjust shock-point coordinates to match mass flux — elliptic region	BREGN
New shock shape parameters by least-squares fit	LEAST
Select points for hyperbolic starting line and write to Unit 2	BRIDGE
Adjust body shape for best match at initial line	BLAYST
Extrapolate elliptic solution to body or boundary-layer edge	BRIDGE
Print elliptic region solution	OUT
Read M.O.C. starting line from Unit 2	START
Read M.O.C. starting line from cards	START
Manage M.O.C. calculation of hyperbolic region	FRMAIN

<u>Operation</u>	<u>Location</u>
Locate next ray	RAY
M.O.C. calculation at point on body surface	BODYB
Manage calculation of Prandtl-Meyer expansion	RAYB
Calculate flow conditions behind Prandtl-Meyer expansion fan	PRNDTL
M.O.C. calculation at point in interior of shock layer	FELD
Perform one cycle of interior point M.O.C. calculation	MOC SOL
Integrate for frozen temperature and velocity along streamline segment	STRMB
Integrate species conservation equations along streamline segment	REACTB
Derivatives of composition and vibrational energy in streamwise direction	DERAB
Interpolate for dependent variables	INTR
Test for completion (time or position)	STIP
Write restart file (Unit 10)	STIP
Rearrange storage omitting alternate points	DIVIDE
Print M.O.C. solution on ray	OUTPUT
Write communication file for BLIMP	OUTPUT
Calculate collision and plasma frequencies	ELDENT
M.O.C. solution at constant pressure boundary	BODYB

<u>Operation</u>	<u>Location</u>
Manage M.O.C. calculation with embedded shock	SHMAIN
Calculate initial angle for embedded shock	FLARE
Locate embedded shock and calculate flow	IMBED
Print diagnostic message and stop — elliptic	TRUBEL
Print diagnostic message and stop — MOC	PAUSE
Print diagnostic and continue	ERRMSG
Print diagnostic message and continue	CNVRGE
Read restart file (Unit 1), free-stream conditions, thermochemistry, body shape	BBIN
Read restart file and restart elliptic region calculation	BREGN
Read restart file and locate desired restart station	START

APPENDIX E

SHOCK SHAPE PARAMETERS

The nonequilibrium shock shape parameters RSHP, S1P, and S1 which have been obtained for various free-stream conditions and thermochemical options are tabulated in Table E-1. Unless otherwise indicated, the reaction set of Ref. 7 was used in making the calculations.

Table E-1. Nonequilibrium Shock Shape Parameters

U_∞ , Kfps	$q_\infty R_N$, gm/cm ²	RSHP/ R_N	S1P	S1 \times 100	RMS Dev $\times 10^4$	Comment
25	2.76×10^{-7}	1.2839	0.08412	—	3.80	No B.L., vib.
23	1.95×10^{-6}	1.1957	0.1473	1.283	4.302	No B.L., vib.
25.1	4.119×10^{-6}	1.1032	0.15163	0.739	7.455	B.L., no vib
14.7	7.11×10^{-6}	1.2566	0.0931	1.372	4.687	Vib., no B.L.
10'	2.0334×10^{-5}	1.1967	0.10437	1.197	2.119	NVIB = 0, w/ B.L.
12		1.1697	0.11161	1.064	5.101	
15		1.1154	0.11879	0.905	1.360	
17.1		1.1173	0.13880	0.927	4.060	
18		1.1186	0.14699	—	5.61	
19		1.1199	0.15474	0.930	7.47	
20		1.1192	0.15872	0.906	8.873	
21		1.1177	0.16137	0.877	10.08	
22		1.1127	0.16130	0.836	9.18	
24		1.1023	0.16430	0.781	5.68	
26		1.0976	0.16614	0.729	7.673	
28		1.0843	0.16117	0.656	4.765	
30	2.0334×10^{-5}	1.0708	0.15227	0.579	4.068	NVIB = 0, w/ B.L.
12.9	3.2×10^{-5}	1.2520	0.0768	1.728	1.584	Vib. + B.L.
10	4.0668×10^{-5}	1.1935	0.10420	1.195	5.718	
12		1.1709	0.11403	1.088	3.186	
15		1.1156	0.11924	0.908	2.446	
18		1.1159	0.14004	0.888	3.048	
20		1.1161	0.14164	0.808	1.638	
22		1.1077	0.14663	0.760	4.194	
25		1.0967	0.13812	0.630	1.920	
28		1.0832	0.13519	0.551	2.214	
30	4.0668×10^{-5}	1.0756	0.13365	0.508	4.208	
10	7.4703×10^{-5}	1.1962	0.10712	1.228	—	
12		1.1683	0.10961	1.045	4.409	
15		1.1068	0.09860	0.751	3.358	
18		1.1282	0.14343	0.910	2.233	
20		1.1225	0.13727	0.783	1.779	
22		1.1132	0.13007	0.675	1.523	
25		1.0997	0.12760	0.582	1.767	
28	7.4703×10^{-5}	1.0859	0.12667	0.516	1.898	
12	1.5225×10^{-4}	1.1695	0.10356	0.988	3.825	
15		1.1263	0.10732	0.817	3.750	
18		1.1313	0.14225	0.905	2.309	
20		1.1264	0.13611	0.777	1.867	
22	1.5225×10^{-4}	1.1166	0.12645	0.656	1.521	Vib. + B.L.
23	1.9×10^{-4}	1.1239	0.1611	0.679	7.302	Vib. + radiation
15	8.7×10^{-4}	1.1109	0.09562	0.622	4.506	Vib. + radiation

APPENDIX F EXAMPLES

The run times shown in Fig. 9 were obtained from calculations made with the input file "ENVELOPE." The sample shown in Fig. F-1 is actually a composite which includes the controls necessary to restart the blunt body calculation and to continue it into the Method-of-Characteristics calculation. All of the computations used the thermochemical data set NEWCHEM displayed in Fig. B-2. The reactions and rates in NEWCHEM are those discussed in Ref. 7.

Consider the following exercise:

Part 1. With NEWCHEM assigned to Unit 8 as in the example, set NEW = .T. to indicate a new run, and INAFT = 0 to limit calculation to the blunt body region in Namelist OPTIONS. Save the output file assigned to Unit 9 and submit the job, allowing 55 sec of CPU time if Cray X/MP is used.

Selected pages from the resulting printout are displayed in Figs. F-2a through F-2e. The table at the bottom of Fig. F-2a displays for each species the electron energy levels (HCFNT) and the degeneracy of each level (FCFNT). The ALPIJ matrix indicates the number of atoms of element *i* in species *j*. The input reaction data are echoed at the top of Fig. F-2b. The shock geometry calculated from the initial shock parameters appears next. The coordinates X, SZ, and SR are dimensionless, as is the curvature CURV. The shock angle SIGMA is in radians. The lower part of the figure is filled with status and error messages. MINRAY is the index of the lowest numbered ray still in the computing grid (the axis is numbered 4) and the number of repeated steps is one less than FLOP. The error messages may be interpreted with the aid of Table 11 and the species listed in Fig. F-1a. For example, B2(11) is the fifth species, i.e., O₂.

The results of the third shock iteration are displayed in Fig. F-2c. The average deviation between the desired and calculated boundary-layer edge points is quite acceptable (1.855×10^{-4}), but the relative error in flow angle fit on the junction ray (MAX DEV) is more than ten times the specified value of RMSTST and, therefore, the "DID NOT CONVERGE" message is issued. Note also that there are 76 records on the restart file.

The results of the 70th successful integration step are shown in Fig. F-2d. Only rays 16 and 17 are still active; 95 percent of the input mass flux on the other rays has been accounted for. The next six lines are written by subroutine BLAYST to report the results of the body adjustment procedure (Section 3.2) which moved the body slightly forward (compare the

first value of ZBDYN to the ZSTAG shown in Fig. F-2c) and decreased the nose diameter by 0.00005 (compare BDCN(2) with BDC(2)). The polynomial coefficients are normalized by the latest shock radius as are the coordinates of the intersection between the junction ray and the boundary-layer edge — BZ,BR.

Parts of the extrapolated results at the boundary-layer edge are shown in Fig. F-2e. Ray 4 is the axis and ray 17 is the junction ray.

Part 2. As part of the exercise, restart at step 65 of the blunt body calculation and attempt to continue onto the afterbody. Assign the restart file, which was written on Unit 9, to Unit 1. Set NEW = .F. in OPTION. Set ITAPE = 1, NRCORD = 65 in RESTART. Also set INAFT = 1 in \$CHANGE and choose ZETAMX = 0.6 in \$SUPER. Note that \$CHANGE must follow \$RESTART, and that this pair can go anywhere in the file between \$OPTIONS and \$SUPER.

The first page of the resulting output is shown in Fig. F-2f and the last page in Fig. F-2g. The Method-of-Characteristics calculation stopped after completing 7 rays with the message "ERROR at STATEMENT 11 SUBROUTINE CFFCNT," which means that the Mach number became subsonic. Sometimes round-off errors will allow computation past the test in CFFCNT but will stop the run with the message "ERROR AT STATEMENT 90 OF SUBROUTINE INTR," which means that the characteristic did not intersect either the previous ray or the known body or shock points. In any event the iteration was evidently diverging. The step size was probably too large for the rapid curvature of the body. The message "ITERATION NOT CONVERGING IN SUBROUTINE FELD," and the following line of numbers were written by subroutine DIGNOS. Since the message appears only once per ray at point number 27, the interior point computation evidently converged on the eighth iteration. To interpret the other numbers in the message, look at the arguments of the call to CNVRGE in FELD.

Part 3. As Part 3 of the exercise, resubmit the job files of Part 2 with just one change; in \$SUPER, decrease ZETAMX to 0.4.

The last two pages of the resulting printout are reproduced as Fig. F-2h. This run was stopped by subroutine STIP because the input time limit of 98 sec was exceeded. If the output file from Unit 10 was saved, the run may be continued by setting ITAPE = 2 and choosing an appropriate value for NRCORD somewhat less than the final value. Since the MOC calculation has a good start, although it is still on the spherical nose, it is probably possible to accelerate the computation by increasing ZETAMX to 0.6. Once the calculation is well past the sphere-cone junction, ZETAMX = 0.8 would probably maintain stability and further increase the marching speed.

The heat-transfer (QDOT) and FRICTION coefficients which appear at the top of Fig. F-2h are meaningless since the input of TWALL was neglected. The flow angle PHI at the boundary-layer edge (NPT=0) is slightly greater than the body angle (PHI BODY). Note that the average equilibrium indicator — AV.CHI — is small and negative close to the body but increases toward the shock indicating that the gas is recombining near the body and dissociating close to the shock where AV.CHI is positive.

```

ENVELOPE
  SPHERE-CONE: NON-EQUILIBRIUM WITH STANDARD RATES
$OPTIONS      LR=1,NVIB=0,INAF=1,NEW=.F.,TUNIT=1,UNIT='CGS' $
NEW=.T.,      ;THIS IS A NEW RUN.
MODEL=0,      ;NON-EQUILIBRIUM AS IN SECTION 2.2.1
NVIB=0,       ;EQUILIBRIUM VIBRATION
UNIT=1,       ;INPUT ALL FREE STREAM CONDITIONS
UNIT='CGS',   ;USE CGS UNITS  DEFAULT
INBLR=1,      ;INCLUDE VISCOUS DISPLACEMENT OPTION
INAF=0        ;DO ONLY BLUNT BODY CALCULATION
$
$UPSTREAM VEL=6.0962E+05,PRES=1.0132E05,TEMP=300.,
VEL=6.0962E+05, ;CENTERLINE VELOCITY IN CM/SEC
PRES=1.0132E05, ;FREE STREAM PRESSURE IN DYNE/CM**2
TEMP=300.,      ;FREE STREAM STATIC TEMPERATURE DEG.K
FRACTN=32.19490E-05,;MOLES/GRAM OF AR  DEFAULT VALUE
72.43929E-04,   ; " " " "
26.96274E-03,   ; " " " "
$
$SHOCK RSHR=0.71527,;RADIUS OF CURVATURE OF SHOCK AT AXIS IN UNITS
S1P=0.13611,    ; SPECIFIED IN OPTIONS NAMELIST
S1=0.00777
$
$BODY REXP=2.,C1=1.27,C2=-1.,MORE=.T. $
REXP=2.,        ; EXPONENT OF (R-RJUNC) TERM--EQN 53
C1=1.27,        ; TWICE THE NOSE RADIUS-SEE EQ.54.
C2=-1.,         ; SEE EQN.54
MORE=.T.,       ; ANOTHER BODY SEGMENT FOLLOWS.
$BODY RJUNC=0.613933,ZJUNC=.472792,REXP=1.,C1=.2642114,MORE=.F. $
RJUNC=0.613933, ;RADIAL COORD. OF SPHERE-CONE JUNCTION-DIMENSIONAL
ZJUNC=.472792,  ;AXIAL COORDINATE OF SPHERE-CONE JUNCTION
REXP=1.0,       ;FIRST POWER OF R FOR CONE
C1=.2642114,    ;TANGENT OF HALF CONE ANGLE
MORE=.F.,       ;LAST SEGMENT
$
$CONTROL      BSIT=3,DELX=.05,XO=.05,DELMIN=1.0E-9,GAMTST=1.E-7,
NBSIT=3,       ; TAKE THREE GLOBAL ITERATIONS
IPRNT=5,       ; STATUS REPORT EVERY 5TH STEP
SKAP=0.5,      ;DECREASE DAMPING--EQN.50. DEFAULT IS .35
PSIRAT=.05,   ;STOP WHEN .95 OF MASS FLUX IS ACCOUNTED FOR.
ERROR=1.0E-6, ;DEFAULT CONVERGENCE CRITERION ALL ITERATIONS.
DELMIN=1.E-9, ;MINIMUM STEP SIZE. INITIAL SIZE=100*DELMIN.
DELX=.05,      ;AVERAGE RAY SPACING. DEFAULT IS 0.04
XO=.05,        ;FIRST OFF AXIS RAY AT X=.05. INCLUDE AXIS.
GAMTST=1.E-07,;MINIMUM MOLE FRACTION --DEFAULT VALUE=1E-7
METHOD=10,     ;USE 9 CORRECTORS.LOMAX ALGORITHM APPENDIX A
TIME=98.
$
$RESTART ITAPE=1,NRCORD=65 $
ITAPE=1,       ;RESTART IN BLUNT BODY CODE IF NEW=.F.
NRCORD=65,     ;RESUME CALCULATION AT 65TH RECORD.
$
$CHANGE      INAF=1, ;IF A RESTART, CHANGE TO INCLUDE M.O.C.CALCULATION
$
$SUPER ZMAX=10.6,NMAX=29,MODRAY=5,ZETAMX=0.4,METHGD=10,ION=1 $

```

Figure F-1. Input file 'ENVELOPE' for nonequilibrium run.

CUNIFLOW														
RUN NO. ENVELOPE														
09/03/88														
SPHERE-CONE: NON-EQUILIBRIUM WITH STANDARD RATES														
PRESSURE DYNE/SQ.CM		TEMPERATURE DEG.K		DENSITY GM/CU.CM		VELOCITY CM/SEC		MOLECULAR WEIGHT						
1.013200E+05		3.000000E+02		1.1764337E-04		6.096200E+05		2.8961483E+01						
INITIAL SHOCK PARAMETERS - RSHP = 0.7153 SIP = 1.36110E-01 S1 = 7.77000E-03														
DELX = 0.0500 XO = 0.0500														
ZBDY	YBDY	BD1	BD2	BDC(1)	BDC(2)	BDC(3)	BDC(4)	BDC(5)						
0.000000E+00	0.000000E+00	2.000000E+00	0.000000E+00	0.000000E+00	1.270000E+00	1.000000E+00	0.000000E+00	0.000000E+00						
4.727920E-01	6.139330E-01	1.000000E+00	0.000000E+00	0.000000E+00	2.642114E-01	0.000000E+00	0.000000E+00	0.000000E+00						
EMISSIVITY = 0.000000E+00 INITIAL WALL TEMP = 0.000000E+00DEG.K														
FREE STREAM COMPOSITION MOLES/GM														
1 O	0.000000E+00	2 N	0.000000E+00	3 E-	0.000000E+00	4 AR	3.219490E-04	5 O2	7.243929E-03					
6 N2	2.896274E-02	7 NO	0.000000E+00	8 NO+	0.000000E+00									
IUNIT	INBLR	INDWT	INAFI	INDIM	IPRNT	NBDY	MODEL	NSPEC	NR	NC	NVIB	NRAD	NXDIV	METHOD
1	1	0	0	1	5	2	0	8	10	4	0	0	20	10
SLAM	SKAP	ERROR	RMSTST	TESTM	TTEST	GAMTST	DELMIN							
-5.000000E-01	5.000000E-01	1.000000E-06	5.000000E-04	1.100000E+00	1.500000E-01	1.000000E-07	1.000000E-09							
FREE STREAM VIBRATIONAL ENERGIES 1.0164367E+08 3.6607761E+06 ERGS/MOLE														
FREE STREAM MACH NO. = 17.5550														
XLMBDA = 4.3150984E+02 HINF = 2.1924662E+02 BIGAM = 1.4001996E+00														
SPECIES														
ALPIJ	HCFNT													
	FCFNT													
O	0.00000E+00	0.76284E+00	0.10885E+01	0.76122E+02	0.16211E+03	0.00000E+00	0.00000E+00	0.00000E+00	0.00000E+00					
1.0.0.0.0.0.0.0.	0.50000E+01	0.30000E+01	0.10000E+01	0.50000E+01	0.10000E+01	0.00000E+00	0.00000E+00	0.00000E+00	0.00000E+00					
N	0.00000E+00	0.92242E+02	0.92495E+02	0.13836E+03	0.42264E+03	0.00000E+00	0.00000E+00	0.00000E+00	0.00000E+00					
0.1.0.0.0.0.0.0.	0.40000E+01	0.60000E+01	0.40000E+01	0.60000E+01	0.60000E+01	0.12000E+02	0.00000E+00	0.00000E+00	0.00000E+00					
E-	0.00000E+00	0.00000E+00	0.00000E+00	0.00000E+00	0.00000E+00	0.00000E+00	0.00000E+00	0.00000E+00	0.00000E+00					
0.0.1.0.0.0.0.0.	0.20000E+01	0.00000E+00	0.00000E+00	0.00000E+00	0.00000E+00	0.00000E+00	0.00000E+00	0.00000E+00	0.00000E+00					
AR	0.00000E+00	0.44686E+03	0.44977E+03	0.00000E+00	0.00000E+00	0.00000E+00	0.00000E+00	0.00000E+00	0.00000E+00					
0.0.0.1.0.0.0.0.	0.10000E+01	0.50000E+01	0.30000E+01	0.00000E+00	0.00000E+00	0.00000E+00	0.00000E+00	0.00000E+00	0.00000E+00					
O2	0.00000E+00	0.37983E+02	0.63353E+02	0.17312E+03	0.23893E+03	0.00000E+00	0.00000E+00	0.00000E+00	0.00000E+00					
2.0.0.0.0.0.0.0.	0.30000E+01	0.20000E+01	0.10000E+01	0.30000E+01	0.30000E+01	0.00000E+00	0.00000E+00	0.00000E+00	0.00000E+00					
N2	0.00000E+00	0.24110E+03	0.28601E+03	0.28783E+03	0.00000E+00	0.00000E+00	0.00000E+00	0.00000E+00	0.00000E+00					
0.2.0.0.0.0.0.0.	0.10000E+01	0.30000E+01	0.60000E+01	0.10000E+01	0.00000E+00	0.00000E+00	0.00000E+00	0.00000E+00	0.00000E+00					
NO	0.00000E+00	0.58052E+00	0.21092E+03	0.22032E+03	0.00000E+00	0.00000E+00	0.00000E+00	0.00000E+00	0.00000E+00					
1.1.0.0.0.0.0.0.	0.20000E+01	0.20000E+01	0.20000E+01	0.40000E+01	0.00000E+00	0.00000E+00	0.00000E+00	0.00000E+00	0.00000E+00					
NO+	0.00000E+00	0.19336E+03	0.28356E+03	0.35028E+03	0.35169E+03	0.00000E+00	0.00000E+00	0.00000E+00	0.00000E+00					
1.1.*	0.0.0.0.	0.10000E+01	0.60000E+01	0.30000E+01	0.00000E+01	0.20000E+01	0.00000E+00	0.00000E+00	0.00000E+00					

a. Output from nonequilibrium run 'ENVELOPE'
Figure F-2. Sample calculations.

NRCORD = 35 FLOP = 8. MINRAY= 4 Y=0.31045E-010.85050E-030.00000		LAST STEP = 0.00000	PSI(MMIN)=			
B2(8) NEGATIVE ON RAY 4RUNGE-KUTTA STEP10 Y = 3.565E-02 DELY = 1.362E-03						
NRCORD = 40 FLOP = 9. MINRAY= 4 Y=0.35104E-010.74751E-030.00000		LAST STEP = 0.00000	PSI(MMIN)=			
B2(11) NEGATIVE ON RAY 4RUNGE-KUTTA STEP10 Y = 3.788E-02 DELY = 1.025E-03						
NRCORD = 45 FLOP = 10. MINRAY= 4 Y=0.38076E-010.81416E-030.00000		LAST STEP = 0.00000	PSI(MMIN)=			
B2(11) NEGATIVE ON RAY 4RUNGE-KUTTA STEP10 Y = 3.919E-02 DELY = 7.431E-04						
NRCORD = 50 FLOP = 11. MINRAY= 4 Y=0.40102E-010.47811E-030.00000		LAST STEP = 0.00000	PSI(MMIN)=			
B2(11) NEGATIVE ON RAY 4RUNGE-KUTTA STEP 3 Y = 4.119E-02 DELY = 5.693E-04						
NRCORD = 55 FLOP = 12. MINRAY= 4 Y=0.41643E-010.35343E-030.00000		LAST STEP = 0.00000	PSI(MMIN)=			
B2(11) NEGATIVE ON RAY 4RUNGE-KUTTA STEP10 Y = 4.293E-02 DELY = 3.894E-04						
NRCORD = 60 FLOP = 13. MINRAY= 7 Y=0.42568E-010.23853E-030.00000		LAST STEP = 0.00000	PSI(MMIN)=			
NRCORD = 65 FLOP = 13. MINRAY= 10 Y=0.44691E-010.52063E-030.14063E-01		LAST STEP = 0.13718E-01	PSI(MMIN)=			
NRCORD = 70 FLOP = 13. MINRAY= 13 Y=0.47318E-010.57717E-030.21453E-01		LAST STEP = 0.23822E-01	PSI(MMIN)=			
NRCORD = 75 FLOP = 13. MINRAY= 15 Y=0.51732E-010.10924E-020.51830E-01		LAST STEP = 0.42974E-01	PSI(MMIN)=			
NRCORD = 80 FLOP = 13. MINRAY= 18 Y=0.57497E-010.10447E-020.52144E-01		LAST STEP = 0.57769E-01	PSI(MMIN)=			
NRCORD = 84Y(3)=0.60230E-01DELY(3)=						
ITERATION NO. 1 SHOCK RADIUS = 0.71527 SIP = 0.13611 S1 = 0.00777						
RMS DEVIATION = 4.3546334E-04 MAX DEV = 1.4883856E-02 ZSTAG = 4.4316737E-02						
NEW SHOCK RADIUS = 7.1415511E-01NEW SHOCK PARAMETERS SIP= 1.3832081E-01 S1= 7.8921060E-03						
SHOCK GEOMETRY						
M	X(M)	SZ(M)	SR(M)	SIGMA	CURV(M)	
1	0.50000E-01	0.12498E-02	0.49979E-01	1.5208	-1.0004	
2	0.10000	0.49970E-02	0.99833E-01	1.4707	-1.0013	
3	0.15000	0.11234E-01	0.14944	1.4207	-1.0022	
4	0.20000	0.19949E-01	0.19867	1.3705	-1.0023	
5	0.25000	0.31117E-01	0.24740	1.3205	-0.9966	
6	0.30000	0.44709E-01	0.29551	1.2705	-0.98617	
7	0.35000	0.60678E-01	0.34289	1.2209	-0.98799	
8	0.40000	0.78966E-01	0.38942	1.1718	-0.97535	
9	0.45000	0.99500E-01	0.43500	1.1235	-0.95781	
10	0.50000	0.12219	0.47955	1.0761	-0.93526	
11	0.55000	0.14694	0.52298	1.0300	-0.90793	
12	0.60000	0.17363	0.56526	0.98538	-0.87635	
13	0.65000	0.20215	0.60633	0.94243	-0.84128	
14	0.70000	0.23238	0.64615	0.90130	-0.80358	
15	0.75000	0.26417	0.68474	0.86210	-0.76416	
16	0.80000	0.29742	0.72208	0.82490	-0.72390	
17	0.85000	0.33200	0.75818	0.78971	-0.68358	
18	0.90000	0.36779	0.79310	0.75653	-0.64383	
19	0.95000	0.40468	0.82684	0.72531	-0.60520	
20	1.0000	0.44258	0.85945	0.69598	-0.56805	
NRCORD = 5 FLOP = 1. MINRAY= 4 Y=0.31000E-050.16000E-050.00000		LAST STEP = 0.00000	PSI(MMIN)=			
NRCORD = 10 FLOP = 1. MINRAY= 4 Y=0.10230E-030.51200E-040.00000		LAST STEP = 0.00000	PSI(MMIN)=			
B2(11) NEGATIVE ON RAY 4RUNGE-KUTTA STEP10 Y = 1.638E-03 DELY = 8.192E-04						
NRCORD = 15 FLOP = 2. MINRAY= 4 Y=0.13823E-020.46930E-030.00000		LAST STEP = 0.00000	PSI(MMIN)=			
NRCORD = 20 FLOP = 2. MINRAY= 4 Y=0.10497E-010.34992E-020.00000		LAST STEP = 0.00000	PSI(MMIN)=			
B2(11) NEGATIVE ON RAY 4RUNGE-KUTTA STEP10 Y = 1.550E-02 DELY = 5.000E-03						
B2(11) NEGATIVE ON RAY 4RUNGE-KUTTA STEP10 Y = 1.834E-02 DELY = 4.147E-03						
NRCORD = 25 FLOP = 4. MINRAY= 4 Y=0.20047E-010.30375E-020.00000		LAST STEP = 0.00000	PSI(MMIN)=			
B2(13) NEGATIVE ON RAY 4RUNGE-KUTTA STEP 9 Y = 2.316E-02 DELY = 3.110E-03						
B2() NEGATIVE ON RAY 4RUNGE-KUTTA STEP10 Y = 2.516E-02 DELY = 2.624E-03						

b. Concluded
Figure F-2. Continued.

```

B2( 11) NEGATIVE ON RAY 4RUNGE-KUTTA STEP10 Y = 2.516E-02 DELY = 2.624E-03
NRCORD = 30 FLOP = 6. MINRAY = 4 Y=0.25945E-010.17364E-020.00000 LAST STEP =0.00000 PSI(MMIN)=

B '3) NEGATIVE ON RAY 4RUNGE-KUTTA STEP 9 Y = 3.016E-02 L = 2.187E-03

B2( 11) NEGATIVE ON RAY 4RUNGE-KUTTA STEP10 Y = 3.268E-02 DELY = 1.728E-03
NRCORD = 35 FLOP = 8. MINRAY = 4 Y=0.31045E-010.85050E-030.00000 LAST STEP =0.00000 PSI(MMIN)=

B2( 8) NEGATIVE ON RAY 4RUNGE-KUTTA STEP10 Y = 3.565E-02 DELY = 1.362E-03
NRCORD = 40 FLOP = 9. MINRAY = 4 Y=0.35104E-010.74751E-030.00000 LAST STEP =0.00000 PSI(MMIN)=

B2( 11) NEGATIVE ON RAY 4RUNGE-KUTTA STEP10 Y = 3.788E-02 DELY = 1.025E-03
NRCORD = 45 FLOP = 10. MINRAY = 4 Y=0.38076E-010.61416E-030.00000 LAST STEP =0.00000 PSI(MMIN)=

B2( 11) NEGATIVE ON RAY 4RUNGE-KUTTA STEP10 Y = 3.949E-02 DELY = 7.431E-04
NRCORD = 50 FLOP = 11. MINRAY = 4 Y=0.40102E-010.47841E-030.00000 LAST STEP =0.00000 PSI(MMIN)=

B2( 11) NEGATIVE ON RAY 4RUNGE-KUTTA STEP 8 Y = 4.119E-02 DELY = 5.693E-04
NRCORD = 55 FLOP = 12. MINRAY = 6 Y=0.41643E-010.35942E-030.00000 LAST STEP =0.00000 PSI(MMIN)=
NRCORD = 60 FLOP = 12. MINRAY = 11 Y=0.44266E-010.77875E-030.16330E-01 LAST STEP =0.17967E-01 PSI(MMIN)=
NRCORD = 65 FLOP = 12. MINRAY = 14 Y=0.48054E-010.42358E-030.34947E-01 LAST STEP =0.38813E-01 PSI(MMIN)=
NRCORD = 70 FLOP = 12. MINRAY = 16 Y=0.53550E-010.17339E-020.66370E-01 LAST STEP =0.65100E-01 PSI(MMIN)=
NRCORD = 76Y(3)=0.59217E-01IDELY(3)=

ITERATION NO. 3 SHRICK RADIUS = 0.71321 STP = 0.13775 S1 = 0.00786
RMS DEVIATION = 1.8551394E-04 MAX DEV = 1.096R413E-02 ZSTAG = 4.4325342E-02

PROGRAM DID NOT CONVERGE
    
```

VALUES AT INTERSECTION OF RAY WITH BODY

RAY	ZB	RB	PHIB	DELTA	FLUX
5	4.56072E-02	4.77592E-02	1.51713E+00	2.82715E-03	5.15241E-04
6	4.94480E-02	9.53713E-02	1.46347E+00	2.86453E-03	2.05542E-03
7	5.58339E-02	1.42691E-01	1.40984E+00	2.90300E-03	4.60399E-03
8	6.47421E-02	1.89576E-01	1.35623E+00	2.95634E-03	8.13373E-03
9	7.61416E-02	2.35887E-01	1.30266E+00	3.02863E-03	1.26071E-02
10	8.99945E-02	2.81490E-01	1.24912E+00	3.12332E-03	1.79765E-02
11	1.06256E-01	3.26258E-01	1.19562E+00	3.24326E-03	2.41847E-02
12	1.24876E-01	3.70065E-01	1.14215E+00	3.39549E-03	3.11659E-02
13	1.45800E-01	4.12792E-01	1.08871E+00	3.58052E-03	3.88441E-02
14	1.68966E-01	4.54325E-01	1.03529E+00	3.80291E-03	4.71354E-02
15	1.94311E-01	4.94552E-01	9.81878E-01	4.06501E-03	5.59476E-02
16	2.21765E-01	5.33366E-01	9.28475E-01	4.36723E-03	6.51811E-02
17	2.51253E-01	5.70662E-01	8.75067E-01	4.70077E-03	7.47275E-02
18	2.82699E-01	6.06339E-01	8.21646E-01	5.11388E-03	8.44827E-02

c. Output from nonequilibrium run 'ENVELOPE'

Figure F-2. Continued.

ENVELOPE										
STEP SIZE = 1.23661E-03			NUMBER OF SUCCESSFUL STEPS = 70				DISTANCE FROM SHOCK = 3.81923E-02 CM.			
RAY	Z CM	R CM	P DYNE/CM**2	I DEG. K	RHD GM/CC	XMW GM/MOL	VTOT CM/SEC	FLOW ANG.		
MOL/GM	HTOT ERG/GM	S CAL/GM K	AVER. CHI E-	FL. DENS. #/CC	MACH NO. D2	FLUX RATIO N2	RAD ERG/GM-SEC NO	PSI GM/SEC ND+		
16	1.5564476E-01	3.8206978E-01	2.2325419E+07	6.3910102E+03	9.7413745E-04	2.3185549E+01	3.2834429E+05	5.2895499E+01		
	1.8845574E+11	2.5706930E+00	-3.7726495E-01	4.7952845E+15	1.9270028E+00	1.0189992E+00	0.0000000E+00	2.4212094E+00		
	1.3215459E-02	3.9715914E-03	8.1702828E-06	3.2194900E-04	8.1912302E-05	2.4422657E-02	1.1004040E-03	8.1702828E-06		
17	1.7504269E-01	4.1001600E-01	2.0307999E+07	6.1597107E+03	9.2882058E-04	2.3423526E+01	3.5009930E+05	5.0066035E+01		
	1.8852134E+11	2.5513161E+00	-5.2232149E-01	3.6275310E+15	2.1015584E+00	1.5468919E+00	0.0000000E+00	4.2133719E+00		
	1.3146853E-02	3.1671880E-03	6.4821975E-06	3.2194900E-04	9.8414458E-05	2.4807058E-02	1.1376942E-03	6.4821975E-06		
BODY POLYNOMIALS BEFORE ADJUSTMENT										
ZBDY	YBDY	BDC(L)								
0.0000000E+00	0.0000000E+00	0.0000000E+00	1.7806877E+00	-1.0000000E+00	0.0000000E+00	0.0000000E+00	0.0000000E+00	0.0000000E+00	0.0000000E+00	0.0000000E+00
6.6290936E-01	8.6080545E-01	0.0000000E+00	2.6421140E-01	0.0000000E+00	0.0000000E+00	0.0000000E+00	0.0000000E+00	0.0000000E+00	0.0000000E+00	0.0000000E+00
BODY POLYNOMIALS AFTER ADJUSTMENT										
ZBDYN	YBDYN	BDCN(L)								
4.4247911E-02	0.0000000E+00	0.0000000E+00	1.7798565E+00	-1.0000000E+00	0.0000000E+00	0.0000000E+00	0.0000000E+00	0.0000000E+00	0.0000000E+00	0.0000000E+00
7.0684784E-01	8.6040365E-01	0.0000000E+00	2.6421140E-01	0.0000000E+00	0.0000000E+00	0.0000000E+00	0.0000000E+00	0.0000000E+00	0.0000000E+00	0.0000000E+00
BZ = 2.5107916E-01BR = 5.7039527E-01 BODY ANGLE = 8.7506723E-01										

d. Output from nonequilibrium run 'ENVELOPE'
Figure F-2. Continued.

M	ZB	INT	ARC	PHIB
4	4.450953E-02	0.000000E+00	0.000000E+00	1.5707963E+00
5	4.580719E-02	4.775916E-02	4.777177E-02	1.5171293E+00
6	4.944804E-02	9.507134E-02	9.508626E-02	1.4634730E+00
7	5.583392E-02	1.420910E-01	1.422873E-01	1.4088371E+00
8	6.474207E-02	1.899767E-01	1.910107E-01	1.3562295E+00
9	7.614162E-02	2.354869E-01	2.367042E-01	1.3026556E+00
10	8.999453E-02	2.814904E-01	2.830654E-01	1.2491180E+00
11	1.062562E-01	3.262576E-01	3.289147E-01	1.1956162E+00
12	1.248764E-01	3.700646E-01	3.739147E-01	1.1421474E+00
13	1.457999E-01	4.127920E-01	4.291701E-01	1.0887061E+00
14	1.689662E-01	4.544249E-01	4.767271E-01	1.0352855E+00
15	1.943109E-01	4.945521E-01	5.242727E-01	9.818778E-01
16	2.217645E-01	5.331667E-01	5.718142E-01	9.284747E-01
17	2.510791E-01	5.703952E-01	6.193596E-01	8.750672E-01
18	2.821434E-01	6.069199E-01	6.669174E-01	8.311211E-01

M	DELTA	PSIBAR	QDOT	ENRAD	FRICT	TW	GWALL
4	0.000000E+00	0.000000E+00	0.000000E+00	0.000000E+00	0.000000E+00	0.000000E+00	0.000000E+00
5	2.827150E-03	5.183409E-04	7.319805E+11	0.000000E+00	1.9679694E-03	0.000000E+00	0.000000E+00
6	2.864526E-03	2.054753E-03	7.274668E+11	0.000000E+00	3.9327244E-03	0.000000E+00	0.000000E+00
7	2.903000E-03	4.602322E-03	7.1998594E+11	0.000000E+00	5.8907991E-03	0.000000E+00	0.000000E+00
8	2.956339E-03	8.1206064E-03	7.096316E+11	0.000000E+00	7.8384079E-03	0.000000E+00	0.000000E+00
9	3.028633E-03	1.2602004E-02	6.965088E+11	0.000000E+00	9.7710838E-03	0.000000E+00	0.000000E+00
10	3.1233159E-03	1.7968942E-02	6.8074053E+11	0.000000E+00	1.1683439E-02	0.000000E+00	0.000000E+00
11	3.243259E-03	2.417404E-02	6.6245593E+11	0.000000E+00	1.3568769E-02	0.000000E+00	0.000000E+00
12	3.3954916E-03	3.115117E-02	6.4190650E+11	0.000000E+00	1.5419618E-02	0.000000E+00	0.000000E+00
13	3.5805186E-03	3.8824070E-02	6.1921279E+11	0.000000E+00	1.7225950E-02	0.000000E+00	0.000000E+00
14	3.8029141E-03	4.7109362E-02	5.9464618E+11	0.000000E+00	1.8977251E-02	0.000000E+00	0.000000E+00
15	4.0650068E-03	5.5911368E-02	5.6848887E+11	0.000000E+00	2.0661817E-02	0.000000E+00	0.000000E+00
16	4.3672306E-03	6.5132821E-02	5.4103710E+11	0.000000E+00	2.2266414E-02	0.000000E+00	0.000000E+00
17	4.7007701E-03	7.4663995E-02	5.125030E+11	0.000000E+00	2.3778744E-02	0.000000E+00	0.000000E+00
18	5.110348E-03	8.4399288E-02	4.8348615E+11	0.000000E+00	2.5180581E-02	0.000000E+00	0.000000E+00

d. Concluded
Figure F-2. Continued.

VALUES AT BOUNDARY LAYER EDGE FOLLOW

ENVELOPE

STEP SIZE = 1.23661E-03 NUMBER OF SUCCESSFUL STEPS = 70 DISTANCE FROM SHOCK = 3.81922E-02 CM.

RAY	Z CM HTDT ERG/GM	R CM S CAL/GM K	P DYNE/CM+2 AVER. CHI	T DEG K EL. DENS. #/CC COMPOSITION IN AR	RHO GM/CC MACH NO. MOLFS PER GRAM O2	XMW GM/MOL FLUX RATIO N2	VTOT CM/SEC RAD. ERG/GM-SEC NO	FLOW ANG. PSI GM/SEC NO1
4	3.1744542E-02 1.8775110E+11 1.3462238E-02	0.0000000E+00 2.5931505E+00 1.0748181E-02	4.1935464E+07 -3.0623044E-04 2.3533478E-05	7.6963009E+03 1.9915681E+16 3.2194900E-04	1.4045979E-03 9.0134611E-04 3.7403379E-05	2.1432845E+01 1.0000000E+00 2.1113243E-02	1.7398792E+02 0.0000000E+00 9.2728000E-04	0.0000000E+00 0.0000000E+00 2.3533478E-05
5	3.0547773E-02 1.8775905E+11 1.3460315E-02	3.4161276E-02 2.6921945E+00 1.0687135E-02	4.1751641E+07 -8.6274630E-04 2.3391011E-05	7.6876040E+03 1.9744023E+16 3.2194900E-04	1.4009725E-03 1.5471073E-01 3.7850373E-05	2.1447384E+01 1.0000000E+00 2.1143251E-02	2.9819011E+04 0.0000000E+00 9.2845161E-04	7.9718770E+01 1.8796141E-02 2.3391011E-05
6	3.3234265E-02 1.8778287E+11 1.3456386E-02	6.8223587E-02 2.6892877E+00 1.0508989E-02	4.1259716E+07 -2.3300416E-02 2.2980788E-05	7.6623997E+03 1.9744023E+16 3.2194900E-04	1.3917496E-03 3.0802846E-01 3.7557622E-05	2.1489531E+01 1.0000000E+00 2.1230067E-02	5.9225683E+04 0.0000000E+00 9.3337639E-04	8.0318565E+01 7.4958043E-02 2.2980788E-05
7	3.7710863E-02 1.8782237E+11 1.3447189E-02	1.0208758E-01 2.6844759E+00 1.0216132E-02	4.0441761E+07 -8.5332011E-03 2.2302119E-05	7.6201637E+03 1.8492123E+16 3.2194900E-04	1.2767065E-03 4.6264730E-01 3.9288410E-05	2.1559818E+01 1.0000000E+00 2.1373628E-02	8.8595530E+04 0.0000000E+00 9.3975008E-04	7.8492197E+01 1.6789417E-01 2.2302119E-05
8	4.3976469E-02 1.8778767E+11 1.3435801E-02	1.3565300E-01 2.6777972E+00 9.8112644E-02	3.9202846E+07 -1.7811790E-02 2.1367290E-05	7.5607309E+03 1.9270061E+16 3.2194900E-04	1.3541382E-03 6.1862150E-01 4.0534638E-05	2.1657436E+01 1.0000000E+00 2.1571614E-02	1.1778270E+05 0.0000000E+00 9.4962000E-04	7.0006127E+01 2.9660711E-01 2.1367290E-05
9	5.2025021E-02 1.8794381E+11 1.3421455E-02	1.6881919E-01 2.6593202E+00 9.7014012E-02	3.7851941E+07 -3.3730648E-02 2.0192512E-05	7.4823845E+03 1.6124756E+16 3.2194900E-04	1.3253963E-03 7.7614487E-01 4.2018642E-05	2.1781634E+01 1.0000000E+00 2.1820856E-02	1.4668421E+05 0.0000000E+00 9.6217353E-04	7.3311577E+01 0.0000000E+00 2.0192512E-05
10	6.1842990E-02 1.8801975E+11 1.3403492E-02	2.0148613E-01 2.6591387E+00 8.8962260E-02	3.6118508E+07 -4.8076217E-02 1.8800469E-05	7.3857725E+03 1.4611948E+16 3.2194900E-04	1.2899782E-03 1.3526041E-01 4.4278399E-05	2.1931134E+01 1.0000000E+00 2.2116722E-02	1.7515473E+05 0.0000000E+00 9.7700908E-04	7.0446085E+01 6.551273E-01 1.8800469E-05
11	7.3406913E-02 1.8809955E+11 1.3381681E-02	2.3355621E-01 2.6473712E+00 8.0082368E-02	3.4129901E+07 -6.2661027E-02 1.7222017E-05	7.2698110E+03 1.2950766E+16 3.2194900E-04	1.2481144E-03 1.0963289E+00 4.7663786E-05	2.2103942E+01 1.0000000E+00 2.2453197E-02	2.0304933E+05 0.0000000E+00 9.9362780E-04	6.7501104E+01 8.8187691E-01 1.7222017E-05
12	8.6682256E-02 1.8817827E+11 1.3356869E-02	2.6493626E-01 2.6341652E+00 7.2528811E-02	3.1931900E+07 -9.0684794E-02 1.5497613E-05	7.1340531E+03 1.1208058E+16 3.2194900E-04	1.2003517E-03 1.2590518E+00 5.1581988E-05	2.2297046E+01 1.0000000E+00 2.2822387E-02	2.3020526E+05 0.0000000E+00 1.0123277E-03	6.4518157E+01 1.1364047E+00 1.5497613E-05
13	1.0162035E-01 1.8825209E+11 1.3328619E-02	2.9554080E-01 2.6197017E+00 6.4494639E-02	2.9582794E+07 -1.3095272E-01 1.3674371E-05	6.9780579E+03 1.4548020E+16 3.2194900E-04	1.1475933E-03 1.4234978E+00 5.6499969E-05	2.2506639E+01 1.0000000E+00 2.3214889E-02	2.5646091E+05 0.0000000E+00 1.0325644E-03	6.1531843E+01 1.4163144E+00 1.3674371E-05
14	1.1815729E-01 1.8832074E+11 1.3296341E-02	3.2529555E-01 2.6041782E+00 5.6193493E-02	2.7149885E+07 -1.8715599E-01 1.806864E-05	6.8019440E+03 1.7618223E+16 3.2194900E-04	1.0911189E-03 1.5296118E+00 6.2816904E-05	2.2728166E+01 1.0000000E+00 2.3620124E-02	2.8165524E+05 0.0000000E+00 1.0540767E-03	5.8570813E+01 1.7195281E+00 1.806864E-05
15	1.3621325E-01 1.8838806E+11 1.3250091E-02	3.5414132E-01 2.5878012E+00 4.7867359E-02	2.4705227E+07 -2.6573033E-01 9.9536483E-06	6.6061849E+03 1.1923105E+16 3.2194900E-04	1.0325555E-03 1.7573643E+00 7.1061114E-05	2.2956333E+01 1.0000000E+00 2.4026530E-02	3.0564838E+05 0.0000000E+00 1.0767312E-03	5.5689358E+01 2.0396645E+00 9.9536483E-06
16	1.5509395E-01 1.8845574E+11 1.3215876E-02	3.8203719E-01 2.5707505E+00 3.9726527E-02	2.2316132E+07 -3.7916578E-01 8.1712156E-06	6.3909993E+03 4.7938081E+16 3.2194900E-04	9.7372635E-04 1.9269066E+00 8.1871889E-05	2.3185151E+01 1.0000000E+00 2.4422294E-02	3.2832860E+05 0.0000000E+00 1.1000672E-03	5.2902517E+01 2.3769661E+00 8.1712156E-06
17	1.7649814E-01 1.8852132E+11 1.3163374E-02	4.0895910E-01 2.5532584E+00 3.2000877E-02	2.0020463E+07 -5.3869943E-01 6.5121892E-06	6.1572420E+03 3.5920748E+16 3.2194900E-04	9.1550625E-04 2.0986269E+00 9.6447380E-05	2.3409960E+01 1.0000000E+00 2.4796902E-02	3.4963331E+05 0.0000000E+00 1.1250767E-03	5.0226672E+01 2.7237663E+00 6.5121892E-06

DRAG = 1.5211207E+07 DYNES

e. Data extrapolated to boundary-layer edge
Figure F-2. Continued.

CUNIFLOW

RUN NO. ENVELOP
09/02/88

SPHERE-CONE: NON-EQUILIBRIUM WITH STANDARD RATES

CONTINUATION OF RUN ENVELOP FROM RECORD 85 SEGMENT 1

NRCORD = 70 FLOP = 12 MINRAY = 17 Y-O.54066E-010.51623E-030.58648E-01 LAST STEP = 0.65100E-01 PSI(MMIN)=
NRCORD= 75Y(3)=0.59216E-01DELTA(3)=

ITERATION NO. 3 SPOCK RADIUS = 0.71321 S1P = 0.13775 S1 = 0.00786
RMS DEVIATION = 1.8557528E-04 MAX DEV = 1.0975208E-02 ZSTAG = 4.4325342E-02

PROGRAM DID NOT CONVERGE

VALUES AT INTERSECTION OF RAY WITH BODY

RAY	ZB	RB	PHIB	DELTA	FLUX
5	4.56072E-02	4.77592E-02	1.51713E+00	2.82715E-03	5.15241E-04
6	4.94480E-02	9.53713E-02	1.46347E+00	2.86453E-03	2.05542E-03
7	5.58339E-02	1.42691E-01	1.40984E+00	2.90300E-03	4.60399E-03
8	6.47421E-02	1.89576E-01	1.35623E+00	2.95634E-03	8.13373E-03
9	7.61416E-02	2.35887E-01	1.30266E+00	3.02863E-03	1.26071E-02
10	8.99945E-02	2.81490E-01	1.24912E+00	3.12332E-03	1.79765E-02
11	1.06256E-01	3.26258E-01	1.19562E+00	3.24326E-03	2.41847E-02
12	1.24876E-01	3.70065E-01	1.14215E+00	3.39549E-03	3.11659E-02
13	1.45800E-01	4.12792E-01	1.08871E+00	3.58052E-03	3.88441E-02
14	1.68966E-01	4.54325E-01	1.03529E+00	3.80287E-03	4.71354E-02
15	1.94311E-01	4.94552E-01	9.81878E-01	4.06488E-03	5.59476E-02
16	2.21765E-01	5.33366E-01	9.28475E-01	4.36705E-03	6.51810E-02
17	2.51253E-01	5.70662E-01	8.75067E-01	4.70052E-03	7.47275E-02
18	2.82699E-01	6.06339E-01	8.21646E-01	5.11355E-03	8.44827E-02

f. First page of output from restart of 'ENVELOPE'
Figure F-2. Continued.

13	1.2773801E-02	2.4569253E-03	5.7414683E-06	3.2194900E-04	1.4661433E-04	2.5023863E-02	1.4150867E-03	5.74146E-06	
14	1.5294762E-01	4.3706170E-01	3.6671519E+05	4.8138121E+01	2.3065263E+07	1.0776382E-03	6.1321534E+03	3.8614996E+01	
	0.0000000E+00	2.3820716E+01	2.2244809E+00	3.3023484E+12	3.4271009E+15	1.8700647E+12	5.8444484E+01	-9.9224071E-02	
	1.2646465E-02	2.2462753E-03	5.2783341E-06	3.2194900E-04	1.6130769E-04	2.5090214E-02	1.5134992E-03	5.2783341E-06	
15	1.5095667E-01	4.3884205E-01	3.6575260E+05	4.4850754E+01	2.4654687E+07	1.0590181E-03	6.7907669E+03	4.1579966E+01	
	0.0000000E+00	2.4479122E+01	2.3712289E+00	2.6198701E+12	2.1569527E+15	1.8935983E+12	3.6326707E+01	8.3336497E-01	
	1.1285557E-02	1.3527857E-03	3.3488716E-06	3.2194900E-04	8.9935179E-04	2.5584548E-02	1.4007486E-03	3.3488716E-06	
16	1.5000721E-01	4.3956531E-01	4.0161767E+05	4.0599772E+01	2.1952440E+07	8.8827734E-04	8.6085062E+03	4.3533444E+01	
	0.0000000E+00	2.8961483E+01	2.2613649E+00	0.0000000E+00	0.0000000E+00	0.0000000E+00	0.0000000E+00	1.0000000E+00	
	0.0000000E+00	0.0000000E+00	0.0000000E+00	3.2194900E-04	7.2439290E-03	2.6962740E-02	0.0000000E+00	0.0000000E+00	
ELAPSED TIME = 2.99 SEC		DRAG = 2.338E+07 DYNFS							
ITERATION IN SUBROUTINE FELD		IS NOT CONVERGING.							
27	0.6099033	0.2178657	0.6163378	0.2103410	0.6195616	0.2205489	0.8319507	0.5387694	
NRCORD = 6									
27	0.6168989	0.2236159	0.6224822	0.2171849	0.6254600	0.2259747	0.8222203	0.5483861	
NRCORD = 7									
ERROR AT STATEMENT 11 OF SUBROUTINE FELD									

g. Last page of output from restart of 'ENVELOPE'
Figure F-2. Continued.

RAY	RUN	SIGMA	PI	DELTA	SBAR	Z BODY	R BODY	PHI BODY
105	ENVEL	4.2371691E+01	5.1688036E-01	5.5835152E-03	2.6667898E-02	3.2901702E-01	5.3769437E-01	3.2096135E+01
		SURFACE DISTANCE=		C.0211 FEET	ENTROPY=	0.259222E+01 CAL/GM/K		
		TW		GWALL	FRICT	QDOT		
		0.000000E+00		0.000000E+00	1.1894032E-03	1.7676375E-01		

NPT	Z (CM)	R (CM)	U (CM/SEC)	PHI (DEG)	P (DYNE/CM**2)	RHO (GM/CC)	T (DEG K)	PSI (GM/CM**25EC)
MOL/GM	RAD	ERG/GM-SEC	XMW (GM/MOLE)	MACH NO.	PLASMA FREQ	EL. DENS (#/CC)	COLL. FREQ.	EL. COND
U	N	E	AR	O2	N2	NO	NO	AV. CHI
0	3.2605027E-01	5.4242440E-01	3.8401063E+05	3.2890944E+01	1.1204538E+07	5.6153050E-04	5.7112237E+03	3.9461822E+00
	0.0000000E+00	2.3797742E+01	2.4097680E+00	2.0525460E+12	1.3239357E+15	9.2827984E+11	4.5484273E+01	-4.4562820E-01
	1.3055733E-02	1.9207921E-03	3.9132402E-06	3.2194900E-04	1.2718885E-04	2.5413470E-02	1.1738338E-03	3.9132402E-06
3	3.2303836E-01	5.4722661E-01	3.8399156E+05	3.3587818E+01	1.1869465E+07	5.9304830E-04	5.7350148E+03	8.2473657E+00
	0.0000000E+00	2.3824332E+01	2.4053180E+00	2.1078910E+12	1.3962957E+15	9.8167767E+11	4.5360911E+01	-3.7860747E-01
	1.3004431E-02	1.8783069E-03	3.9077817E-06	3.2194900E-04	1.3306756E-04	2.5415541E-02	1.2121839E-03	3.9077817E-06
5	3.1907500E-01	5.5354570E-01	3.8447519E+05	3.4402660E+01	1.2716890E+07	6.3418225E-04	5.7549719E+03	1.4326885E+01
	0.0000000E+00	2.3861825E+01	2.4059738E+00	2.1683991E+12	1.4776090E+15	1.0500872E+12	4.4875306E+01	-3.1632115E-01
	1.2937059E-02	1.8138585E-03	3.8671266E-06	3.2194900E-04	1.4283481E-04	2.5423246E-02	1.2612626E-03	3.8671266E-06
7	3.1559268E-01	5.5909782E-01	3.8509592E+05	3.5049801E+01	1.3452951E+07	6.7041094E-04	5.7670472E+03	2.0071587E+01
	0.0000000E+00	2.3894850E+01	2.4089050E+00	2.2154821E+12	1.5424731E+15	1.1096946E+12	4.4328946E+01	-2.7493676E-01
	1.2878531E-02	1.7566391E-03	3.8187343E-06	3.2194900E-04	1.5118411E-04	2.5430941E-02	1.3031402E-03	3.8187343E-06
9	3.1193794E-01	5.6492485E-01	3.8591614E+05	3.5677795E+01	1.4217774E+07	7.0857028E-04	5.7751080E+03	2.6518137E+01
	0.0000000E+00	2.3929780E+01	2.4139972E+00	2.2591865E+12	1.6039295E+15	1.1718245E+12	4.3651178E+01	-2.4100270E-01
	1.2817146E-02	1.6959733E-03	3.7570354E-06	3.2194900E-04	1.6032389E-04	2.5439721E-02	1.3463068E-03	3.7570354E-06
11	3.0831017E-01	5.7070888E-01	3.8688627E+05	3.6268096E+01	1.4969209E+07	7.4662372E-04	5.7786997E+03	3.3351788E+01
	0.0000000E+00	2.3964855E+01	2.4209147E+00	2.2970838E+12	1.6581919E+15	1.2330852E+12	4.2885943E+01	-2.1485848E-01
	1.2755649E-02	1.6351820E-03	3.6861751E-06	3.2194900E-04	1.6986013E-04	2.5448904E-02	1.3888028E-03	3.6861751E-06
13	3.0509255E-01	5.7583897E-01	3.8790633E+05	3.6780499E+01	1.5623554E+07	7.8035358E-04	5.7784893E+03	3.9784771E+01
	0.0000000E+00	2.3996790E+01	2.4288670E+00	2.3252370E+12	1.6990867E+15	1.2866635E+12	4.2113742E+01	-1.9711298E-01
	1.2700090E-02	1.5799271E-03	3.6138246E-06	3.2194900E-04	1.7883435E-04	2.5457727E-02	1.4264850E-03	3.6138246E-06
15	3.0249355E-01	5.7998275E-01	4.1622524E+05	3.7338338E+01	1.6220111E+07	8.8428295E-04	5.3975565E+03	4.5721540E+01
	0.0000000E+00	2.4466210E+01	2.7196464E+00	1.7959547E+12	1.0136123E+15	1.3624797E+12	2.3725485E+01	-1.8510082E-01
	1.1947691E-02	7.3664419E-04	1.9024737E-06	3.2194900E-04	3.6335909E-04	2.5687694E-02	1.8115460E-03	1.9024737E-06
17	3.0092924E-01	5.8247684E-01	4.1437901E+05	3.7443822E+01	1.6652091E+07	9.0160650E-04	5.4311956E+03	4.9692013E+01
	0.0000000E+00	2.4449555E+01	2.6984364E+00	1.8510490E+12	1.0767551E+15	1.3960071E+12	2.4598157E+01	-1.6662388E-01
	1.1970974E-02	7.6890415E-04	1.9821789E-06	3.2194900E-04	3.5377987E-04	2.5673626E-02	1.8073424E-03	1.9821789E-06
19	2.9965835E-01	5.8450313E-01	4.1606127E+05	3.7590353E+01	1.7026171E+07	9.2718857E-04	5.4097441E+03	5.3006675E+01
	0.0000000E+00	2.4493737E+01	2.7170668E+00	1.8280012E+12	1.0501082E+15	1.4291149E+12	2.3433663E+01	-1.5072022E-01
	1.1873349E-02	7.1918035E-04	1.8797883E-06	3.2194900E-04	3.7825861E-04	2.5674154E-02	1.8561121E-03	1.8797883E-06
21	2.9852156E-01	5.8631559E-01	4.1937353E+05	3.7719559E+01	1.7369291E+07	9.5735062E-04	5.3608132E+03	5.6089824E+01
	0.0000000E+00	2.4566702E+01	2.7548209E+00	1.7677829E+12	9.8206217E+14	1.4621508E+12	2.1420031E+01	-1.4051299E-01
	1.1712205E-02	6.3816102E-04	1.7025933E-06	3.2194900E-04	4.2225813E-04	2.5678091E-02	1.9294339E-03	1.7025933E-06
23	2.9746465E-01	5.8800071E-01	4.2297875E+05	3.7839869E+01	1.7694724E+07	9.8868861E-04	5.3047841E+03	5.9082687E+01
	0.0000000E+00	2.4643973E+01	2.7971174E+00	1.6981379E+12	9.0620619E+14	1.4945478E+12	1.9337061E+01	-1.3417580E-01

**h. Typical output from MOC calculation run number 'ENVELOPE'
Figure F-2. Continued.**

	1. 1536876E-02	5. 5859239E-04	1. 5212845E-06	3. 2194900E-04	4. 7528197E-04	2. 5683235E-02	1. 9988969E-03	1. 5212845E-06
25	2. 9646288E-01	5. 8959790E-01	4. 2664015E+05	3. 7948571E+01	1. 8008678E+07	1. 0202861E-03	5. 2481751E+03	5. 2044053E+01
	0. 0000000E+00	2. 4721550E+01	2. 8406055E+00	1. 6128821E+12	8. 1749731E+14	1. 5256746E+12	1. 7088254E+01	-1. 0335748E-01
	1. 1361493E-02	4. 7968947E-04	1. 3298643E-06	3. 2194900E-04	5. 4518468E-04	2. 5704897E-02	2. 0346662E-03	1. 3298643E-06
27	2. 9550922E-01	5. 9111839E-01	4. 3055656E+05	3. 8022503E+01	1. 8306503E+07	1. 0493980E-03	5. 2080005E+03	6. 4981555E+01
	0. 0000000E+00	2. 4821791E+01	2. 8835090E+00	1. 4540553E+12	6. 6442037E+14	1. 5508502E+12	1. 3663009E+01	8. 6648403E-02
	1. 1134898E-02	3. 8012794E-04	1. 0508619E-06	3. 2194900E-04	6. 9980695E-04	2. 5796003E-02	1. 9522949E-03	1. 0508619E-06
28	2. 9470460E-01	5. 9240126E-01	4. 3628319E+05	3. 8034583E+01	1. 8503962E+07	1. 0677164E-03	5. 2249768E+03	6. 7551168E+01
	0. 0000000E+00	2. 5067027E+01	2. 9326828E+00	1. 0873727E+12	3. 7156773E+14	1. 5522391E+12	7. 6340131E+00	5. 3090896E-01
	1. 0487464E-02	2. 4023323E-04	5. 7759710E-07	3. 2194900E-04	1. 1999261E-03	2. 6042352E-02	1. 5999646E-03	5. 7759710E-07
29	2. 9400224E-01	5. 9352108E-01	4. 4053032E+05	3. 7885081E+01	1. 8605337E+07	1. 0557221E-03	5. 4037706E+03	6. 9831428E+01
	0. 0000000E+00	2. 5493896E+01	2. 9412299E+00	6. 6586147E+11	1. 3933136E+14	1. 5192914E+12	2. 9246982E+00	8. 4051804E-01
	9. 2492967E-03	1. 4318161E-04	2. 1904948E-07	3. 2194900E-04	2. 1232116E-03	2. 6395080E-02	9. 9191911E-04	2. 1904948E-07
30	2. 9333463E-01	5. 9458550E-01	4. 4391530E+05	3. 7148036E+01	1. 8369145E+07	9. 8318023E-04	5. 9665797E+03	7. 1935825E+01
	0. 0000000E+00	2. 6551979E+01	2. 9073766E+00	2. 4352428E+11	1. 8636555E+13	1. 4103916E+12	4. 2140452E-01	9. 7230348E-01
	6. 1956562E-03	7. 0998179E-05	3. 1461211E-08	3. 2194900E-04	3. 9917882E-03	2. 6772928E-02	3. 0859389E-04	3. 1461211E-08
31	2. 9290617E-01	5. 9526863E-01	4. 4671553E+05	3. 6118980E+01	1. 7942228E+07	8. 7329982E-04	7. 1565969E+03	7. 9836562E+01
	0. 0000000E+00	2. 8961483E+01	2. 7543098E+00	0. 0000000E+00	0. 0000000E+00	0. 0000000E+00	0. 0000000E+00	1. 0000000E+00
	0. 0000000E+00	0. 0000000E+00	0. 0000000E+00	3. 2194900E-04	7. 2439290E-03	2. 6962740E-02	0. 0000000E+00	0. 0000000E+00

ELAPSED TIME = 27.29 SEC. DRAG = 2.752E+07 DYNES

NRCORD = 106

NRCORD = 107

NRCORD = 108

NRCORD = 109

h. Concluded
Figure F-2. Concluded.

Example 2. The second example to be considered (Fig. F-3) illustrates input for a calculation of equilibrium air flow over a flared body. The free-stream conditions are obtained from fits to the 1953 Standard Atmosphere. Specifying cgs units explicitly was unnecessary.

Figure F-4a is a reproduction of the first page of the output from run EQUILI. Notice that the altitude and velocity are printed out in English units and that the thermochemical properties are not printed. The results of the third marching pass are shown in Fig. F-4b. There were no integration failures ($FLOP = 1$) and the RMS deviation between specified and computed body points is certainly acceptable, but the relative error between calculated flow angle and the angle of the body surface at the junction ray is approximately 1 percent, so the message "PROGRAM DID NOT CONVERGE" is printed. DELTA and FLUX are zero because the boundary-layer option was not selected ($INBLR = 0$). Printout from the thirteenth data surface is shown in Fig. F-4c. $AVER.CHI = 0.0$ at all points as it should for this equilibrium calculation. No composition data are obtained when $MODEL = 2$, so the electron density is reported as zero.

The M.O.C. printout at the flare discontinuity is reproduced in Figs. F-4d - F-4g. The message at the bottom of Fig. F-4d indicates that the next ray would ordinarily be located at the dimensionless station $ZRAY = 1.6772$ but since this station is downstream of the segment end $ZCHECK = 1.626$, Ray 59 is placed at the junction point and printed. Now the code discovers that this junction is a discontinuity, so it calculates Ray 60 normal to the cylinder (body segment 2) at the junction point (Fig. F-4e) and then calls subroutine FLARE to determine the initial inclination of the imbedded shock, Fig. F-4f. The match error is that between the flow angle calculated from momentum and energy conservation and the specified body angle. The flow conditions just downstream and just upstream of the shock at the body surface are printed as Ray 61, Fig. F-4g. Note that the point identifier and the point coordinates are repeated. Figure F-4h reproduces the first ray downstream of the discontinuity.

```

EQUILIB
SAMPLE INPUT FOR EQUILIBRIUM AIR FLOW OVER SPHERE-CYLINDER-CONE
$OPTIONS
MODEL=2.           ;SPECIFIES EQUILIBRIUM AIR
IUNIT=0.           ;FREE STREAM CONDITIONS FROM 1953 STANDARD ATMOSPHERE
INBLR=0.           ;NO VISCOUS INTERACTION
INAFI=1.           ;INCLUDE M.O.C. CALCULATIONS
UNIT='CGS'        ;METRIC UNITS FOR INPUT
$
$UPSTREAM
VEL=4.8768E5.     ;CENTERLINE VELOCITY CM/SEC
ALT=2.7432E6.     ;ALTITUDE IN CM
$
$SHOCK
RSHK=2.16135.    ;CM RADIUS OF CURVATURE OF SHOCK AT AXIS
S1P=0.09867.     ;
S1=0.0061.       ;
$
$BODY
REXP=2.           ;EXPONENT OF (R-RJUNC)
C1=3.81.          ;CM TWICE THE NOSE RADIUS
C2=-1.            ;SINCE THIS IS A SPHERE
MORE=.T.         ;ANOTHER BODY SEGMENT FOLLOWS
$
$BODY
RJUNC=1.905.      ;CM--RADIAL COORDINATE SPHERE-CONE JUNCTION
ZJUNC=1.905.      ;CM--AXIAL COORDINATE SPHERE-CONE JUNCTION
REXP=1.           ;
C1=0.00.          ;TANGENT OF CONE HALF-ANGLE
MORE=.T.         ;
$
$BODY
ZJUNC=3.50.       ;BEGINNING OF FLARE
RJUNC=1.905.      ;
REXP=1.           ;EXPONENT OF (Z - ZJUNC)
ZEAP=1.           ;TANGENT OF FLARE ANGLE
CO=0.07.          ;
MORE=.F.         ;THIS IS LAST BODY SEGMENT
$
$CONTROL
NBSIT=3.          ;NOT MORE THAN 3 SHOCK-SHAPE ITERATIONS
IPRNT=5.          ;STATUS REPRNT EVERY 5TH STEP FROM SHOCK
DELX=.05.         ;AVERAGE RAY SPACING, DEFAULT IS .04
XO=.05.           ;POSITION OF FIRST NON-AXIS RAY
METHOD=10.        ;PROBABLY UNNECESSARY
DELMIN=1.0E-6.    ;MINIMUM STP SIZE--INITIAL STEP=1.0E-4*RSHK
PSIRAT=0.10.      ;DEFAULT MARCHING STOPS WITH 10% OF FLUX LEFT
ERROR=1.0E-5.     ;CONVERGENCE CRITERION FOR MOST ITERATIONS
NOUT=15.          ;USE 15 POINTS TO START M.O.C. CALCULATION
$
$SUPER
ZMAX=6.25.        ;BODY IS 6.25 CM LONG
ZETAMX=0.8.       ;M.O.C. RAY SPACING IS 0.8*Z.F.L. ALLOWANCE
NMAX=35.          ;MAXIMUM NUMBER OF STREAMLINES IN MESH.
MODRAY=10.        ;PRINT EVERY 10TH RAY
NCORN(2)=2.       ;SIGNALS THAT THIS CORNER IS A COMPRESSION
$

```

Figure F-3. Sample input for equilibrium airflow over flared body.

```

CAL BLUNT BODY PROGRAM
RUN NO. EQUIL1
09/08/88
SAMPLE INPUT FOR EQUILIBRIUM AIR FLOW OVER A SPHERE-CYLINDER-CONE
ALITUDE = 9.000000E+04 FT. VELOCITY = 1.600000E+04 FT/SEC
PRESSURE DYNE/50.CM    TEMPERATURE DEG.K    DENSITY GM/CCU.CM    VELOCITY CM/SEC    MOLECULAR WEIGHT
1.7609575E+04          2.2396411E+02          2.7388232E-05          4.8768000E+05          2.8961483E+01
INITIAL SHOCK PARAMETERS - RSHP = 2.1613 SIP = 9.86700E-02 S1 = 6.10000E-03
DELX = 0.0500 XO = 0.0500
ZBDY      YBDY      BD1      BD2      BDC(1)      BDC(2)      BDC(3)      BDC(4)      BDC(5)
0.000000E+00 0.000000E+00 2.000000E+00 0.000000E+00 0.000000E+00 3.810000E+00 -1.000000E+00 0.000000E+00 0.000000E+00
1.905000E+00 1.905000E+00 1.000000E+00 0.000000E+00 0.000000E+00 0.000000E+00 0.000000E+00 0.000000E+00 0.000000E+00
3.500000E+00 1.905000E+00 1.000000E+00 1.000000E+00 7.000000E-02 0.000000E+00 0.000000E+00 0.000000E+00 0.000000E+00
EMISSIVITY = 0.000000E+00 INITIAL WALL TEMP = 2.222222E+02 DEG.K
IUNIT  INBLR  INDWT  INAFT  INDIM  IPRNT  NBDY  MODEL  NSPEC  NR  NC  NVIB  NRAD  NKDIV  METHOD
0       0       0       1       1       5       3       2       6       0  0  0     0     20     10
SLAM      SKAP      ERROR      RMSTST      TESTM      TTEST      GAMTST      DELMIN
-5.000000E-01 3.500000E-01 1.000000E-05 5.000000E-04 1.100000E+00 1.500000E-01 1.000000E-05 1.000000E-06
FREE STREAM MACH NO. = 16.2088
XLMBDA = 3.6990057E+02 HINF = 1.8847597E+02 BIGAN = 1.4079086E+00
    
```

SHOCK GEOMETRY						
M	X(M)	SZ(M)	SR(M)	STGMA	CURV(M)	
1	0.50000E-01	0.12496E-02	0.49979E-01	1.5208	-0.99920	
2	0.10000	0.49931E-02	0.99834E-01	1.4709	-0.99668	
3	0.15000	0.11215E-01	0.14944	1.4212	-0.99222	
4	0.20000	0.19889E-01	0.19868	1.3717	-0.98548	
5	0.25000	0.30977E-01	0.24743	1.3227	-0.97607	
6	0.30000	0.44429E-01	0.29558	1.2742	-0.96367	
7	0.35000	0.60185E-01	0.34303	1.2264	-0.94798	
8	0.40000	0.78170E-01	0.38967	1.1794	-0.92886	
9	0.45000	0.98301E-01	0.43544	1.1335	-0.90634	
10	0.50000	0.12048	0.48024	1.0888	-0.88057	
11	0.55000	0.14462	0.52403	1.0455	-0.85189	
12	0.60000	0.17059	0.56675	1.0037	-0.82075	
13	0.65000	0.19830	0.60837	0.96348	-0.78768	
14	0.70000	0.22762	0.64886	0.92495	-0.75326	
15	0.75000	0.25845	0.68822	0.88816	-0.71806	
16	0.80000	0.29067	0.72645	0.85315	-0.68262	
17	0.85000	0.32417	0.76356	0.81990	-0.64740	

a. First page of output from run 'EQUIL'
Figure F-4. Output from Example 2.

```

ITERATION NO. 3 SHOCK RADIUS = 2.18226 SIP = 0.10333 S1 = 0.00639
RMS DEVIATION = 2.5188678E-04 MAX DEV = 1.0793289E-02 ZSTAG = 4.7660161E-02
PROGRAM DID NOT CONVERGE
VALUES AT INTERSECTION OF RAY WITH BODY
RAY      ZB      RR      PHIB      DELTA      FLUX
5        4.89585E-02 4.75923E-02 1.51625E+00 0.00000E+00 0.00000E+00
6        5.28488E-02 9.50364E-02 1.46171E+00 0.00000E+00 0.00000E+00
7        5.93176E-02 1.42185E-01 1.40719E+00 0.00000E+00 0.00000E+00
8        6.83422E-02 1.88895E-01 1.35268E+00 0.00000E+00 0.00000E+00
9        7.98922E-02 2.35021E-01 1.29821E+00 0.00000E+00 0.00000E+00
10       9.39288E-02 2.80427E-01 1.24376E+00 0.00000E+00 0.00000E+00
11       1.10406E-01 3.24977E-01 1.18934E+00 0.00000E+00 0.00000E+00
12       1.29270E-01 3.68542E-01 1.13495E+00 0.00000E+00 0.00000E+00
13       1.50464E-01 4.10994E-01 1.08059E+00 0.00000E+00 0.00000E+00
14       1.73921E-01 4.52212E-01 1.02625E+00 0.00000E+00 0.00000E+00
15       1.99571E-01 4.92081E-01 9.71938E-01 0.00000E+00 0.00000E+00
16       2.27340E-01 5.30488E-01 9.17639E-01 0.00000E+00 0.00000E+00
17       2.57150E-01 5.67328E-01 8.63345E-01 0.00000E+00 0.00000E+00
18       2.88919E-01 6.02500E-01 8.09045E-01 0.00000E+00 0.00000E+00
    
```

b. Results of the third marching pass
Figure F-4. Continued.

STEP SIZE = 1.09113E-02		NUMBER OF SUCCESSFULL STEPS = 13				DISTANCE FROM SHOCK = 9.01273E-02 CM.				
RAY	Z CM HTDT ERG/GM	R CM S CAL /GM K	P DYNE/CM**2 AVER. CHI	I DEG.K EL. DENS. #/CC	RHO GM/CC MACH NO.	XMW GM/MOL FLUX RATIO	VTDT CM/SEC RAD ERG/GM-SEC	FLDW ANG. PSI GM/SEC		
4	9.0127331E-02 1.2027657E+11	0.000000E+00 4.5209805E+03	6.2255604E+06 0.000000E+00	5.7622539E+03 0.000000E+00	3.0339272E-04 3.9591136E-02	2.3341083E+01 1.000000E+00	6.1816089E+03 0.000000E+00	0.000000E+00 0.000000E+00		
5	9.2741701E-02 1.2043612E+11	1.1456402E-01 4.5207264E+03	6.2010024E+06 0.000000E+00	5.7584693E+03 0.000000E+00	3.0244369E-04 1.5706729E-01	2.3344877E+01 1.3281012E+00	2.4514737E+04 0.000000E+00	7.2079614E+01 6.6293433E-02		
6	1.0057523E-01 1.2090573E+11	2.0887324E-01 4.5190199E+03	6.1279185E+06 0.000000E+00	5.7469474E+03 0.000000E+00	2.9962719E-04 3.0641202E-01	2.3356479E+01 1.3821923E+00	4.7769841E+04 0.000000E+00	7.5938671E+01 2.7528583E-01		
7	1.1359881E-01 1.2166365E+11	3.1267567E-01 4.5184646E+03	6.0081252E+06 0.000000E+00	5.7273231E+03 0.000000E+00	2.9502696E-04 4.5710740E-01	2.3376329E+01 1.4713183E+00	7.1125511E+04 0.000000E+00	7.5082886E+01 6.566002E-01		
8	1.3176298E-01 1.2267584E+11	4.1572576E-01 4.5162103E+03	5.8447790E+06 0.000000E+00	5.6990405E+03 0.000000E+00	2.8878481E-04 6.0775598E-01	2.3405067E+01 1.5935927E+00	9.4302776E+04 0.000000E+00	7.3019912E+01 1.2569909E+00		
9	1.5499696E-01 1.2388917E+11	5.1778477E-01 4.5129049E+03	5.6424129E+06 0.000000E+00	5.6611670E+03 0.000000E+00	2.8111475E-04 7.5793681E-01	2.3443726E+01 1.7458302E+00	1.1716735E+05 0.000000E+00	7.0489992E+01 2.1357776E+00		
10	1.8320764E-01 1.2526628E+11	6.1867895E-01 4.5084040E+03	5.4068644E+06 0.000000E+00	5.6103267E+03 0.000000E+00	2.7224761E-04 9.0735005E-01	2.3493127E+01 1.9244666E+00	1.3960439E+05 0.000000E+00	6.7751841E+01 3.3598161E+00		
11	2.1627910E-01 1.2674244E+11	7.1804777E-01 4.5024124E+03	5.1450108E+06 0.000000E+00	5.5544962E+03 0.000000E+00	2.6248975E-04 1.0557659E+00	2.3554432E+01 2.1240398E+00	1.6150102E+05 0.000000E+00	6.4829262E+01 4.9943300E+00		
12	2.5407265E-01 1.2825126E+11	8.1581948E-01 4.4946306E+03	4.8640797E+06 0.000000E+00	5.4835410E+03 0.000000E+00	2.5216011E-04 1.2030023E+00	2.3628639E+01 2.3394400E+00	1.8274779E+05 0.000000E+00	6.2090298E+01 7.0986598E+00		
13	2.9642780E-01 1.2975540E+11	9.1186343E-01 4.4850066E+03	4.5708885E+06 0.000000E+00	5.4001064E+03 0.000000E+00	2.4150370E-04 1.3488098E+00	2.3715232E+01 2.5650953E+00	2.0324168E+05 0.000000E+00	5.9277463E+01 9.7189004E+00		
14	3.4316408E-01 1.3123056E+11	1.0059423E+00 4.4736397E+03	4.2711847E+06 0.000000E+00	5.3041962E+03 0.000000E+00	2.3069482E-04 1.4928973E+00	2.3812828E+01 2.7965399E+00	2.2289289E+05 0.000000E+00	5.6513014E+01 1.2888557E+01		
15	3.9408382E-01 1.3257337E+11	1.0979635E+00 4.4600379E+03	3.9697130E+06 0.000000E+00	5.1931121E+03 0.000000E+00	2.2001372E-04 1.6353905E+00	2.3923254E+01 3.0304247E+00	2.4162824E+05 0.000000E+00	5.3807220E+01 1.8629347E+01		
16	4.4897555E-01 1.3372457E+11	1.1879303E+00 4.4440803E+03	3.6706938E+06 0.000000E+00	5.0653543E+03 0.000000E+00	2.0964706E-04 1.7772316E+00	2.4046526E+01 3.2662154E+00	2.5879299E+05 0.000000E+00	5.1164006E+01 2.0864573E+01		
17	5.0761795E-01 1.3471750E+11	1.2754712E+00 4.4265156E+03	3.3785497E+06 0.000000E+00	4.9232293E+03 0.000000E+00	1.9962316E-04 1.9195831E+00	2.4178680E+01 3.5035804E+00	2.7614550E+05 0.000000E+00	4.8590498E+01 2.5911976E+01		

c. Output from the 13th data surface
Figure F-4. Continued.

18	2.2664170E+00 1.2118949E+11	2.7755577E+00 2.8584668E+01	4.2398526E+05 4.4497830E+00	2.314938	1	1.1485604E+06	1.5431604E-04	2.5596172E+03	2.9028	+02
19	2.2664170E+00 1.2116292E+11	2.8173468E+00 2.8658443E+01	4.3012818E+05 4.6336845E+00	2.3833239E+01		1.2762196E+06	1.8328308E-04	2.4007915E+03	3.3306065E+02	

ELAPSED TIME = 11.90 SEC. DRAG = 3.739E+07 DYNES

NRCORD = 50

NRCORD = 51

NRCORD = 52

NRCORD = 53

NRCORD = 54

NRCORD = 55

NRCORD = 56

NRCORD = 57

END OF SEGMENT 2 ENCOUNTERED. ZCHECK = 1.62622RAY = 1.6772

**d. Method-of-Characteristics (MOC) printout at junction between body segments
Figure F-4. Continued.**

RAY	RUN	STGMA	P1	DELTA	SRAR	Z BODY	R BODY	PHI BODY
60	EQUILLI	2.2608884E+01	0.0000000E+00	0.0000000E+00	0.0000000E+00	3.5716178E+00	1.8897424E+00	0.0000000E+00
SURFACE DISTANCE= 0.1492 FEET ENTRDFY= 0.452488E+04 CAL/GM/K								
NPT	Z (CM) H (ERG/GM)	R (CM) XMW (GM/MOLE)	U (CM/SEC) MACH NO.	PHI (DEG)	P (DYNE/CM**2)	RHO (GM/CC)	T (DEG K)	PSI (GM/CM**2SEC)
0	3.5716178E+00 1.2706976E+11	1.8897424E+00 2.5308991E+01	3.4708042E+05 3.0023494E+00	0.0000000E+00	1.8427304E+05	1.6198288E-05	3.4639020E+03	0.0000000E+00
2	3.5716178E+00 1.3915998E+11	2.1128516E+00 2.5726545E+01	3.9247076E+05 3.4918577E+00	1.2501963E+00	1.8910437E+05	1.7432646E-05	3.3575214E+03	1.7576660E+01
3	3.5716178E+00 1.3767735E+11	2.1664152E+00 2.5847257E+01	3.9202531E+05 3.5142407E+00	1.5535826E+00	1.9115021E+05	1.7854330E-05	3.3292268E+03	2.2559311E+01
4	3.5716178E+00 1.3625374E+11	2.2147141E+00 2.5960211E+01	3.9147134E+05 3.5333160E+00	1.8621495E+00	1.9348410E+05	1.8292354E-05	3.3035540E+03	2.7264468E+01
5	3.5716178E+00 1.3434391E+11	2.2756044E+00 2.6107912E+01	3.9056431E+05 3.5557335E+00	2.3079408E+00	1.9725772E+05	1.8941975E-05	3.2709770E+03	3.3514469E+01
6	3.5716178E+00 1.3273058E+11	2.3237040E+00 2.6229891E+01	3.8968044E+05 3.5723895E+00	2.7021266E+00	2.0095473E+05	1.9544298E-05	3.2446724E+03	3.8727604E+01
7	3.5716178E+00 1.3006274E+11	2.3986331E+00 2.6424492E+01	3.8794361E+05 3.5945624E+00	3.4452401E+00	2.0884432E+05	2.0722242E-05	3.2039873E+03	4.7419784E+01
8	3.5716178E+00 1.2822006E+11	2.4457535E+00 2.6556639E+01	3.8665160E+05 3.6081022E+00	3.9652994E+00	2.1486344E+05	2.1612128E-05	3.1764080E+03	5.3287306E+01
9	3.5716178E+00 1.2625327E+11	2.4924050E+00 2.6693455E+01	3.8516040E+05 3.6204222E+00	4.5426251E+00	2.2215234E+05	2.2666264E-05	3.1475597E+03	5.9454464E+01
10	3.5716178E+00 1.2317130E+11	2.5609570E+00 2.6900415E+01	3.8266283E+05 3.6367499E+00	5.4916202E+00	2.3514298E+05	2.4529474E-05	3.1024250E+03	6.9279051E+01
11	3.5716178E+00 1.2093397E+11	2.6328387E+00 2.7103043E+01	3.8228198E+05 3.6722498E+00	6.5889215E+00	2.5175326E+05	2.6856124E-05	3.0566702E+03	8.0746327E+01
12	3.5716178E+00 1.2081745E+11	2.7117626E+00 2.7307875E+01	3.8749565E+05 3.7626124E+00	7.9017570E+00	2.7419765E+05	2.9942651E-05	3.0085716E+03	9.5131377E+01
13	3.5716178E+00 1.2075757E+11	2.8012502E+00 2.7566141E+01	3.9437491E+05 3.8847795E+00	9.4495729E+00	3.0510622E+05	3.4413783E-05	2.9403150E+03	1.1443609E+02
14	3.5716178E+00 1.2079594E+11	2.8883801E+00 2.7834904E+01	4.0196294E+05 4.0248228E+00	1.0924363E+01	3.4066698E+05	3.9934431E-05	2.8567441E+03	1.3716489E+02
15	3.5716178E+00 1.2085835E+11	2.9733860E+00 2.8133520E+01	4.1095278E+05 4.2040568E+00	1.2305714E+01	3.8118269E+05	4.7123253E-05	2.7379206E+03	1.6434380E+02
16	3.5716178E+00 1.2092355E+11	3.0566982E+00 2.8383751E+01	4.1949611E+05 4.3931400E+00	1.3595616E+01	4.2797908E+05	5.6250268E-05	2.5981639E+03	1.9741769E+02
17	3.5716178E+00 1.2125035E+11	3.1422820E+00 2.8565594E+01	4.2786711E+05 4.5962418E+00	1.4854366E+01	4.8546981E+05	6.8349392E-05	2.4410104E+03	2.4014923E+02
18	3.5716178E+00 1.2138494E+11	3.2308893E+00 2.8686894E+01	4.3569166E+05 4.8335274E+00	1.6081562	5.5898798E+05	8.5787912E-05	2.2488404E+03	2.97175 +02
19	3.5716178E+00 1.2122828E+11	3.3240820E+00 2.8749670E+01	4.4336492E+05 5.1607391E+00	1.7000694E+01	6.5991258E+05	1.1399029E-04	2.0023963E+03	3.7810726E+02
20	3.5716178E+00 1.2116685E+11	3.4233964E+00 2.8732957E+01	4.5076647E+05 5.5778695E+00	1.8545738E+01	8.0541397E+05	1.5954105E-04	1.7451197E+03	5.0097734E+02
21	3.5716178E+00 1.2116389E+11	3.4315589E+00 2.8729862E+01	4.5128818E+05 5.6117028E+00	1.8633039E+01	8.1963085E+05	1.6410193E-04	1.7263794E+03	4.9410808E+02
ELAPSED TIME = 13.25 SEC. DRAG = 3.739E+07 DYNES								

e. Method-of-Characteristics (MOC) printout, ray normal to cylinder at beginning of flare
Figure F-4. Continued.

18	3.5716178E+00 1.2138494E+11	3.2308893E+00 2.8686894E+01	4.3569166E+05 4.8335274E+00	1.608156.	1	5.5898798E+05	8.5787912E-05	2.2488404E+03	2.97171	-02
19	3.5716178E+00 1.2122828E+11	3.3240820E+00 2.8749670E+01	4.4336492E+05 5.1607391E+00	1.7300694E+01		6.5991258E+05	1.1399029E-04	2.0023963E+03	3.7810726E+02	
20	3.5716178E+00 1.2116685E+11	3.4233964E+00 2.8732957E+01	4.5076647E+05 5.5778695E+00	1.8545738E+01		8.0541397E+05	1.5954105E-04	1.7451197E+03	5.0097734E+02	
21	3.5716178E+00 1.2116389E+11	3.4315589E+00 2.8729862E+01	4.5128818E+05 5.6117028E+00	1.8633039E+01		8.1963085E+05	1.6410193E-04	1.7263794E+03	4.9410808E+02	

ELAPSED TIME = 13.28 SEC. DRAG = 3.739E+07 DYNES

4.004 DEG. FLARE . INITIAL ANGLE OF IMBEDDED SHOCK IS 22.102 DEGREES.
MATCH ERROR = -0.51098E-09

**f. Printout from Subroutine 'FLARE'
Figure F-4. Continued.**

RAY	RUN	SIGMA	PI	DELTA	SBAR	Z BODY	R BODY	PHI BODY
61	EQUILI	2.2608884E+01	0.0000000E+00	0.0000000E+00	0.0000000E+00	3.5716178E+00	1.8897424E+00	0.0000000E+00
		SURFACE DISTANCE = 0.1492 FEET		ENTROPY = 0.452619E+04 CAL/GM/K				

NPT	Z (CM)	R (CM)	U (CM/SEC)	PHI (DEG)	P (DYNE/CM**2)	RHO (GM/CC)	T (DEG K)	PSI (GM/CM**25EC)
0	3.5716178E+00 1.2706963E+11	1.8897424E+00 2.5122641E+01	3.3831252E+05 2.7152198E+00	4.0041729E+00	2.3821002E+05	2.0128301E-05	3.5769782E+03	0.0000000E+00
0	3.5716178E+00 1.2706976E+11	1.8897424E+00 2.5308991E+01	3.4708042E+05 3.0023494E+00	0.0000000E+00	1.8427304E+05	1.6198288E-05	3.4639020E+03	0.0000000E+00

IMBEDDED SHOCK ANGLE = 22.102 DEGREES

NRCORD = 58

**g. Flow conditions at discontinuity (first block is behind the shock)
Figure F-4. Continued.**

RAY 62	RUN EQUIL1	SIGMA 2.1939355E+01	PI 0.0000000E+00	DÉLTA 0.0000000E+00	SBAR 0.0000000E+00	Z BODY 3.8532913E+00	R BODY 1.9094595E+00	PHI BODY 4.0041729E+00
		SURFACE DISTANCE= 0.1585 FEET ENTROPY= 0.452619E+04 CAL/GM/K						

NPT	Z (CM) H (ERG/GM)	R (CM) XMW (GM/MOLE)	U (CM/SEC) MACH NO.	PHI (DEG)	P (DYNE/CM**2)	RHD (GM/CC)	T (DEG K)	PSI (GM/CM**2SEC)
0	3.8532913E+00 1.2708131E+11	1.9094595E+00 2.5131878E+01	3.3882339E+05 2.8647017E+00	4.0041729E+00	2.3473815E+05	1.9878261E-05	3.5704941E+03	0.0000000E+00
1000	3.8532913E+00 8.2652335E+10	2.0041299E+00 2.8753026E+01	3.4810096E+05 4.0684789E+00	1.3910075E+01	5.7994711E+05	1.3808125E-04	1.9371982E+03	8.7883301E+00
1000	3.8532913E+00 8.1950046E+10	2.0041299E+00 2.8675346E+01	3.7050730E+05 5.3858427E+00	5.2728956E-01	1.7986706E+05	5.0270998E-05	1.2343517E+03	8.7883301E+00
2	3.8532913E+00 1.3916387E+11	2.1185736E+00 2.5753059E+01	3.9343426E+05 3.5103895E+00	1.0773014E+00	1.8260359E+05	1.6914754E-05	3.3448021E+03	2.7276783E+01
3	3.8532913E+00 1.3768035E+11	2.1735639E+00 2.5876392E+01	3.9306017E+05 3.5341977E+00	1.3540628E+00	1.8401581E+05	1.7277420E-05	3.3157321E+03	3.2261344E+01
4	3.8532913E+00 1.3825069E+11	2.2232647E+00 2.5992989E+01	3.9261377E+05 3.5553998E+00	1.6153918E+00	1.8544153E+05	1.7632853E-05	3.2888084E+03	3.6967711E+01
5	3.8532913E+00 1.3434568E+11	2.2861589E+00 2.6146039E+01	3.9186593E+05 3.5809657E+00	1.9838249E+00	1.8781686E+05	1.8153966E-05	3.2543692E+03	4.3219216E+01
6	3.8532913E+00 1.3273213E+11	2.3360588E+00 2.6272423E+01	3.9111255E+05 3.6002124E+00	2.3208388E+00	1.9028587E+05	1.8640911E-05	3.2265413E+03	4.8435003E+01
7	3.8532913E+00 1.3006481E+11	2.4142646E+00 2.6476919E+01	3.8968190E+05 3.6284459E+00	2.9073731E+00	1.9524764E+05	1.9544628E-05	3.1821717E+03	5.7127877E+01
8	3.8532913E+00 1.2822311E+11	2.4637890E+00 2.6612205E+01	3.8850791E+05 3.6443850E+00	3.3617421E+00	1.9980468E+05	2.0288289E-05	3.1530997E+03	6.3001280E+01
9	3.8532913E+00 1.2628268E+11	2.5130451E+00 2.6751573E+01	3.8722305E+05 3.6603163E+00	3.8389425E+00	2.0473942E+05	2.1105772E-05	3.1220904E+03	6.9172217E+01
10	3.8532913E+00 1.2318213E+11	2.5859347E+00 2.6966564E+01	3.8500847E+05 3.6828684E+00	4.6421741E+00	2.1395421E+05	2.2591914E-05	3.0725067E+03	7.8998390E+01
11	3.8532913E+00 1.2094839E+11	2.6629617E+00 2.7173454E+01	3.8485298E+05 3.7234599E+00	5.6186152E+00	2.2648503E+05	2.4492581E-05	3.0230696E+03	9.0468463E+01
12	3.8532913E+00 1.2083833E+11	2.7481095E+00 2.7381215E+01	3.9023621E+05 3.8188686E+00	6.8025627E+00	2.4390634E+05	2.7043431E-05	2.9710888E+03	1.0485410E+02
13	3.8532913E+00 1.2073802E+11	2.8452081E+00 2.7641147E+01	3.9712444E+05 3.9448671E+00	8.2885907E+00	2.6964706E+05	3.0934857E-05	2.8986864E+03	1.2418955E+02
14	3.8532913E+00 1.2076472E+11	2.9390999E+00 2.7904888E+01	4.0460664E+05 4.0862437E+00	9.7652979E+00	3.0037454E+05	3.5856093E-05	2.8124063E+03	1.4696103E+02
15	3.8532913E+00 1.2084852E+11	3.0319395E+00 2.8191370E+01	4.1341022E+05 4.2657603E+00	1.1178439E+01	3.3599496E+05	4.2342167E-05	2.6913708E+03	1.7419613E+02
16	3.8532913E+00 1.2093471E+11	3.1219881E+00 2.8425794E+01	4.2174902E+05 4.4556564E+00	1.2502935E+01	3.7746585E+05	5.0639650E-05	2.5491609E+03	2.0734117E+02
17	3.8532913E+00 1.2127671E+11	3.2141965E+00 2.8593175E+01	4.2990374E+05 4.6605735E+00	1.3787697E+01	4.2880689E+05	6.1714340E-05	2.3902078E+03	2.5018893E+02
18	3.8532913E+00 1.2140270E+11	3.3093103E+00 2.8698462E+01	4.3749039E+05 4.9029128E+00	1.5031325E+01	4.9489897E+05	7.7805360E-05	2.1961561E+03	3.0744398E+02
19	3.8532913E+00 1.2124118E+11	3.4090929E+00 2.8747192E+01	4.4492144E+05 5.2389850E+00	1.6273636E+01	5.8484748E+05	1.0364870E-04	1.9515139E+03	3.8883043E+02
20	3.8532913E+00 1.2118656E+11	3.5157260E+00 2.8727913E+01	4.5235303E+05 5.6793184E+00	1.7749661E+01	6.9749831E+05	1.4264006E-04	1.6900817E+03	5.1179620E+02
21	3.8532913E+00 1.2116934E+11	3.5471082E+00 2.8714086E+01	4.5466353E+05 5.8447865E+00	1.8086756E+01	7.4580591E+05	1.6052262E-04	1.6050354E+03	5.2750759E+02

ELAPSED TIME = 13.51 SEC. DRAG = 3.739E+07 DYNES

ERROR AT STATEMENT 90 OF SUBROUTINEINTR

**h. First ray downstream of embedded shock
Figure F-4. Concluded.**

NOMENCLATURE

A_k	Constant in radiation rate of k^{th} process
A_{k_i}	Constant in expression for rate of i^{th} reaction, Eq. (21)
A_{ij}	Matrix specifying reactions affected by j^{th} vibrator
a_f	“Frozen” sound speed; $a_f^2 = \bar{C}_p \mathcal{R} \Sigma \bar{\gamma}_j \bar{T} / (\bar{C}_p - \mathcal{R} \Sigma \bar{\gamma}_j)$
B_k	Constant in radiation rate of k^{th} process
B_{k_i}	Constant in expression for rate of i^{th} reaction, Eq. (21)
b_j	Constant in harmonic oscillator formula for chemical potential
C_H	Stanton number
C_P	Specific heat of mixture
C_{p_j}	Specific heat at constant pressure of j^{th} species
C_f	Coefficient of friction
C_{k_i}	Constant in expression for rate of i^{th} reaction, Eq. (21)
D_i	Constant specifying reaction type, Eq. (22)
D_{k_i}	Constant in expression for rate of i^{th} reaction, Eq. (21)
D_{ik}	Binary diffusion coefficient
\bar{E}_{j_l}	Energy of l^{th} electronic level of j^{th} species, cal per molecule
\bar{F}_j	Molar free energy of j^{th} species, ergs/mole
ΔF_i	Change of free energy in i^{th} reaction in Eq. (19)
F1-F5	Profile integrals used in boundary-layer calculation

G	Boundary-layer enthalpy ratio
\mathcal{G}	Rate of change of static enthalpy due to chemical and vibrational relaxation, Eq. (A-24)
g_{jt}	Degeneracy of 1 th electronic level of j th species
H	Total enthalpy
\bar{h}_j	Static enthalpy of j th species, ergs/mole
\bar{h}_j^0	Heat of formation of j th species, ergs/mole
\bar{I}_j	Rotational contribution to species enthalpy, ergs/mole
J	Jacobian of transformation from z, r to x, y coordinates
K_i	Equilibrium constant i th reaction
k'_{bi}	Backward reaction rate constant i th reaction
k'_{fi}	Forward reaction rate constant i th reaction
\overline{M}	Molecular weight, gm/mole
m_e	Mass of electron, gm
M	Ray index, also any species
N_c	Number of elements
N_R	Number of reactions
N_{rad}	Number of radiative processes
N_S	Number of species
N_{vib}	Number of nonequilibrium vibrators
n_j	Number of atoms in j th species

\bar{N}_e	Electron number density, cm^{-3}
\bar{N}_j	Number density of j th species, cm^{-3}
O	Number of vibrational levels in cut-off oscillator
\bar{p}	Pressure, dynes/ cm^2
p	Dimensionless pressure, $\bar{p}/(\rho_\infty \bar{U}_\infty^2)$
Q_{ij}	Source term in species conservation, Eq. (22)
\bar{R}	Radius of curvature
\mathcal{R}	Universal gas constant = 8.313405×10^7 ergs/mole $^\circ\text{K}$
r	Coordinate normal to axis
\bar{R}_{ad}	Total energy radiated, $\text{ergs gm}^{-1} \text{sec}^{-1}$
\bar{S}	Streamline coordinate
\bar{s}	Boundary-layer history parameter
\bar{T}	Translational temperature
T_{vj}	Vibrational temperature of j th oscillator
U	Resultant velocity = \bar{U}/\bar{U}_∞
\bar{U}_∞	Free-stream velocity at centerline
u	Velocity component normal to ray = \bar{u}/\bar{U}
V_j	Modifies reaction to account for nonequilibrium of j th vibrator
v	Velocity component along ray = \bar{v}/\bar{U}_∞
w_j	Source function for nonequilibrium vibration - defined, Eq. (16)

W_i	Constant specifying reaction type
X_i	Mass fraction of i^{th} species
x	Coordinate along shock
y	Coordinate normal to shock
z	Coordinate along axis from shock vertex
Z_i	Constant specifying reaction type
α_{jk}	Number of atoms of type k in species j
β	Mach angle, also $\cos^2 \phi_b$
Γ	Averaged specific heat ratio (frozen)
$\bar{\gamma}_j$	Concentration of j^{th} species, moles/gm
γ_j	Concentration of j^{th} species, moles/free-stream mole
$\bar{\delta}$	Boundary-layer velocity thickness, cm
$\bar{\epsilon}$	Vibrational energy, erg/gm
$\bar{\mu}$	Viscosity, $\text{gm cm}^{-1} \text{sec}^{-1}$
$\bar{\mu}_j^0$	Chemical potential of j^{th} species, ergs/mole, Eq. (4)
ν_{ij}	Stoichiometric coefficient of species j in reaction i
$\bar{\tau}$	Vibrational relaxation time, cm, Eq. (27)
τ_a	} constants in expression for $\bar{\tau}$, Eq. (27)
τ_b	
τ_c	
τ_d	

$\bar{\theta}_j$	Characteristic vibrational temperature, °K
η	Boundary-layer coordinate normal to body; also coordinate normal to a streamline
ϕ_{ii}	Viscosity cross-section (\AA^2)
ϕ	Flow angle with respect to z-axis; azimuthal angle
ψ	Mass flux
$\pi(s)$	Boundary-layer pressure gradient parameter
$\bar{\pi}$	$(1/s) \int_0^s \pi(s) ds$
κ	Local shock curvature
κ	} Constants used in determining new shock shape
λ	
Λ	$\overline{U_\infty^2} \overline{M_\infty} / \mathcal{R} \overline{T_\infty}$, constant in dimensionless state equation
σ	Shock angle with respect to Z-axis
$\bar{\sigma}$	Stefan-Boltzmann Constant = $5.6687 \times 10^{-5} \text{ erg cm}^{-2} (\text{°K})^{-4} \text{ sec}$
ω	0 two-dimensional flow 1 axisymmetric flow
Ω	Solid angle
$\bar{\rho}$	Density, gm cm^{-3}
χ_j	Degree of nonequilibrium of ith reaction, Eq. (24)

Subscripts

∞	Evaluated in free stream at centerline
0	Evaluated at stagnation point

- b Evaluated at body surface
- sh Evaluated at shock
- e Evaluated at boundary-layer edge
- N Normal to shock
- t Tangent to shock
- am Local free-stream value at shock location

Superscripts

- Indicates dimensional quantity
- o Evaluated at 0°K and 1 atm pressure
- * Pertaining to products of a reaction

Note: The nondimensional quantities used throughout this report are referenced to free-stream values according to the following system:

<u>Types of Quantity</u>	<u>Reference</u>
Length	\bar{R}_{sh}
Velocity	\bar{U}_{∞}
Density	$\bar{\rho}_{\infty}$
Pressure	$\bar{\rho}_{\infty} \bar{U}_{\infty}^2$
Energy of mixture	$\mathcal{R} \bar{T}_{\infty} / \bar{M}_{\infty}$
Energy of particular species	$\mathcal{R} \bar{T}_{\infty}$
Molecular weight	\bar{M}_{∞}
Concentration (γ_j)	$\sum_{j=1}^{NS} \bar{\gamma}_{j\infty} = \bar{M}_{\infty}^{-1}$